Summer 2011

Simulation of spatial and temporal trends in hydrodynamic conditions of Upper Mississippi River Pool 8

Thomas Jess II Smith
University of Iowa

SIMULATION OF SPATIAL AND TEMPORAL TRENDS IN HYDRODYNAMIC CONDITIONS OF UPPER MISSISSIPPI RIVER POOL 8

by

Thomas Jess Smith II

A thesis submitted in partial fulfillment
of the requirements for the
Master of Science degree in
Civil and Environmental Engineering
in the Graduate College of
The University of Iowa

July 2011

Thesis Supervisors: Professor Larry J. Weber
Adjunct Assistant Professor Douglas J. Schnoebelen
Associate Research Engineer Nathan C. Young

Graduate College
The University of Iowa
Iowa City, Iowa

CERTIFICATE OF APPROVAL

_____

MASTER'S THESIS

_____

This is to certify that the Master's thesis of

Thomas Jess Smith II

has been approved by the Examining Committee
for the thesis requirement for the Master of Science
degree in Civil and Environmental Engineering at the July 2011 graduation.

Thesis Committee: _____
Larry J. Weber, Thesis Supervisor

_____
Douglas J. Schnoebelen, Thesis Supervisor

_____
Nathan C. Young, Thesis Supervisor

_____
A. Jacob Odgaard

To my Dad

Continuous effort – not strength or intelligence – is the key to unlocking our potential.

-*Winston Churchill*

ACKNOWLEDGMENTS

I would like to first acknowledge all the help and support I received from the faculty and staff at IIHR – Hydroscience and Engineering. Larry Weber, Nathan Young, and Douglas Schnoebelen have all continuously mentored and guided me through this whole process and made my time at the institute very beneficial. Larry, Nate, and Doug all provided guidance with conceptual ideas and helped form my work into the success it has become. I would like acknowledge Jesse Piotrowski for all his effort in helping me with the technical aspects of my work. Through his tireless efforts, he ensured that this work came together. I want to thank Mike Kundert for all his help with graphics and plots for this work as well. I would also like to thank the numerous faculty, students and staff at IIHR which helped with everyday activities that really fine-tuned the thesis.

I would like to thank members of the United States Geological Survey at the Upper Midwest Environmental Sciences Center, Barry Johnson, Jim Rogala, Jeff Houser, and Brian Ickes. They continuously aided in conceptual guidance and data collection which made this work possible. I would like to thank Marvin Hubbell, Karen Haggerty and Jon Hendrickson all with the U.S. Army Corps of Engineers. Their help and support in data collection and securing funding has greatly benefited the project. The experience with everyone at these organizations has been beneficial, not only to me, but ensuring that future generations will understand the importance of hydraulic modeling in the Upper Mississippi River.

Finally I would like to acknowledge my family. Their constant support and wisdom have molded me into the person I have become today, and I would not have succeeded without them. Lastly, I would like to acknowledge my future wife Kelly Davis, she has seen me through this trying time, and has constantly been providing me with support. My family and Kelly really have guided me on the path of success and have ensured that I continue along it throughout my life and career.

ABSTRACT

The Upper Mississippi River is in interest to river managers and biologists due to its vast ecosystem and past anthropogenic impacts. In order to help restore the river to a more natural state, river managers and biologists need a strong understanding of the hydrodynamics of the system. A two-dimensional hydrodynamic model was developed in Pool 8 of the Upper Mississippi River and utilized for river management applications. The model was constructed using SMS 10.0 grid generation software and processed with SRH-2D hydrodynamic software. SRH-2D used Manning's roughness coefficients to calibrate the model to observed water surface elevation data collected by the USGS. The model was validated to an observed water surface elevation profile, percent discharge, and velocity magnitude comparison through 17 transects within the model. The calibrated and validated model was used for river management and biological applications; steady state discharge library, drawdown scenario, hypothetical island, travel time study, and habitat suitability assessment. The results showed that the two-dimensional hydrodynamic model could accurately develop a library of discharge scenarios, simulate drawdown scenarios, represent a hypothetical island, develop stream traces for travel time calculations, and create habitat suitability maps based on field data. The completion of these applications with the two-dimensional model shows the efficiently and accuracy of the model, and how two-dimensional numerical models are important tools in bridging the gap between engineers and scientists.

TABLE OF CONTENTS

LIST OF TABLES

LIST OF FIGURES

LIST OF CONVERSION FACTORS AND DATUMS

Inch/Pound to SI

Multiply	By	To obtain
	Length	
inch (in.)	2.54	centimeter (cm)
foot (ft)	0.3048	meter (m)
mile (mi)	1.609	kilometer (km)
	Area	
acre	4047	square meter (m^2)
square mile (mi^2)	2.59	square kilometer (km^2)
	Flow Rate	
cubic foot per second (ft^3/s)	0.02832	cubic meter per second (m^3/s)

Vertical coordinate information is referenced to the North American Vertical Datum of 1988 (NAVD 88)

Horizontal coordinate information is referenced to the North American Datum of 1983 (NAD 83)

CHAPTER 1: INTRODUCTION

1.1 Background

The Mississippi River is the largest river in the United States, and one of the longest rivers in the world, being surpassed only by the Amazon and Nile. The Mississippi drains an area approximately 1,245,025 mi^2 (3,224,600 km^2) which covers approximately 41 percent of the 48 contiguous states (Knox, 2007). The Mississippi River is a vital economic, social, and environmental resource that has been the focus of many projects in order to improve its current and future state.

The Upper Mississippi River Management Act of 1986 (Public Law 99-662) defines the Upper Mississippi River (UMR) as the commercially navigable reaches of six floodplain rivers above Cairo, Illinois, excluding the Missouri River (Delaney, 1998). In addition, Public Law 99-662 states the following, "To ensure the coordinated development and enhancement of the Upper Mississippi River system, it is hereby declared to be the intent of Congress to recognize that system as a nationally significant ecosystem and a nationally significant commercial navigation system. Congress further recognizes that the system provides a diversity of opportunities and experiences" (Delaney, 1998). These statements greatly explain why the UMR has been of great interest to numerous stakeholders including both government, and nongovernment agencies. Engineers and biologists are being drawn to the UMR because of its large, diverse ecosystems and continued anthropogenic impacts. The creation of the UMR lock and dam system in the 1930's to aid in navigation has significantly altered the hydrologic and geomorphic characteristics of the river. The lock and dam system has created 27 pools from Minneapolis, Minnesota to Granite City, Illinois in the UMR (United States Geological Survey, 2011b). The natural state of the UMR has changed dramatically from a historically meandering river connected to broad floodplains to a series of pools that are often isolated from the surrounding floodplains by levees. This situation has often had

negative effects on native biota from changing hydrologic conditions, loss of habitat, increased sedimentation, and loss of connectivity to the main river. In order for scientists to aid water managers, communities and stakeholders in rehabilitating or restoring UMR ecosystems, it is critical to link the hydrodynamic framework with biology and ecology to provide a complete understanding of the ecosystems in the UMR.

Pool 8 in the UMR is a pool of interest because the complex braided areas of this pool provide a rich habitat for native species. Effective long-term ecosystem and resource managements in Pool 8 are critical for river stakeholders with implications for similar sections of the Mississippi and other large rivers. Pool 8 has been the site of several biological research studies by the United States Geological Survey (USGS) Upper Midwest Environmental Science Center (UMESC) located in La Crosse, Wisconsin. UMESC is an ideal location for mobilizing research scientists for Pool 8 studies. In addition, Pool 8 is part of the Mississippi River Long Term Resource Monitoring Program (LTRMP) (United States Geological Survey, 2011a) so there is a vast amount of biological data available about the pool, and much of it has been available since 1988 (United States Geological Survey, 2011a). However, biological data is most valuable when coupled with a hydrodynamic framework to more fully understand and use this information for adaptive management and long-term planning.

Computer generated hydrodynamic models are essential to bridging the gap between biologists and engineers. Hydrodynamic models are a tool that provides essential data on discharge, velocity, and water depth, which are the primary parameters of hydrodynamics. These models provide the necessary frame work to understand processes within hydraulics and how these affect ecosystems. Hydrodynamic models also guide us in making comparisons to real world events, which can tell us if the model results or field data (or both) are in error (Silberstein, 2006). In addition, hydrodynamic models are tools that allow biologists and river managers to simulate a range of scenarios

in which they can better understand the flow regimes of the river, along with spatial and temporal distribution of the hydrodynamic properties which effect biota.

1.2 Motivation

The motivation behind this project has stemmed from an increased need of hydrodynamic data to better understand biological processes on the Mississippi River. The University of Iowa Lucille A. Carver Mississippi Riverside Research Station (LACMRERS) (The University of Iowa, 2010) researchers, the U.S. Army Corps of Engineers, and UMESC have identified Pool 8 as a critical resource with a rich data set for study (Schnoebelen, 2009-2010). Initial work in the area began with data collection and developing a three-dimensional hydrodynamic model for Round Lake, a backwater area located in Pool 8 (Schubert, 2009). The previous three-dimensional model was developed to study simple nitrate transport and reaction in Round Lake. Velocity and discharge measurements were collected by IIHR – Hydroscience and Engineering staff in November 2008 and June 2009 for the three-dimensional model, which were used as the boundary conditions for the model along with calibration and validation of the model (Schubert, 2009). Flow was simulated through the three-dimensional model and particle residence time and species transport applications were used to understand how the hydrodynamics effected the removal of nitrogen within the lake (Schubert, 2009). Water quality sampling was also conducted for the three-dimensional model and was collected by the USGS UMESC in conjunction with IIHR staff in the summer of 2009 (Schubert, 2009). The three-dimensional model was able to predict flow patterns along with nutrient processing fairly accurately according to the results from the study when compared to water quality samples. The previous three-dimensional model provided a proof of concept for the current study, in which the concept was applied to a larger study area.

Hydrodynamic model simulations can save resources for restoration and biology projects by predicting scenarios that otherwise would need to be physically modeled or

experienced. Models can help predict and avoid unintended outcomes. Lastly, models can provide a library of hydrodynamic events which river managers and biologists can reference for future work. This library of flow events, ranging from low to high, contains data with all output parameters from the model that can be targeted for adaptive management projects.

1.3 Objectives

The overall objective of the study was to select and develop a two-dimensional hydrodynamic model for Pool 8 of the Upper Mississippi River near La Crosse, Wisconsin. The model would resolve multidirectional flow in the main channel and backwater areas with the goal of being used for current and future management techniques. Specific objectives of the model include:

- Build a library of flow scenarios ranging from low to high flows based on correspondence with the UMESC and U.S. Army Corps of Engineers, Rock Island District.
- Simulate one and two foot drawdown scenarios with a comparison of the flow conditions during the drawdowns.
- Implement a hypothetical island within the pool and evaluate the local flow regime.
- Evaluate residence time for three flow conditions (10,000, 33,000 and 100,000 cubic feet per second (ft^3/s).
- Conduct a habitat suitability assessment for emergent vegetation.
- Couple the hydrodynamic results with an ecological model currently being developed by the University of Illinois and USGS UMSEC.

1.4 Study Location

The Upper Mississippi River (UMR) contains 27 navigation dams which in turn creates a series of navigation pools. These navigation pools stretch from Minneapolis,

Minnesota (Pool 1) to Granite City, Illinois (Pool 26). The study area is located in the UMR of Pool 8 near La Crosse, Wisconsin (Figure 1.1 and Figure 1.2). Pool 8 is approximately 23 mi (37 km) long and is bounded upstream and downstream by Lock and Dam 7 and Lock and Dam 8, respectively. Along with the lock and dams, there are wing dams and engineered islands in Pool 8 that are maintained by the United States Army Corps of Engineers, St. Paul District to help sustain the 9.00 foot (2.74 meter) navigation channel within the pool.

1.5 Selection of a Two-Dimensional Numerical Model

1.5.1 Numerical Models

There are three classifications of numerical models: one-, two-, and three-dimensions, as represented in the spatial domain. In application, model dimensionality should be based on a variety of factors, including desired objectives, applications, time, and resources (Cunge, Holly and Verwey, 1980). Each model type has its advantages and disadvantages depending on the project requirements. Projects that require high resolution detail and the vertical component typically require a three dimensional model, while projects that are strictly looking at inundation can use a one dimensional model. Computational run time is also a factor. Additional dimensions and higher grid resolution requires modelers to devote a greater amount of time to mesh development, along with a longer simulation time for the model (Anderson, 1995).

One-dimensional models cannot solve multidirectional flow. However, they are extremely useful in mapping inundation because they can clearly illustrate wet and dry cross-sections within the model (Bates and De Roo, 2000). Velocity, depth, and discharge are calculated in one-dimensional models using a series of cross-sections which are perpendicular to channel flow, and since one-dimensional models eliminate multidirectional aspects of flow by maintaining a constant velocity, the parameters are all averaged over the depth and the cross-sections. One-dimensional models are

computationally efficient due to the use of the cross-section averages for the Navier-Stokes equations. While the model is efficient and can be used on large scales, there are some limitations besides the lack of resolution. Inexperienced modelers run the risk of improperly placing the cross sections within the model domain, which can be troublesome since the one-dimensional models interpolate linearly between cross-sections to obtain data. Placing cross sections along equipotential flow lines ensures the model will give accurate results (Bates and De Roo, 2000).

Three-dimensional models are powerful tools for physical representations of river sections even in complex, meandering rivers. These types of models use the full set of Navier-Stokes equations which increases computational run-time. Three-dimensional models show detail in all three physical dimensions and are recommended for complex domains, but are not efficient over long reaches. It has been reported that if a model domain exceeds approximately three miles (five kilometers), a two-dimensional model using simpler numerical schemes is recommended (Bates and De Roo, 2000). Two-dimensional models are often a good compromise in that they can accurately show detail and still be numerically efficient (Bates and De Roo, 2000).

One assumption made in two-dimensional models is that vertical mixing is negligible (Lai, 2009). In general, this is a valid assumption in that many open channel flows are already well mixed and the horizontal dimensions in the fluid domain greatly exceed the vertical dimensions (Jirka, 2001). By vertically averaging the Navier-Stokes equation, depth-averaged two-dimensional equations can be obtained (Lai, 2009). These depth-averaged (Equations (1.1) through (1.3) below) are defined as the Saint-Venant shallow water equations.

$$\frac{\partial h}{\partial t}+\frac{\partial (hU)}{\partial x}+\frac{\partial (hV)}{\partial y}=0 \tag{1.1}$$

$$\frac{\partial (hU)}{\partial t}+\frac{\partial (hUU)}{\partial x}+\frac{\partial (hVU)}{\partial y}=\frac{\partial (hT_{xx})}{\partial x}+\frac{\partial (hT_{xy})}{\partial y}-gh\frac{\partial z}{\partial x}-\frac{\tau_{bx}}{\rho} \tag{1.2}$$

$$\frac{\partial(hV)}{\partial t}+\frac{\partial(hUV)}{\partial x}+\frac{\partial(hVV)}{\partial y}=\frac{\partial(hT_{xy})}{\partial x}+\frac{\partial(hT_{yy})}{\partial y}-gh\frac{\partial z}{\partial y}-\frac{\tau_{by}}{\rho} \tag{1.3}$$

In the equations above, t is time, x and y are horizontal Cartesian coordinates, and h is water depth. The gravitational acceleration is g, while U and V are the depth-averaged velocity components in the x and y directions, respectively. The depth-averaged stresses due to turbulence and dispersion are represented by T_{xx}, T_{xy}, and T_{yy}. The water surface elevation is z, which takes into account the depth, h, and bed elevation z_b. The water density is ρ, and the bed shear stresses are τ_{bx} and τ_{by} (Lai, 2009).

The depth-averaged Saint-Venant equations, in relation to the full Navier-Stokes equations, remove the horizontal component. This means that vertical differential terms are eliminated, thus making the equations simplier (Cunge, Holly and Verwey, 1980). When the equations are simplified, it has been seen that computational efficieny and capacity increase (Lai, 2009; Piotrowski, 2010).

The depth-averaged turbulent stress and dispersion terms can be seen in equations (1.4) though (1.6). The effective stresses are calculated using the Boussinesq's formulation (Lai 2009).

$$T_{xx}=2(\upsilon+\upsilon_t)\frac{\partial U}{\partial x}-\frac{2}{3}k \tag{1.4}$$

$$T_{xy}=(\upsilon+\upsilon_t)(\frac{\partial U}{\partial y}+\frac{\partial V}{\partial x}) \tag{1.5}$$

$$T_{yy}=2(\upsilon+\upsilon_t)\frac{\partial V}{\partial y}-\frac{2}{3}k \tag{1.6}$$

In the above equations, k is the turbulent kinetic energy, υ is the kinematic viscosity of water, and υ_t is the turbulent eddy viscosity. In this study, the depth-averaged parabolic turbulence model was used for computational efficiency. The parabolic equation can be seen in equation (1.7).

$$\upsilon_t=C_tU_*h \tag{1.7}$$

In the above equation, U_* is the bed frictional velocity and C_t is the model constant which can range from 0.3 to 1.0. The default value set in the model is 0.7, which was determined by Yong Lai (Lai, 2009).

The bed shear stress is derived using the Manning's resistance equation (Lai 2009). The bed shear stress equations are (1.8) and (1.9) below.

$$\tau_{bx} = \rho(\frac{gn^2}{h^{1/3}})U\sqrt{U^2+V^2} \tag{1.8}$$

$$\tau_{by} = \rho(\frac{gn^2}{h^{1/3}})V\sqrt{U^2+V^2} \tag{1.9}$$

In the above equations, n is the spatially varying Manning's value. The Manning's value is used as a spatial tuning parameter for the numerical model, which again will be fully discussed in Chapter 3.

While two-dimensional models are efficient at modeling multidirectional flow, they sometimes may lack certain details which scientists might find necessary. For example, if a project wants to capture local flow patterns, to enable scientists and biologists to better assess detailed habitat suitability, meso-scale features must be incorporated (Crowder, 2002). However, for the scope of the current project (pool scale study) it was determined that meso-scale features within the bathymetry could be considered negligible and a two-dimensional study would provide a satisfactory amount information while minimizing computation time needed to capture all objectives.

1.5.2 Numerical Discretization

Anderson (1995) stated that, "…discretization is the process by which a closed-form mathematical expression, such as a function or a differential or integral equation involving functions, all of which are viewed as having an infinite continuum of values throughout some domain, is approximated by analogous (but different) expressions which prescribe values at only a finite number of discrete points or volumes in the domain". In

order for the governing equations to be discretized the time step (Δt) and computational element size (Δx) are required in the domain. The time derivative can be discretized using an explicit or implicit scheme. Explicit schemes solve the time derivative in a forward looking mode and are easier to set up and program (Anderson, 1995). The method contains one unknown so that it explicitly solves for the unknown, which is generally straightforward. The method allows for a small time step and is typically used for transient problems. The stability is achieved when the Courant-Friedrichs-Lewy (CFL) condition is satisfied for convergence. The resulting CFL number must be less than or equal to one for stability (Anderson, 1995). This can be seen in equation (1.10).

$$C = c\frac{\Delta t}{\Delta x} \leq 1 \tag{1.10}$$

In the above equation, C is known as the Courant number, and for stability to be achieved $\Delta t \leq \Delta x/c$ for the numerical solution.

Implicit schemes solve the time derivative in a backward looking mode. This scheme allows for stability to be maintained over larger Δt values, while requiring fewer iterations. A disadvantage to using the implicit scheme is it involves solving a system of algebraic equations simultaneously, which is not easy to program (Anderson, 1995). Also, a matrix in the computations must be inverted, adding to the complexity. Computer time per time step is greater than the explicit scheme. The implicit scheme is not accurate for large time steps, greater than a second, and a larger time step increases truncation error. The implicit scheme is primarily used for steady state problems (Anderson, 1995).

The current study used the Sedimentation and River Hydraulics Two-Dimensional (SRH-2D) flowing model developed by the U.S. Bureau of Reclamation (Lai, 2009). Numerical discretization of the governing flow equations in this model are by a segregated finite-volume approach (Lai, 2009). The domain of the solution is constructed upon a hybrid unstructured mesh, with arbitrary cell size and shape. Dependent variables

are stored at the geometric center of the cell and the governing equations are integrated over the cells using the Gauss integral, while using the Euler implicit time discretization method (Lai, 2009).

1.5.3 Steady and Unsteady State Numerical Models

SRH-2D can simulate steady state and unsteady state solutions, while implementing steady and unsteady state discharges through inlets and exits. The differences between the two, solutions and discharges (boundary conditions), must be known in order to understand exactly how SRH-2D converges a solution. The user can select steady state or unsteady state as the solver for the governing equations in SRH-2D. If a steady state solution is selected, only one iteration is used per time step. If the unsteady state solution is selected, multiple iterations are completed per time step (Lai, 2009). When a steady state solution is selected, only the final solution can be used, however, in an unsteady state solution, intermediate outputs can be used as solutions (United States Bureau of Reclamation, 2008). The steady solver converged solutions much faster than the unsteady solver, which makes it beneficial when computational time is an issue. The unsteady state solver converged solutions in approximately twice time of the steady state solver.

SRH-2D can also simulate steady state and unsteady state discharges through inlets and exits. The only difference between the two options is that in the unsteady model, discharge is time dependent. For the purpose of this study, SRH-2D uses a steady state solver, which reduced computational time, with a steady state discharge through inlets. The model is still solving the equations dynamically; just the final output is only sought after, with no need for intermediate solutions.

1.6 Flow Scenarios and Pool Scale Drawdowns

Steady state simulations were used for all simulations completed with the hydrodynamic model. The flow scenarios for the steady state simulations were developed

by the USGS (Johnson, 2010-2011; Ickes, 2011). The first flow scenarios were a low, average, and high flow. These were determined to be 11,000 ft^3/s, 33,000 ft^3/s, and 95,000 ft^3/s (311 m^3/s, 934 m^3/s, and 2,690 m^3/s). Later in the development of the model, more scenarios were added until there was a library of steady state flow scenarios from 10,000 ft^3/s to 100,000 ft^3/s (283 m^3/s to 2831 m^3/s) at intervals of 10,000 ft^3/s (283 m^3/s). The flow scenarios will be discussed in detail later in Chapter 4.

The purpose of a large scale pool drawdown is to expose previously inundated areas to promote growth of vegetation, which in turn increases new species activity and development of habitats. Water level management of the pool is designed to restore the temporal fluctuations within the pool (Water Level Management Task Force, 2007). Two historic drawdowns were completed in Pool 8 during the years of 2001 and 2002. The results of the drawdowns were increased discharge and sediment transport in the main channel, some erosion in secondary channels, reduction in the need for dredging, increase in aquatic plant coverage, increase in water clarity and submersed macrophytes, and an increase in animal habitat and occupation of pool 8 (Water Level Management Task Force, 2007).

There are numerous benefits to implementing a drawdown condition to pools in the UMR, with an overall goal of improving the ecosystems within the pool and guiding the pool back to its once natural state. The drawdowns conducted with the numerical model for this study were a one and two foot drawdown, where three flow conditions were simulated during each of the two drawdowns and a comparison was completed for each flow condition during both drawdowns, of exposed area along with velocity and depth.

1.7 Pool 8 Island Construction

Historically, the Upper Mississippi River system has been described as a main channel--with secondary channels, backwater areas, and natural levees--separating the

floodplain areas. The natural levees acted as barriers between the main flow and the floodplain ensuring that ecological processes within the pool could be seasonally completed. One example is winter habitats for fish and waterfowl, essential to the river ecology, and were protected by natural levees. These natural levees were often the highest land forms within the floodplains and also acted as platforms for terrestrial vegetation (Hendrickson, 2010). The construction of the Lock and Dam system in the 1930s has inundated floodplains along with valuable habitat area once inhabited by various species. Species have been forced to relocate due to the higher water surface elevations. The resulting pools did have a higher water surface elevations to stabilize flows, but wind induced wave action has also caused erosion of the natural levees along with blurring the habitats of main channel flows and floodplain areas, making it difficult for temporal biotic activities to occur (Hendrickson, 2010).

Since the early 1990s over ten miles of islands have been constructed in Pool 8 to help restore the river back to a more natural state (Hendrickson and Buesing, 2000). The construction of the islands in the recent years were designed to recreate past habitats for fish, animals, and birds along with improving sediment transport within the pool. The islands were constructed to replace the historic natural islands or levees that were inundated or eroded with the creation of Pool 8. Islands were rebuilt on or nearby historic islands. The island rebuilding goals were to create winter fish habitat, redistribute flow into relic channels, improve flow over floodplain areas, aid in temporal disconnectivity, and reduce wind induced wave action in shallow areas of the pool (Hendrickson and Buesing, 2000).

One goal of the present hydrodynamic modeling study was to place a hypothetical island in Pool 8 and evaluate the resulting hydrodynamics. The goals of the hypothetical island were to create a low flow zone in deep water, reduce wind fetch, and redistribute flow into relic channels. The island was placed in the lower portion of the pool (near river mile 683, Figure 1.4) based on discussions with UMESC researcher (Rogala, 2009-

2011). A complete evaluation of the island implemented in this study will be discussed in Chapter 4.

1.8 Travel Time Study

Physical processes, for example transport and mixing, within large scale river reaches are the main drivers for biogeochemical behavior of the aquatic ecosystems. These physical processes determine spatial and temporal locations of suspended substances while controlling the environmental conditions for the rate of biogeochemical processes. For biologists and scientists to better understand biogeochemical processes within large rivers, a first order description of the physical process occurring in rivers needs to be known, which can be expressed as a residence time (Rueda, Monreno-Ostos and Armengol, 2011). Knowing the residence time within Pool 8 can help predict the removal rate of nutrients within the pool, and help express flow patterns within the backwater areas, where nutrient build up is most common (Schubert, 2009). The current study is utilizing steady state simulations with stream traces created in Tecplot 360, which will results in the calculation of a travel time instead of a residence time. The difference between a residence time and travel time needs to be fully understood. A residence time is calculated by timing a particle that is injected at the model inlet until it reaches the exit of the model domain. The travel time, for the current study, is calculated by having a particle travel a certain distance by implementing a time step function. Travel times and residence times are not the same; therefore a travel time is not the ideal parameter that would be used for the calculations of nutrient removal. Biologists and river managers can utilize travel times and stream traces to assess when and where containments might be if they enter Pool 8 through one of the inlets, which would greatly effects the water quality.

Travel times for this study were completed using particle tracking with Tecplot 360. This process is beneficial in understanding flow patterns within the pool using

stream traces, while being able to incorporate particle tracking to calculate travel times within the pool. This process is difficult due to the nature of steady state simulations that were run with the model. Unsteady, three-dimensional models are more accurate for particle tracking and calculating residence times. Schubert (2009) was able to use FLUENT three dimensional modeling software to accurately track particles through the study area, the upper portion of Pool 8, which can be seen in Figure 1.3. The study was able to show nitrogen removal within the backwater area, and how it related to the physical processes. The residence time was calculated along with nutrient removal accurately because of the unsteady nature and size of the model. This study was able to calculate travel times at the pool scale within reason due to the difficulty of stream path creation with steady state simulations. The results are further discussed in Chapter 4.

1.9 Habitat Suitability Assessment

Habitat suitability assessments are complex, and complete assessments require consideration of numerous variables. Specific studies have been completed that not only take into consideration the hydrodynamics of a habitat within a river reach, but also the more complex aspects, such as local fluctuations with energy and velocity gradients and flow variations for specific areas (Crowder, 2002). Studies have also shown that it is important to capture meso-scale features within the bathymetry in order to understand highly dynamic local flow patterns which can have biological importance (Crowder and Diplas, 2000; He, Wu, and Wang, 2006). While the complexity of habitat suitability assessments are greatly studied, numerical efficiency must also be taken into consideration when conducting these studies. Often a balance is needed between an appropriate level of detail and project goals. A study completed comparing a one and two dimensional hydrodynamic model used for a Physical Habitat Simulation System (PHABSIM) showed that the two-dimensional numerical model was more appropriate for the habitat suitability study in the comparison (Ghanem, Steffler and Hicks, 1996).

For the current study, a simple habitat suitability assessment using depth and velocity for emergent vegetation was completed. The objective was to demonstrate how a two-dimensional numerical model at a pool scale could be efficient in predicting emergent vegetation habitat over a range of flow scenarios. This is important for resource management because biological field data is typically collected under a limited number of flow conditions making future predictions difficult. This study was able to use field depth, velocity, and presence in conjunction with simulated hydrodynamics in order to create an accurate habitat suitability assessment for Pool 8.

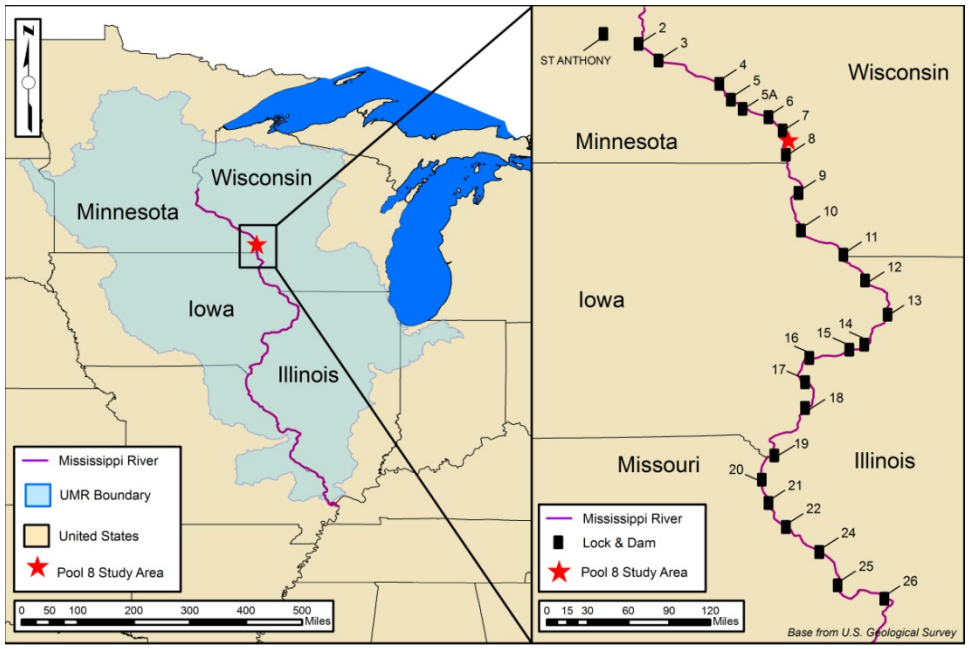

Figure 1.1. Aerial map of study area within the UMR basin showing the location of Pool 8 in the lock and dam system (Data Source: USGS, 2010b).

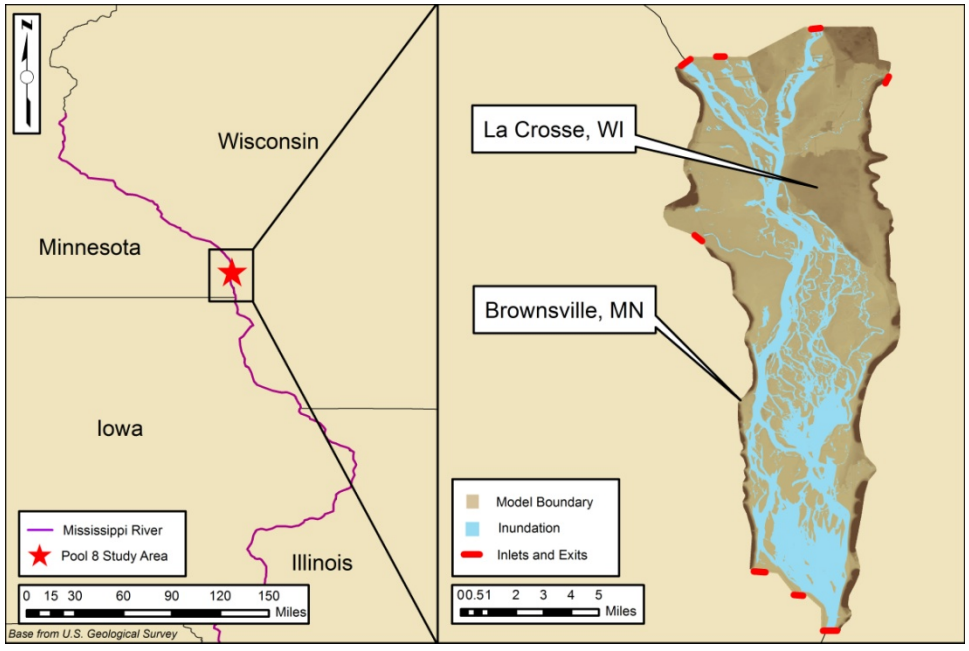

Figure 1.2. Aerial map of study area on the Mississippi River and detailed features of the study area Pool 8 (Data Source: USGS, 2010b).

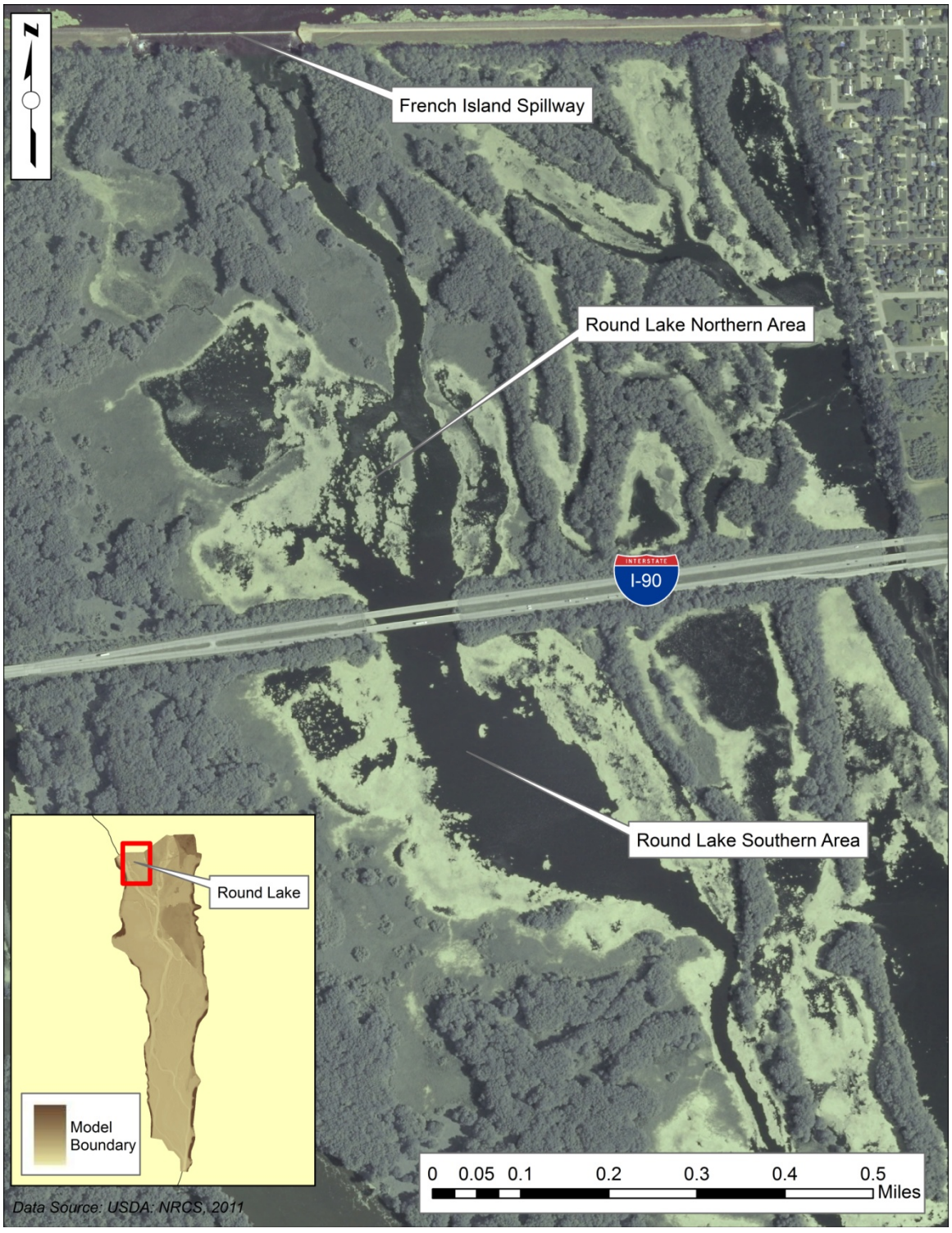

Figure 1.3. Aerial map showing Round Lake and its location within Pool 8 (Data Source: NRCS, 2011).

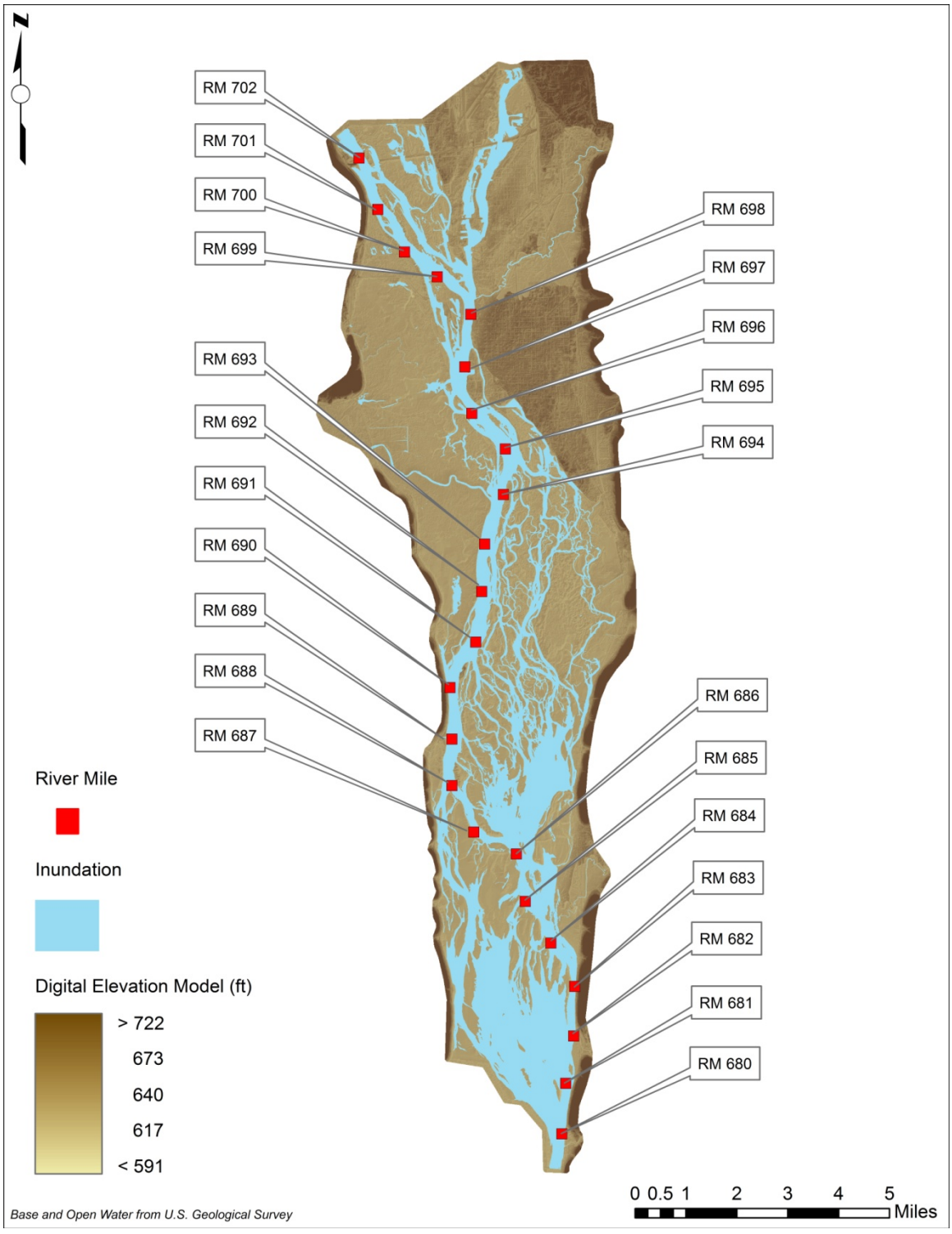

Figure 1.4. River miles along Pool 8 used for spatial references (Data Source: USGS, 2010b). Data flooded by dark brown extends to elevation 1,178 feet and data flooded by light brown extends to elevation 561 feet.

CHAPTER 2: DATA COMPILATION, ANALYSIS, AND PROCSESSING

2.1 Overview

The creation of a numerical flow model involves several steps of data compilation, analysis, and processing. Initially, the process begins with a compilation of a database of elevations for the pool or stream to be modeled, typically known as a digital elevation model (DEM). The DEM for the study area to be modeled is constructed using the Geographic Information System software, ArcGIS (ESRI, 2011). Once the DEM has been created, it is then used as the base or framework for the generation of the mesh for a modeled area. The mesh size and shape (structured, unstructured, or hybrid) depends on the objectives and detail needed for the model. The mesh for this study was created using the grid generation software, Surface Water Modeling Software 10.0 (SMS) (AQUAEVO, 2011) which was then physically linked to the DEM. Once this linkage is completed, flow simulations can be run through the mesh. The Sedimentation and River Hydraulics – Two-Dimensional (SRH-2D) (United States Bureau of Reclamation, 2008) numerical modeling software was then used to process the stream flow scenarios through the model. The model results were then analyzed using post-processing software, Tecplot 360 (Tecplot, 2010) and ArcGIS for graphic output. Other data outputs were summarized in tables using Microsoft Excel spreadsheets and simple statistics (Microsoft, 2011).

2.2 Model Extent, Bathymetry and Topography

The model extent was created using a 120,000 ft^3/s (3,399 m^3/s) steady flow condition through Lock and Dam 8, which was the largest historic discharge through Lock and Dam 8 when the data was collected in 2009 from the USACE source (USACE, 2011a). The simulations were steady state and therefore continuity had to be maintained, which meant the inflow had to equal the outflow in the model. Using this principle, Lock

and Dam 8 was used as the starting point to define the boundary conditions. The model extent was based on the inundation of the 120,000 ft^3/s (3,399 m^3/s) plus a 30 ft (10 m) buffer. This ensured that all the inundation would be captured in the model domain. The model extent was then used to define the DEM boundary. All the available bathymetry data for Pool 8 were originally from the U.S. Army Corps of Engineers through the Upper Mississippi River Restoration-Environmental Management Program (UMRR-EMP) with data processed by UMESC (United States Geological Survey, 2011a). The seamless bathymetry and topography data for the Pool 8 model were collected from the years of 1989 through 1991, with some updates to main channel surveys (Rogala, 2009 – 2011). In areas where additional topography was required for the model extent, data were acquired through the National Seamless Map server provided by the UMESC (United States Geological Survey, 2010a). UMESC was able to provide seamless bathymetry and topography for Pool 8 at the scale of one meter resolution which extended into the floodplain. In order to have the correct model extent, extra topographic data was needed, which was taken from the National Seamless Map server at 98 ft (30 m) resolution. A majority of the areas that required the extra topographic data were in the low land areas around the edges of the model domain. In areas were the data overlapped, the high resolution data were taken. The model extent can be seen in Figure 2.1.

2.3 Digital Elevation Model

The seamless bathymetry and topography gathered from the UMESC were used as the DEM for the hydrodynamic model. The DEM required some modification for the Stoddard Island Complex located in the southeast area of Pool 8 (Figure 2.2) because of missing elevations from crucial physical features. There were two rock sills that needed to be added to the DEM so that the Stoddard Island Complex was correctly represented. Figure 2.2. displays the rock sills that were added to the DEM.

The first rock sill was in the most northern part of the Stoddard Island Complex and was referred to as Rock Sill A, and the second rock sill was located on the west side of the complex and was referred to as Rock Sill B (Figure 2.2). Geometry data on both sills were acquired from the United States Army Corps of Engineers (Hendrickson, 2010-2011).

The most northern sill, rock sill A, was constructed higher than the original geometrical designs. The rock sill was built into the DEM based on elevation recommendation from the United States Army Corps of Engineers. Both rock sills were built referencing the 1912 Mean Sea Level (MSL) datum. In order for the structures to be accurately placed into the DEM, their elevations were converted to the North American Vertical Datum of 1988 (NAVD 88), the datum used for all topographic features during the development of the model. NAVD 88 was the datum determined to be the most accurate compared to past datum because over time benchmarks from past datum have been destroyed and affected by shifts in the earth's crust. The NAVD 88 datum was created to minimize these problems (Natinal Oceanic and Atmospheirc Administration, 2011). The spatial orientation of the structures matched the existing DEM orientation, which referenced North American Datum of 1983 (NAD 83) UTM Zone 15. NAD 83 was used for the same reasons NAVD88 was used, being it was the more accurate spatial reference. NAD 83 was more accurate because of shifts in past datum which created large differences that needed to be corrected, as well as past datum referencing the Clark Ellipsoid of 1866 which is no longer applicable to modern geodetics (Schwarz, 1989).

2.4 Stream Flow Data

Lock and Dam 7 and 8 boundary conditions were defined by historic discharge and stage data from federal agency websites. The discharge data were obtained from the USACE website (United State Army Corps of Engineers, 2011a) and (United States

Army Corps of Engineers, 2010). The boundary conditions for the two tributaries that enter the model domain were defined by historic discharge data that was obtained from the USGS website (United States Geological Survey, 2011c).

2.5 Summary

A large amount of existing data were compiled and analyzed in order to construct the hydrodynamic numerical model for Pool 8. Seamless bathymetric and topographic data were used for constructing the final DEM from the U.S. Army Corps of Engineers and UMESC. Topographic data extending past the study area was collected and merged to extend model boundaries. The Rock Sill A and B structures in the Stoddard Island Complex of Pool 8 were manually added to the bathymetry and topography for accuracy. All these data compellations were then used to construct the final DEM. The historic discharge data that defined the inflows and outflows to Pool 8 completed the data sets needed for the model.

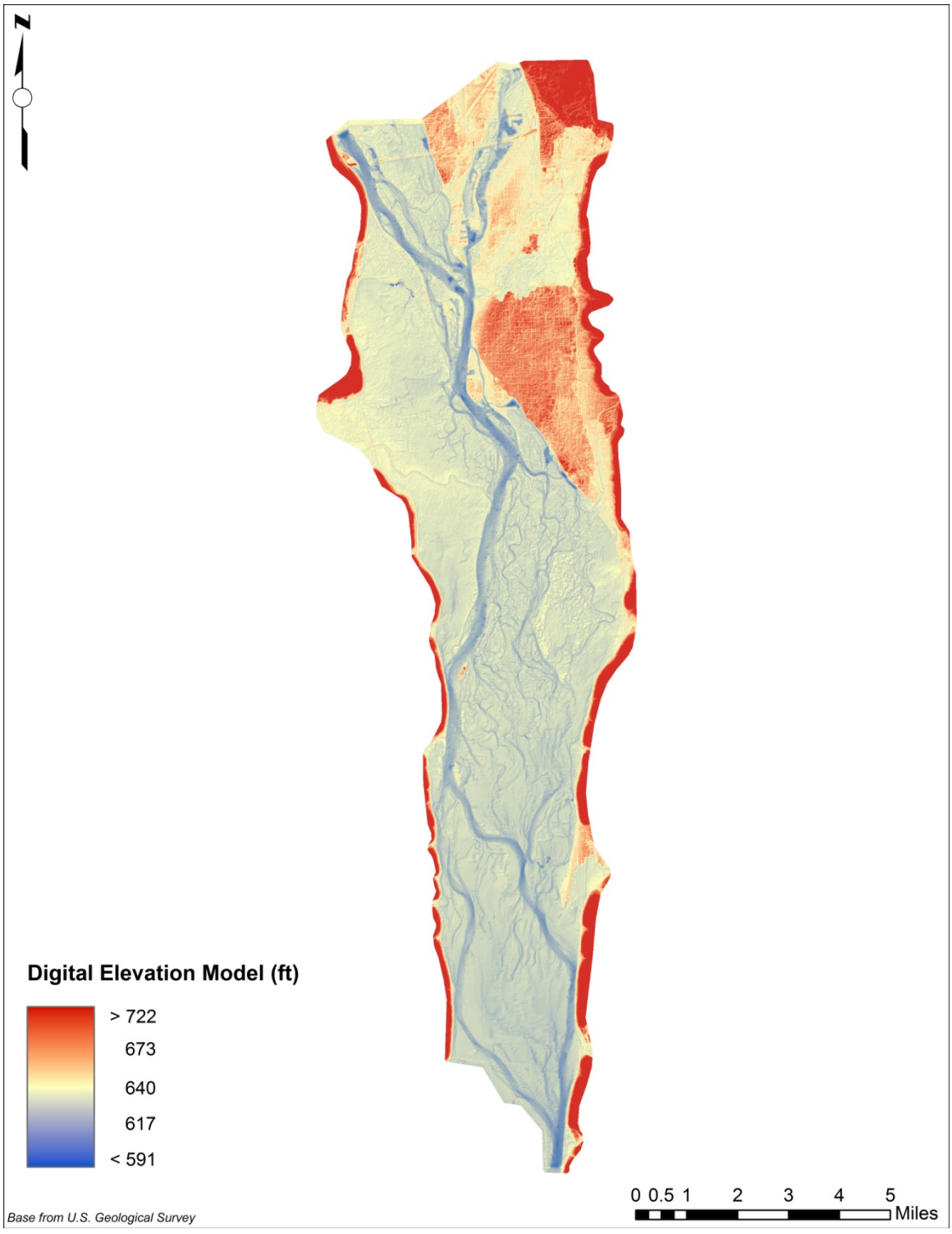

Figure 2.1. Digital Elevation Model used for model construction (Data Source: Rogala, 2009-2011). Data flooded by dark red extends to elevation 1,178 feet and data flooded by dark blue extends to elevation 561 feet.

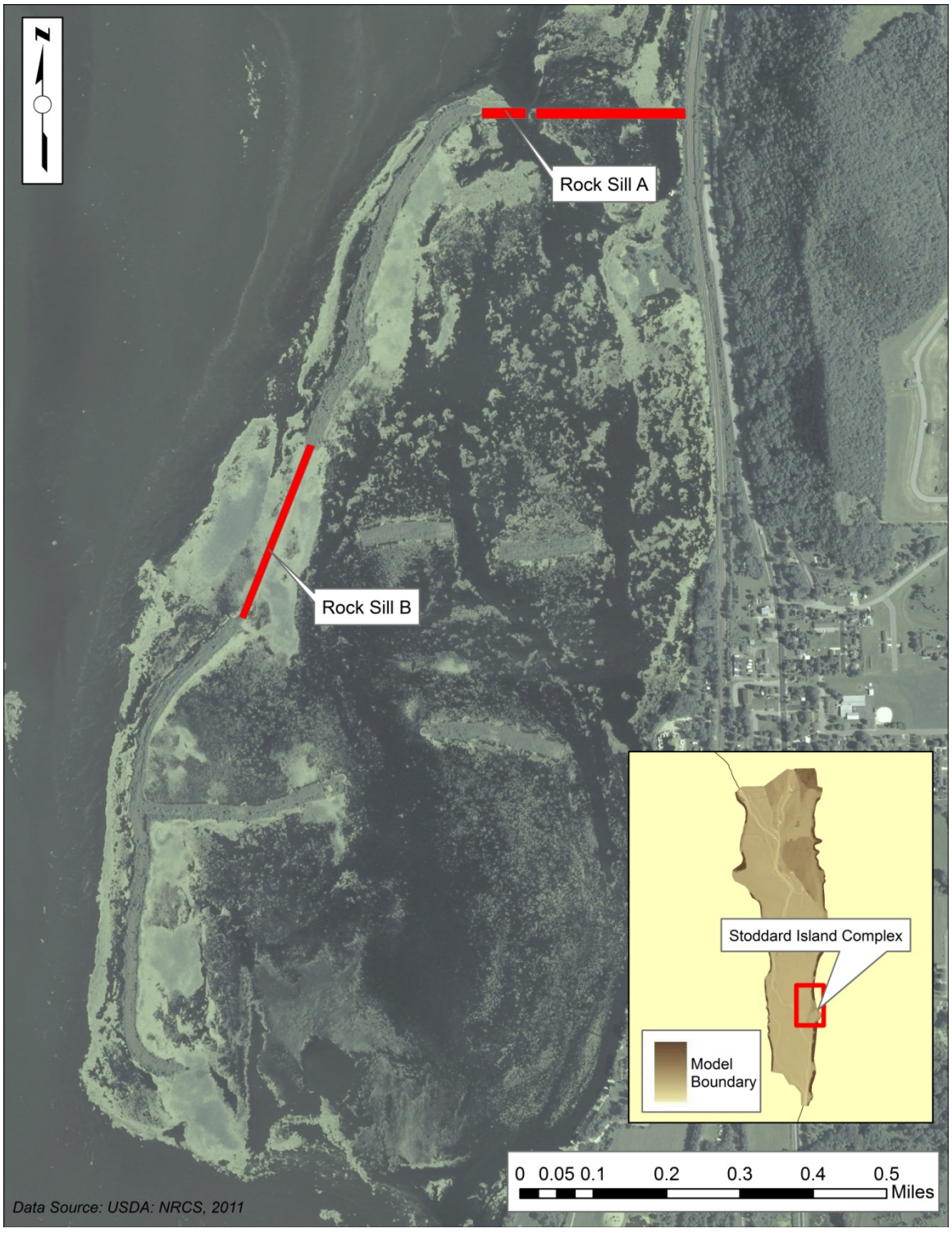

Figure 2.2. Inclusion of Rock Sill A and Rock Sill B within the Stoddard Island Complex located in the south eastern portion of Pool 8 (Data Source: NRCS, 2011).

CHAPTER 3: MODEL DEVELOPMENT

The seamless DEM was used as the base to create the numerical model that simulated the hydraulic flow through the study reach. The model was calibrated using the aerial LiDAR data and validated using the field data collected by the USGS. Flow conditions were determined, simulated and the results were used for the model applications and scenarios. The process of model development and production can be seen as a general flow diagram in Figure 3.1.

3.1 Numerical Methods

Each simulation was run using the steady depth-averaged Saint-Venant equations (equations 1.1-1.3, Chapter 1) along with a parabolic turbulence model found in the SRH-2D software. The parabolic turbulence model was chosen because the developer of the code recommends the parabolic turbulence model for field applications (Lai, 2009). The two-equation k-ε turbulence model is recommended for separated flow (e.g. flow in a 90 degree pipe bend). The model extent included the area as previously defined in Figure 2.1. in Chapter 2. The numerical mesh was generated using the SMS 10.0 mesh generation software. The mesh was composed of an unstructured hybrid mesh that contained 206,594 elements. The number of elements was based on the node spacing, which will be discussed later in this chapter in detail. A hybrid mesh was used so that the large model extent was computationally efficient, and areas of interest maintained high resolution. A mesh sensitivity analysis was not completed for this model because of project time constraints and the mesh resolution was determined to capture the necessary amount of detail set by the USGS personnel.

In the SMS software, the mesh is generated by user defined inputs. Feature arcs are first created by the user which defined the physical features of Pool 8. Feature arcs created the framework for the model, like steel beams create the framework for a building. The feature arcs are created by digitizing grid files from AcrMap. The feature

arcs are given a node density that is set by the user. When feature arcs connect to make a loop--which must consist of three or more feature arcs, polygons can be created by SMS. Each polygon is assigned a material type and mesh type. The material type defines the roughness coefficient used in the model. The mesh type can either be quadrilateral or triangular. Once all polygons are created and node densities are set, SMS will iteratively construct a mesh based on the polygons and node densities. Figure 3.2 through Figure 3.5 show the numerical mesh broken into four sections, which shows the mesh density.

The creation of the mesh began with inputting 18 land cover types defined by the USGS (United States Geological Survey, 2010b) in Pool 8. The high resolution grids were inputted into SMS and feature arcs were used to delineate the boundaries of the land cover types. The 18 land cover types included: agriculture, conifers, deep marsh annual, deep marsh perennial, deep marsh shrub, developed, flood forest, grassland, levee, lowland forest, mud, open water, pasture, plantation, populous community, road, rooted floating aquatics, salix community, sand, sedge meadow, shallow marsh annual, shallow marsh perennial, shrub/scrub, submerged vegetation, upland forest, wet meadow, and wet meadow shrub. These land cover types were used because SRH-2D is limited to 18 different roughness coefficients and these 18 land cover types were the 18 most prominent in Pool 8. After each land cover type was delineated by feature arcs, the node density was chosen based on the land cover type and location. All open water was given a maximum mode density of 98 ft (30 m). The 98 ft resolution was set by the USGS personnel, and was determined by the USGS to capture the correct amount of detail set by the project goals. The open water was the only land cover type that consisted of quadrilateral mesh cells. All other land cover types were assigned node densities from 98 ft (30 m) to 295 ft (90 m) based on their location to the open water. Figure 3.6 shows a zoomed in area of the land cover polygons within the mesh. A ratio of one to two was maintained between adjacent land cover types, as recommended by the SRH-2D manual (United States Bureau of Reclamation, 2008). The only area where the mesh density was

delineated lower than 98 ft (30 m) was in the tributary channel of the Root and La Crosse rivers, and a channel transition area south of the Onalaska dam. The node density was smaller than 98 ft (30 m) so to maintain an accurate representation of the areas. The node density for the entire mesh generally started at 98 ft (30 m) and propagated to the limit of the model domain where it finished at a maximum 295 ft (90 m).

3.2 Boundary Conditions

There are five inlets and three exits within the model boundary, which can be seen in Figure 3.7. Lock and Dam 7 gated spillway is the main inlet accompanied by a 1000 ft (305 m) concrete spillway known as French Island, and a 670 ft (204 m) concrete spillway referenced as Onalaska dam. There are two tributaries that flow into pool 8, the La Crosse and Root Rivers. La Crosse River enters the navigation channel on the south side of the city of La Crosse. The Root River enters the navigation channel on the west side of the pool north of Brownsville, Minnesota. Lock and Dam 8 gated spillway is the main exit in the model, while there are two overflow spillways to the west of the Lock and Dam 8. Reno and Hastings are both concrete overflow spillways that measure 937 and 1,337 ft (286 m and 408 m), respectively. Both Lock and Dam 7 and 8 are controlled by the United States Army Corps of Engineers. Lock and Dam 7, 8, French Island, Onalaska Dam, Reno spillway, and Hastings spillway flow conditions were all taken from historical data that are recorded by the Army Corps at two river gauges located within pool 8 (United State Army Corps of Engineers, 2011a). The two gauges can be seen in Figure 3.7. Flow conditions for the two tributaries, Root and La Crosse Rivers, were taken from historical records proved by the USGS (United States Geological Survey, 2010b). Flow over the overflow spillways was determined from using operation and rating curves along with correspondence with USGS personnel (Rogala, 2009-2011).

The steady state inlet and exit conditions were calculated using an average mass conservation method developed by (Young, 2006). The method looked at desired flow

through Lock and Dam 8, took a five percent range around the desired flow and recorded the corresponding dates during those flows. The flow through all the inlets were then recorded during the dates taken in the previous step, and then averaged. The flow over French Island Spillway and Onalaska Dam were taken from rating curves by using the pool elevation at Lock and Dam 7 during the previous recorded dates. Once the flows through each inlet were calculated based on historic data, the total flow through Lock and Dam 8 was recorded. A percent flow was calculated for each inlet, and then the final flow rates were calculated based on the percent compared to the desired flow. A simple flow chart of the process can be seen in Figure 3.8 along with an example of discharges for the 33,000 ft^3/s (934 m^3/s) flow scenario in Table 3.1.

3.3 Simulation Run Time

Each simulation was run until it was determined that the simulation reached a steady state. When using SRH-2D software, the user is able to implement the use of two water surface elevation (WSE) monitoring points. The first monitoring point was placed in the upper portion of the model near Lock and Dam 7, and the second point was placed in the lower pool at the same location of the USGS pool gauge within the model. SRH-2D outputs a visual graph of both monitoring points during the entire simulation. Once the WSE monitoring points and residual plots level off and become flat, the model is considered to have reached a steady state. In order to make sure the model has reached a steady state, the last output was subtracted from the previous output to compare the difference in water surface elevations. The mean difference between the last two outputs for the calibrated model was 3.28e-06 ft (0.000001 m) and had a standard deviation of 0.01 ft (0.0005 m). This small of a difference between the two outputs shows that the models reached a steady state.

3.4 Model Calibration

The numerical model was calibrated by modifying the Manning's roughness coefficient, a measure of bed friction resistance. A single roughness coefficient for perennially wet areas was selected based on values found in the primary literature (Chow, 1959). All other areas were assigned a coefficient based on land cover (United States Geological Survey, 2010b), values identified by other primary literature (Mays, 2005), and professional experience which established the base roughness coefficients. The base scenario of Manning's roughness values were systematically increased and decreased by two percent, ranging from two to twenty percent. Outliers of plus and minus 100 percent were also included in order to make sure all values were taken into account. Table 3.2 displays all the land cover types, their original values, and calibrated values.

The model was calibrated to a water surface elevation profile along the main channel that was obtained from LiDAR data. The LiDAR data was acquired from the USGS and conducted by the Sanborn Map Company. Flow conditions from the date of the LiDAR survey (November 6, 2007) were simulated for every set of roughness coefficients. The specific flows for the calibrations model can be seen in Table 3.3.

It has been found that when calibrating a two-dimensional model, lower flows are recommended for calibration so roughness can still influence the flow (Papanicolaou et al., 2010). This was held true for the current study since the model was calibrated during November with a flow of approximately 44,000 ft^3/s (1,246 m^3/s) exiting Lock and Dam 8.

A water surface elevation profile along the navigation channel was extracted from the LiDAR and compared to simulated profiles. Figure 3.9 displays the final calibration results. There was a mean difference between measured and simulated water surface elevations of 0.13 ft (0.04 m) and a standard deviation of 0.30 ft (0.09 m). The statistical results can be seen in Table 3.4.

SRH-2D also uses the turbulent eddy viscosity coefficient to calibrate the model, but is not recommended (Lai, 2009). The eddy viscosity coefficient, like the Manning's roughness value, is used in solving the governing 2D equations. Previously stated, the parabolic turbulence model was used for the current study based on recommendation from the code developer (Lai, 2009). The parabolic eddy viscosity coefficient is set to a value of 0.7 as the default by the model, but can range from 0.3 to one. Simulations were run using 0.3, 0.5, 0.7, 0.9, and one as the eddy viscosity coefficient for the parabolic model and were compared. It was determined from evaluating the WSE profiles that the eddy viscosity coefficient had very little effect on the calibrated WSE. Using the parabolic default value of 0.7, as the base condition, the mean difference and standard deviations were calculated and reported in Table 3.5.

3.5 Model Validation

The numerical model was validated using Real Time Kinematic (RTK) Global Navigation Satellite System (GNSS) measurements of the water surface elevation along the main navigation channel. Data collected by the USGS on June 4, 2010 were compared to simulated water surface elevations. Table 3.3 displays the validation flow conditions and Figure 3.10 displays the validation results. There was a mean difference of 0.03 ft (0.01 m) and a standard deviation of 0.13 ft (0.04 m) between the measured and simulated water surface elevations. The validation statistics can be seen in Table 3.4 There was a mean difference of 0.19 ft (0.06 m) found in the lower portion of the pool between the measured and simulated results. The difference was determined to be error in the collection of the field data. Personal correspondence with the USGS field crew that collected data reported a barge interrupted the data collection. The field crew explained they stopped data collection for the barge and continued data collection when the barge wake resided, which still could have affected the data collection. The boundary conditions at Lock and Dam 8 for the model matched the gauge reading set by the

USACE for the day the field data was collected. The four hour discharge data (Table 3.6) shows the discharge was steady throughout the day, with a decrease in discharge during the late afternoon and evening. This decrease during the afternoon could also have contributed to the difference in WSE profiles. It should also be noted that the exit elevation is set at the boundary of the model, while the data reported is at the mesh cell center, this can also be the cause of a small difference at the exit (Lai, 2009).

The numerical model was also validated using discharge and Acoustic Doppler Current Profile (ADCP) measurements across 17 transects within the pool, which can be seen in Figure 3.11 through Figure 3.15. The transect data was recorded by the USGS in the month of May 2010, between the days of the third and tenth. A comparison of the distribution of flow can be seen in Table 3.7. At each transect, simulated UMR discharges were within 16-percent of the measured discharges, within the navigation channel. Secondary channels and backwater areas were within 12-percent. The model was determined to accurately distribute the flow through the main navigation channel, secondary channels, backwater areas, and lower pool.

A majority of the discharge comparisons were within five percent, with the exception of a few sub transects. The higher percent differences could be attributed changes in the bathymetry along with errors in the bathymetry which have propagated during the years the DEM has been manipulated and applied to other applications.

A comparison of velocity magnitudes at each sub transect was also completed for validation of the model. Field velocity was scaled to match simulated velocity based on the percent difference of discharge through a transect. Figure 3.16 through Figure 3.24 are direct comparisons of the velocity magnitudes and when the data falls on the 45-degree line, the measured and simulated data are in perfect agreement. Through personal correspondence with the USGS field crew, some transects were full of vegetation and small areas made data collection difficult. Some transects tended to have measured and simulated data that did not agree well, which could have been due to difficult data

collection and bathymetry that has been altered over time. Coarse discretization within the mesh could also have affected simulated velocity magnitudes in small backwater channels, which could have skewed some transect comparisons. The transects that had the strongest agreement were located within the main channel.

The validation flow conditions were not vastly different from the calibration flow conditions. When a hydrodynamic model is validated, the validated flow conditions should vary from the calibrated flow conditions showing how the model can simulate diverse flow conditions. Since the pool is bounded by a lock and dam system, the flow is controlled, therefore resulting in a small difference between the validation and calibration flow conditions. The calibrated and validated flow conditions were collected between a three year span. By calibrating and validating to data that was collected three years apart, it displays the models ability to persist over time. The model was able to accurately simulate WSE profiles from two cases that were three years apart. The confidence in the model shows stakeholders that this hydrodynamic model will be useful for many future years.

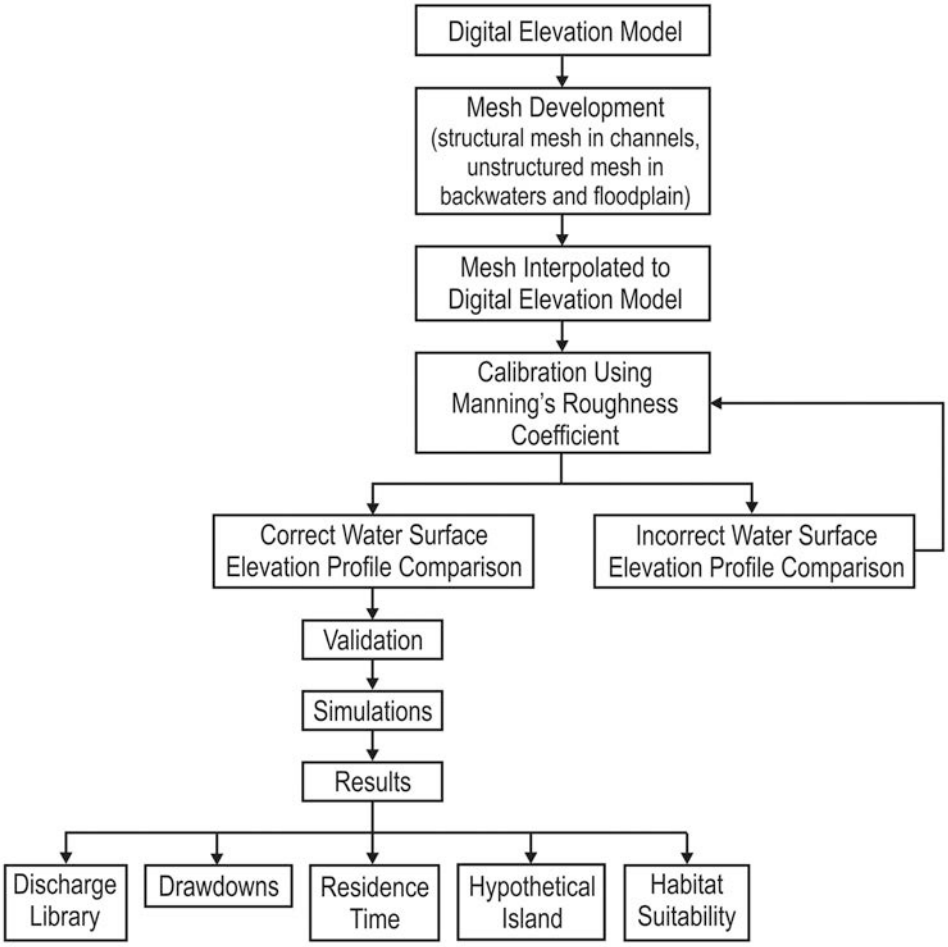

Figure 3.1. Flow diagram of numerical model development and processing.

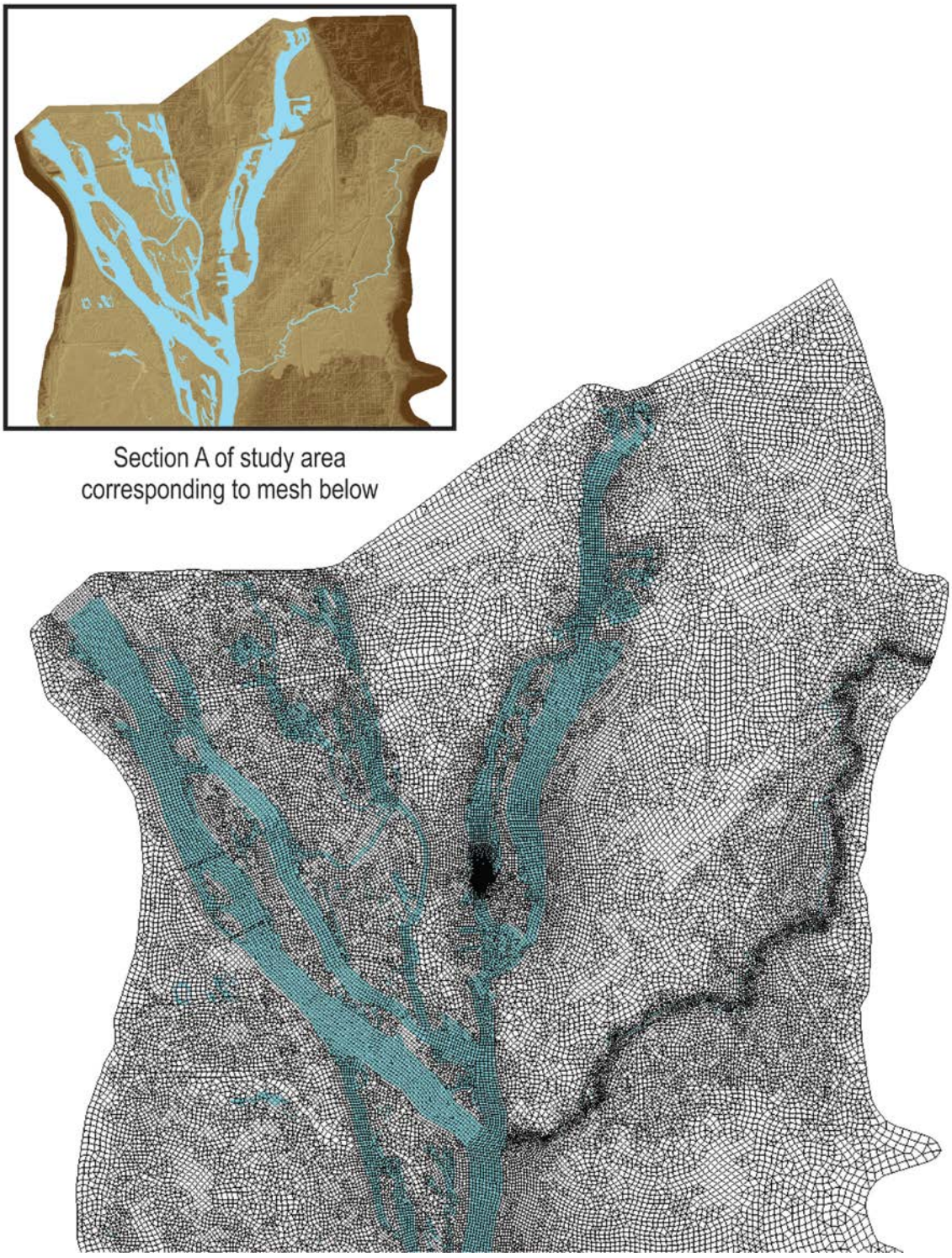

Figure 3.2. Upper portion of Pool 8 study area showing mesh density (section A) (Base Data Source: USGS, 2010b).

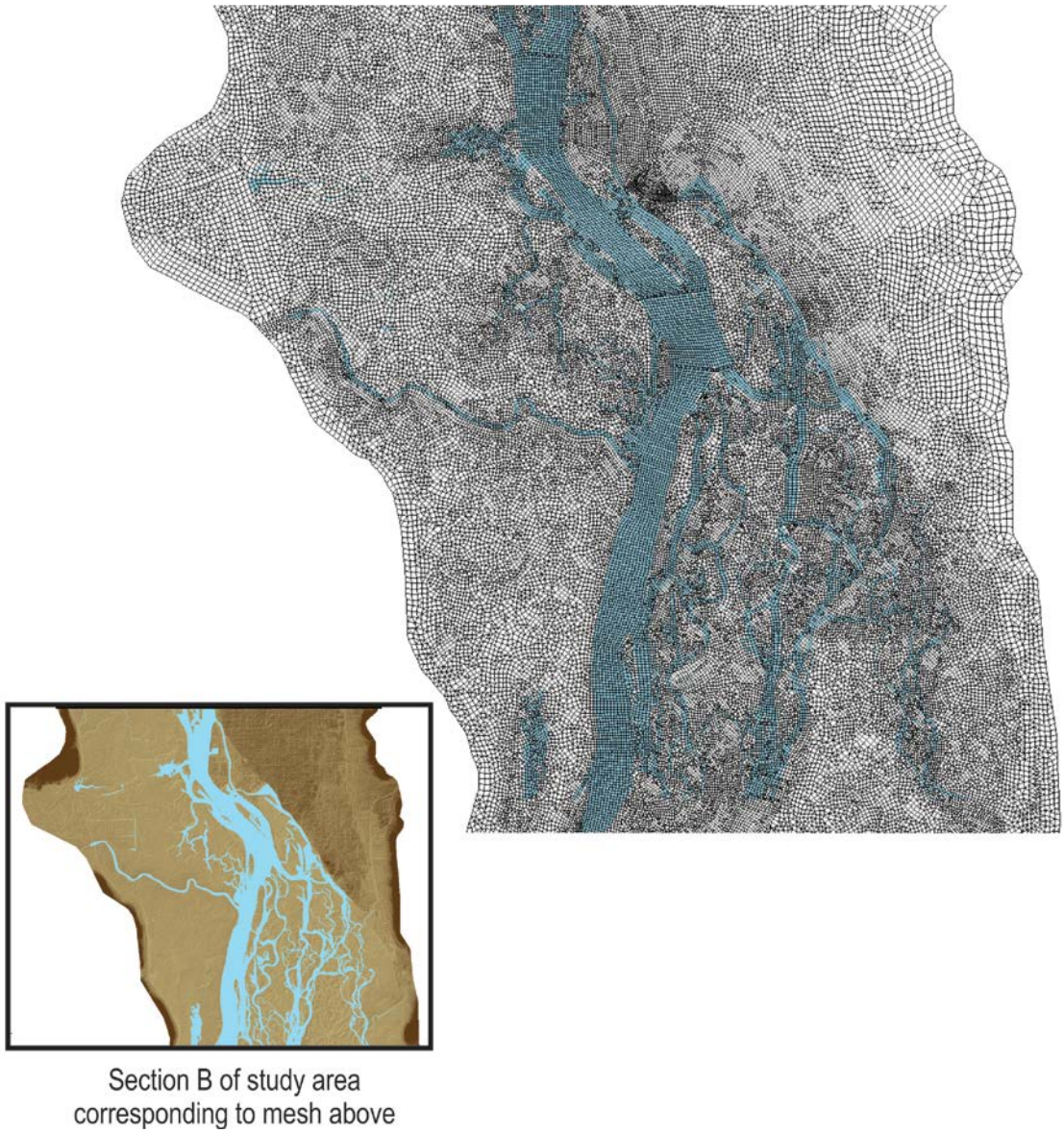

Figure 3.3. Middle upper portion of Pool 8 study area showing mesh density (Section B) (Base Data Source: USGS, 2010b).

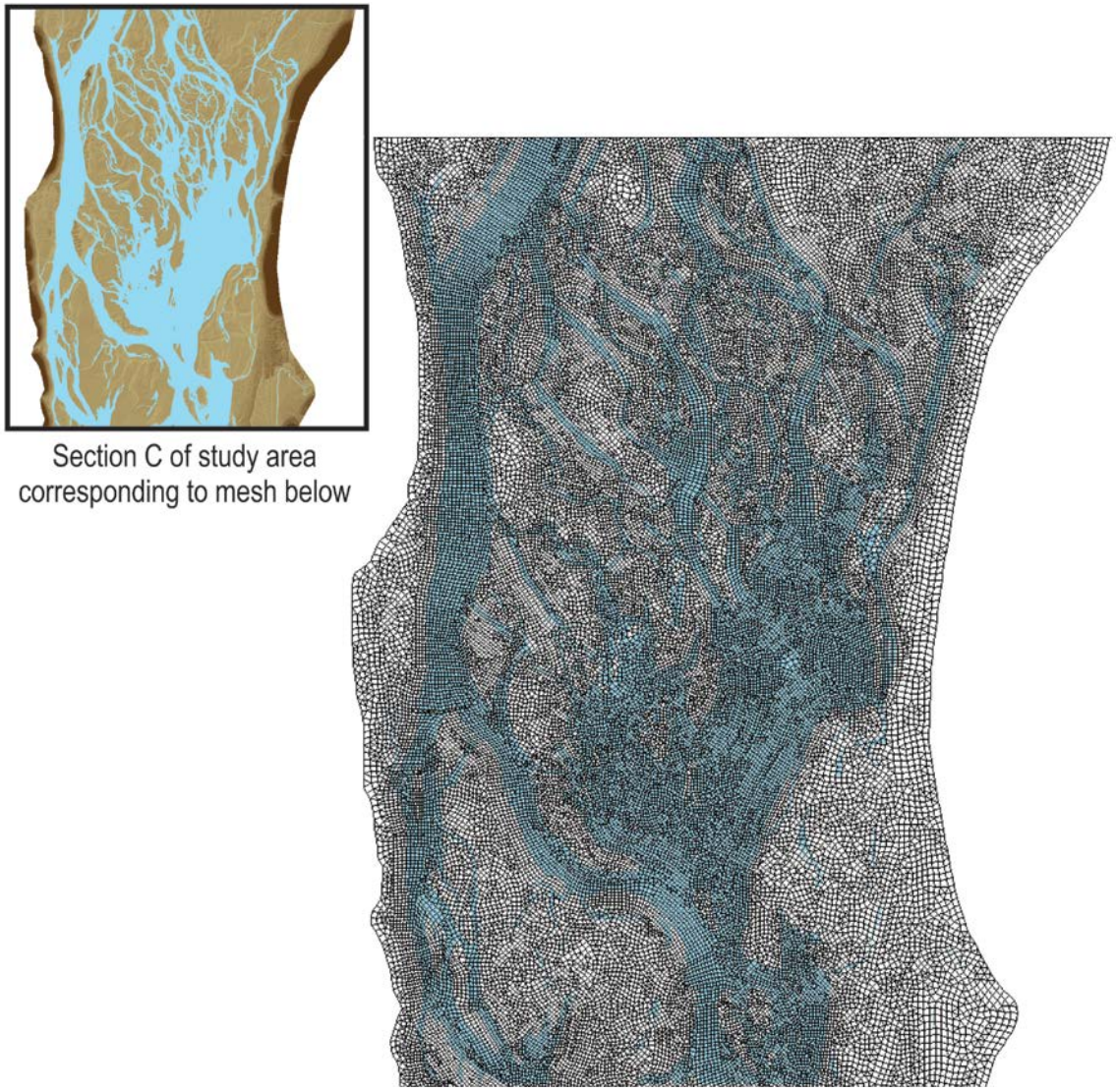

Figure 3.4. Middle lower portion of Pool 8 study area showing mesh density (Section C) (Base Data Source: USGS, 2010b).

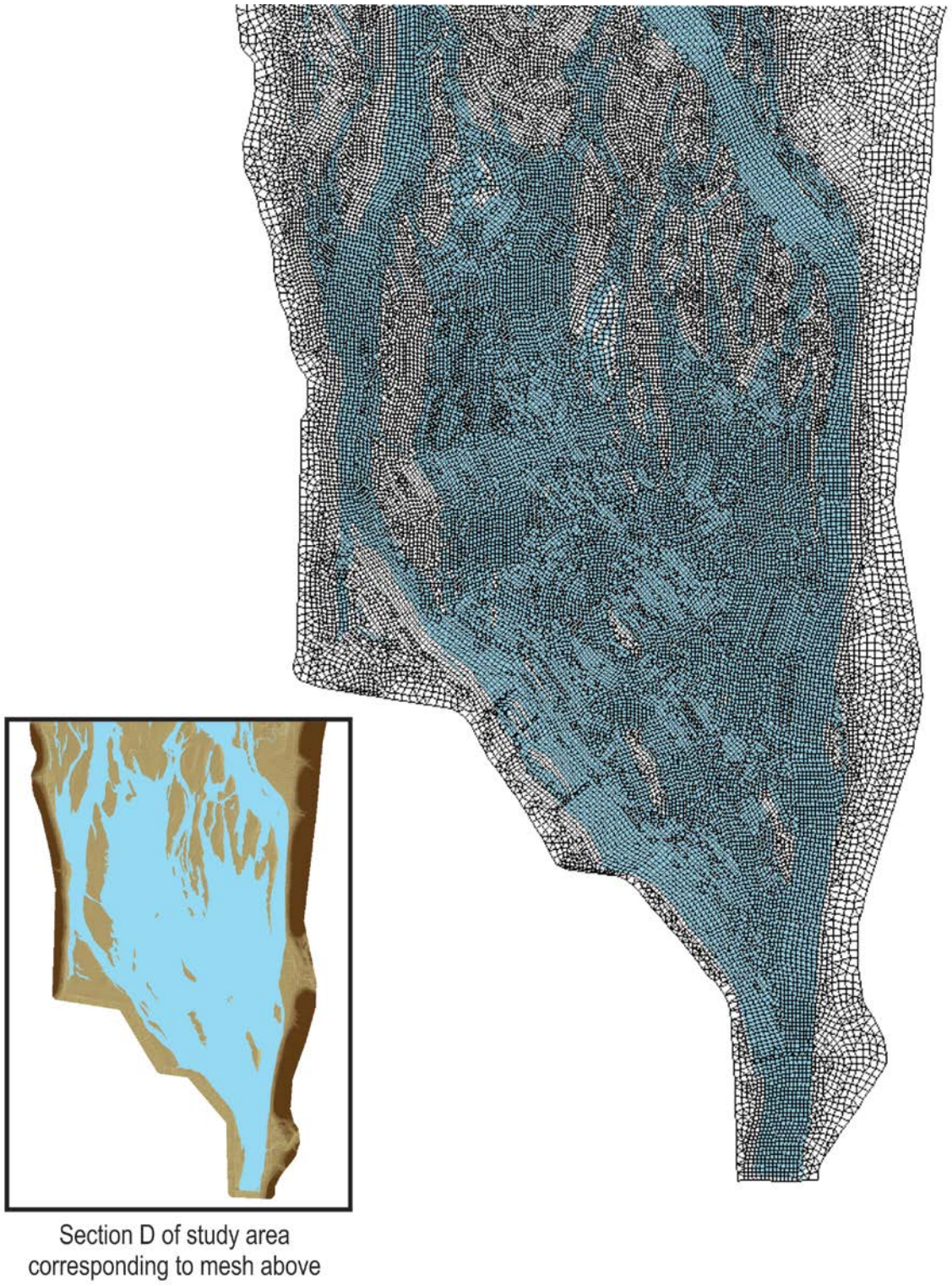

Figure 3.5. Lower portion of Pool 8 study area showing mesh density (Section D) (Base Data Source: USGS, 2010b).

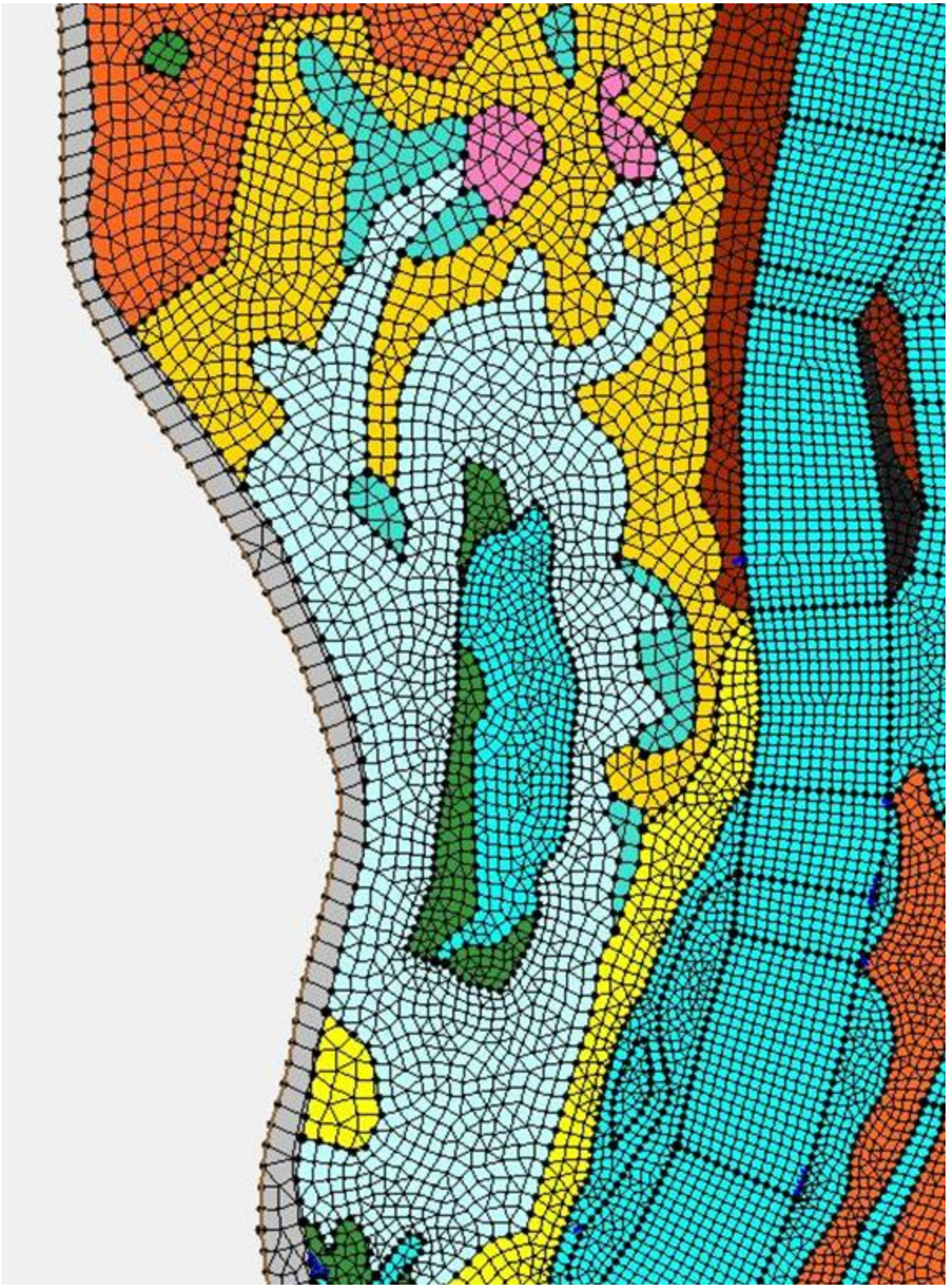

Figure 3.6. Zoomed in section of mesh displaying land cover polygons.

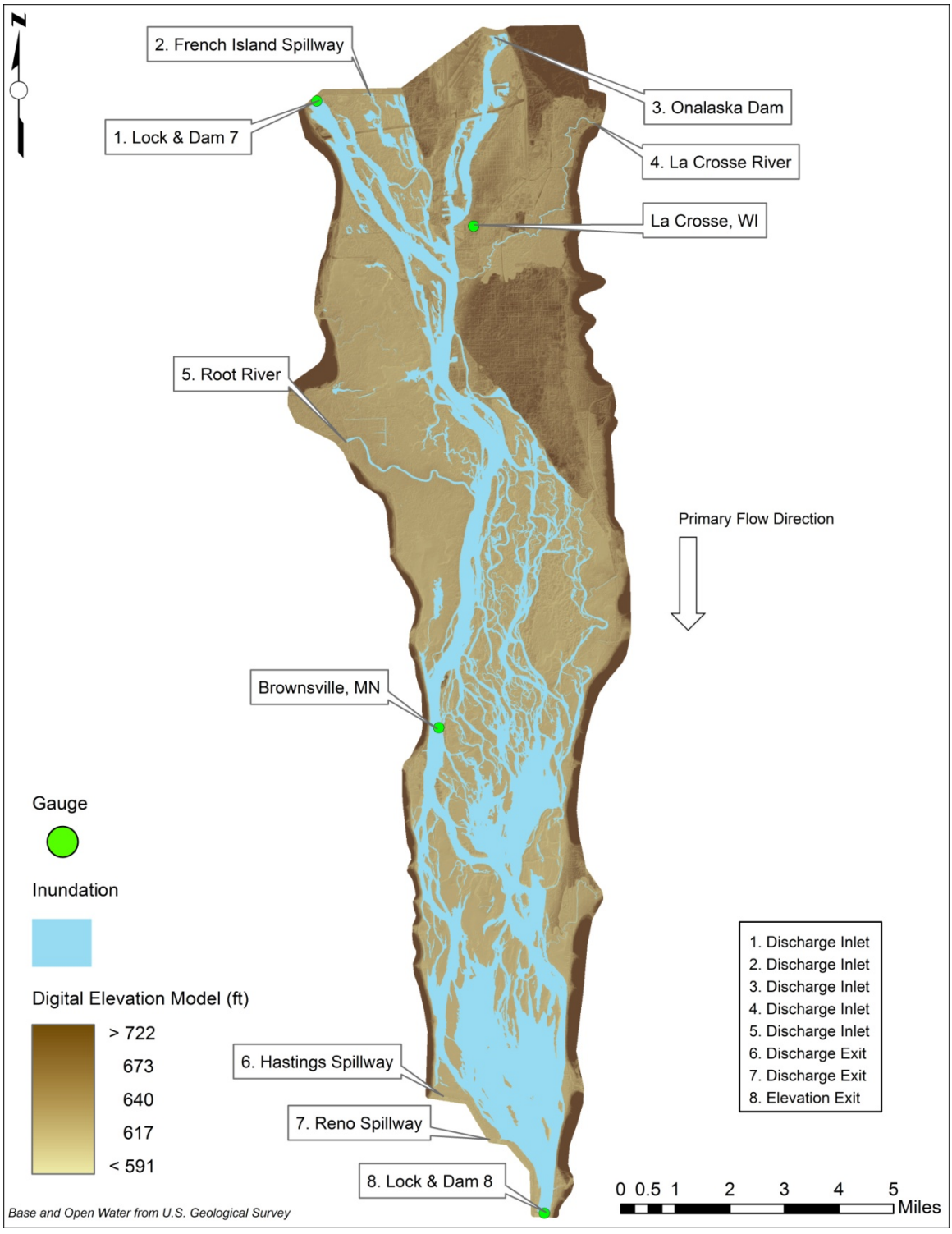

Figure 3.7. Aerial map of inlets, exits, and gauges within the model boundary (Data Source: USGS, 2010b). Data flooded by dark brown extends to elevation 1,178 feet and data flooded by light brown extends to elevation 561 feet.

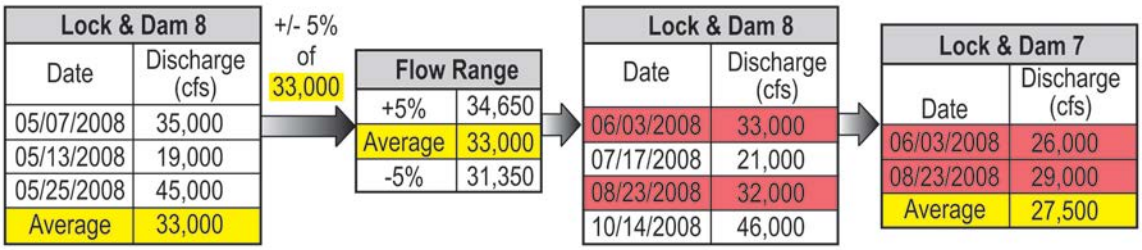

Figure 3.8. Basic flow chart example of inlet averaging calculations.

Table 3.1. Example of discharges for 33,000 ft^3/s flow case.

Boundary	Recorded Discharge (ft^3/s)	Percent of Total through Lock & Dam 8	Adjusted Discharge (ft^3/s)
1. Lock & Dam 7	30,128	89.76	29,754
2. French Island Spillway	1,333	3.97	1,316
3. Onalaska Dam	667	1.98	658
4. La Crosse River	382	1.13	377
5. Root Rover	1,053	3.13	1,040
Total Lock & Dam 8	33,564	100	33,148

Table 3.2. Manning's roughness coefficients.

Manning's Roughness Coefficients		
Land Cover Type	Original Base Values	Calibrated Values
open water	0.0300	0.0240
developed	0.1000	0.0800
roads	0.0130	0.0104
submerged vegetation	0.0300	0.0240
flood forest	0.0500	0.0400
wet meadows	0.0350	0.0280
agriculture	0.0350	0.0280
deep marsh annual	0.0350	0.0280
deep marsh perennial	0.0350	0.0280
grassland	0.0300	0.0240
lowland forest	0.0600	0.0480
populous common	0.0750	0.0600
root float vegetation	0.0600	0.0480
salix common	0.0350	0.0280
sand	0.0300	0.0240
shallow marsh	0.0350	0.0280
upland forest	0.0800	0.0640
misc.	0.0350	0.0280

Table 3.3. Calibration and validation flow rates through inlets and exits.

Calibration Flow Conditions		Validation Flow Conditions	
Inlet	Discharge (ft^3/s)	Inlet	Discharge (ft^3/s)
1. Lock and Dam 7	43,900	1. Lock and Dam 7	27,200
2. French Island Spillway	5,100	2. French Island Spillway	2,500
3. Onalaska Dam	3,200	3. Onalaska Dam	1,250
4. La Crosse	366	4. La Crosse River	313
5. Root River	1,210	5. Root River	622
Exit	Discharge (ft^3/s)	Exit	Discharge (ft^3/s)
6. Reno Spillway	0	6. Reno Spillway	0
7. Hastings Spillway	0	7. Hastings Spillway	0
Exit	Elevation (ft)	Exit	Elevation (ft)
8. Lock and Dam 8	629.53	8. Lock and Dam 8	629.45

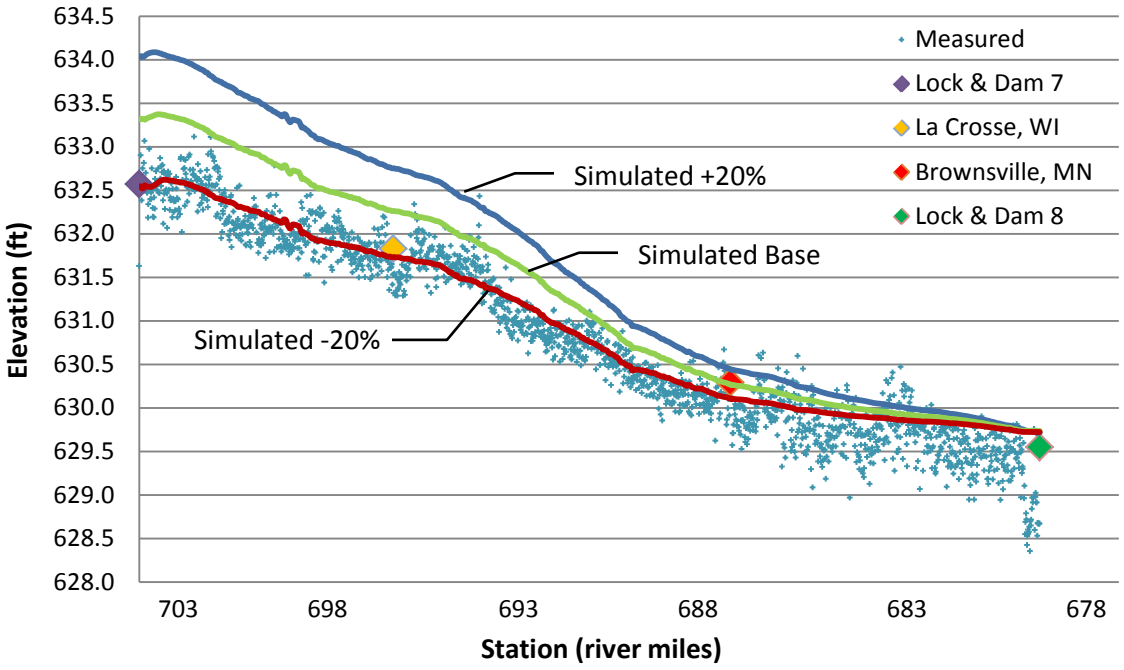

Figure 3.9. Calibration water surface elevation profile showing three calibration roughness value sets of decrease by 20%, base values, and increased by 20%; along with four gauge measurements from upstream to downstream Lock & Dam 7, La Crosse, WI, Brownsville, MN, and Lock & Dam 8.

Table 3.4. Calibration and validation statistics.

Calibration Statistics (ft)		Validation Statistics (ft)	
Mean Difference	0.12	Mean Difference	0.03
Minimum Difference	1.01	Minimum Difference	0.55
Maximum Difference	6.21	Maximum Difference	1.94
Standard Deviation	0.30	Standard Deviation	0.13

Table 3.5. Turbulent eddy viscosity sensitivity results.

Turbulent Eddy Viscosity Coefficient Comparison to Default Value (ft)		
Coefficient	Mean Difference	Standard Deviation
0.3	0.00164	0.00131
0.5	0.00066	0.00066
0.9	0.00098	0.00066
1	0.00131	0.00098

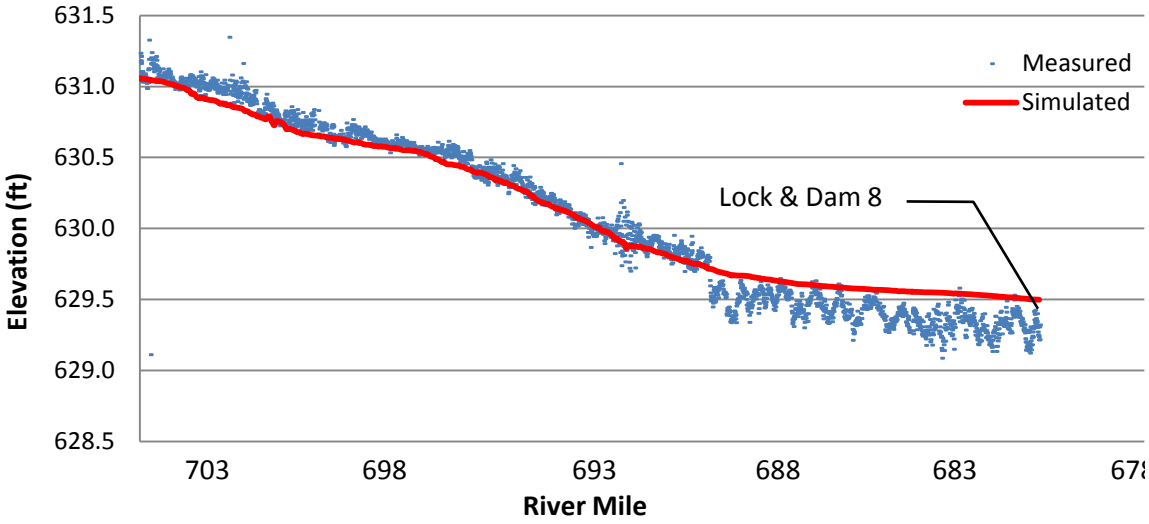

Figure 3.10. Validation water surface elevation profile.

Table 3.6. Four hour gauge data for Lock and Dam 8 during the day of June 4, 2010.

Time (hrs)	Discharge (ft^3/s)
0400	29,100
0800	29,100
1200	29,200
1600	29,500
2000	28,000
2400	27,900

Table 3.7. Validation discharge percent comparison.

				measured data			simulated data			% difference
river mile	transect	sub transect	date	Q (cfs)	total Q (cfs)	% total Q	Q (cfs)	total Q (cfs)	% total Q	% (simulated - field)
701.47	1	a*	5/3/2010	31196.0	33646.5	92.7	24183.0	25747.3	93.9	1.2
		b	5/3/2010	2450.5		7.3	1564.3		6.1	-1.2
700.58	2	a	5/3/2010	1709.7	33176.2	5.2	1483.5	25772.0	5.8	0.6
		b*	5/3/2010	27096.5		81.7	21642.4		84.0	2.3
		c	5/3/2010	4370.0		13.2	2646.0		10.3	-2.9
700.12	3	a*	5/4/2010	30495.8	35794.1	85.2	23296.7	27871.8	83.6	-1.6
		b	5/4/2010	4719.5		13.2	3304.0		11.9	-1.3
		c	5/4/2010	578.7		1.6	1271.0		4.6	2.9
698.74	4	a	5/4/2010	5021.1	35716.1	14.1	3117.9	32216.8	9.7	-4.4
		b*	5/4/2010	30695.0		85.9	29099.0		90.3	4.4
697.41	5	a	5/6/2010	5180.0	32478.1	15.9	3206.1	27728.9	11.6	-4.3
		b*	5/4/2010	27298.2		84.1	24522.8		88.4	4.3
696.79	6	a*	5/5/2010	30164.6	30909.7	97.6	29025.5	29204.7	99.4	1.8
		b	5/6/2010	745.0		2.4	179.2		0.6	-1.8
695.23	7	a*	5/5/2010	31296.0	33465.8	93.5	25489.9	27309.1	93.3	-0.2
		b	5/5/2010	2169.8		6.5	1819.2		6.7	0.2
693.97	8	a*	5/6/2010	24396.7	31702.7	77.0	24030.4	28204.1	85.2	8.2
		b	5/6/2010	1039.9		3.3	454.3		1.6	-1.7
		c	5/6/2010	357.0		1.1	3.7		0.0	-1.1
		d	5/6/2010	3739.3		11.8	3020.2		10.7	-1.1
		e	5/6/2010	2169.8		6.8	695.5		2.5	-4.4
693.37	9	a*	5/6/2010	24496.7	32718.6	74.9	24549.2	26924.7	91.2	16.3
		b	5/6/2010	1109.8		3.4	459.7		1.7	-1.7
		c	5/6/2010	418.8		1.3	2.8		0.0	-1.3
		d	5/6/2010	811.8		2.5	11.9		0.0	-2.4
		e	5/6/2010	48.0		0.1	0.0		0.0	-0.1
		f	5/6/2010	1569.9		4.8	943.5		3.5	-1.3
		g	5/6/2010	359.1		1.1	3.3		0.0	-1.1
		h	5/6/2010	540.2		1.7	132.2		0.5	-1.2
		i	5/6/2010	294.8		0.9	140.2		0.5	-0.4
		j	5/6/2010	3069.5		9.4	681.9		2.5	-6.8
692.54	10	a*	5/7/2010	23597.0	32193.9	73.2	22949.1	29268.2	78.4	5.3
		b	5/7/2010	2049.7		6.4	2279.3		7.8	1.4
		c	5/8/2010	117.9		0.4	188.7		0.6	0.3
		d	5/7/2010	1060.0		3.3	695.5		2.4	-0.9
		e	5/8/2010	3239.7		10.0	2065.8		7.1	-3.0
		f	5/7/2010	2129.5		6.6	1089.9		3.7	-2.9
691.42	11	a	5/7/2010	377.1	32713.7	1.2	7.9	27708.6	0.0	-1.1
		b*	5/7/2010	23696.9		72.4	22937.9		82.8	10.3
		c	5/7/2010	1749.6		5.3	906.2		3.3	-2.1
		d	5/8/2010	1329.8		4.1	334.7		1.2	-2.9
		e	5/7/2010	5179.3		15.8	3397.8		12.3	-3.6
		f	5/7/2010	381.0		1.2	124.1		0.4	-0.7
688.71	12	a*	5/8/2010	18971.4	31946.7	59.4	16804.7	26960.8	62.3	2.9
		b	5/8/2010	489.0		1.5	652.9		2.4	0.9
		c	5/8/2010	12486.3		39.1	9503.2		35.2	-3.8
687.23	13	a	5/8/2010	6839.2	33535.7	20.4	6582.5	27524.7	23.9	3.5
		b*	5/8/2010	10298.5		30.7	8532.4		31.0	0.3
		c	5/8/2010	16398.0		48.9	12409.7		45.1	-3.8
685.56	14	a	5/9/2010	5377.7	32358.1	16.6	3425.1	22037.0	15.5	-1.1
		b	5/9/2010	1380.6		4.3	688.5		3.1	-1.2
		c*	5/9/2010	18597.8		57.5	12051.3		54.7	-2.8
		d	5/9/2010	1691.3		5.2	1211.1		5.5	0.3
		e	5/9/2010	5310.6		16.4	4660.9		21.1	4.7
682.79	15	a	5/9/2010	3806.4	32382.8	17.4	3788.8	29452.1	19.0	1.6
		b	5/9/2010	879.2		2.5	1571.3		5.0	2.5
		c	5/9/2010	14699.6		42.5	17559.7		55.4	12.9
		d*	5/9/2010	12997.6		37.6	6532.4		20.6	-17.0
681.25	16	a	5/10/2010	9438.4	35536.0	26.6	8636.8	30935.1	27.9	1.3
		b*	5/10/2010	26097.6		73.4	22298.3		72.1	-1.3
680.36	17	a	5/10/2010	34177.6	34177.6	100.0	30970.6	30970.6	100.0	0.0

*Indicates that the navigation channel is within that specific transect.

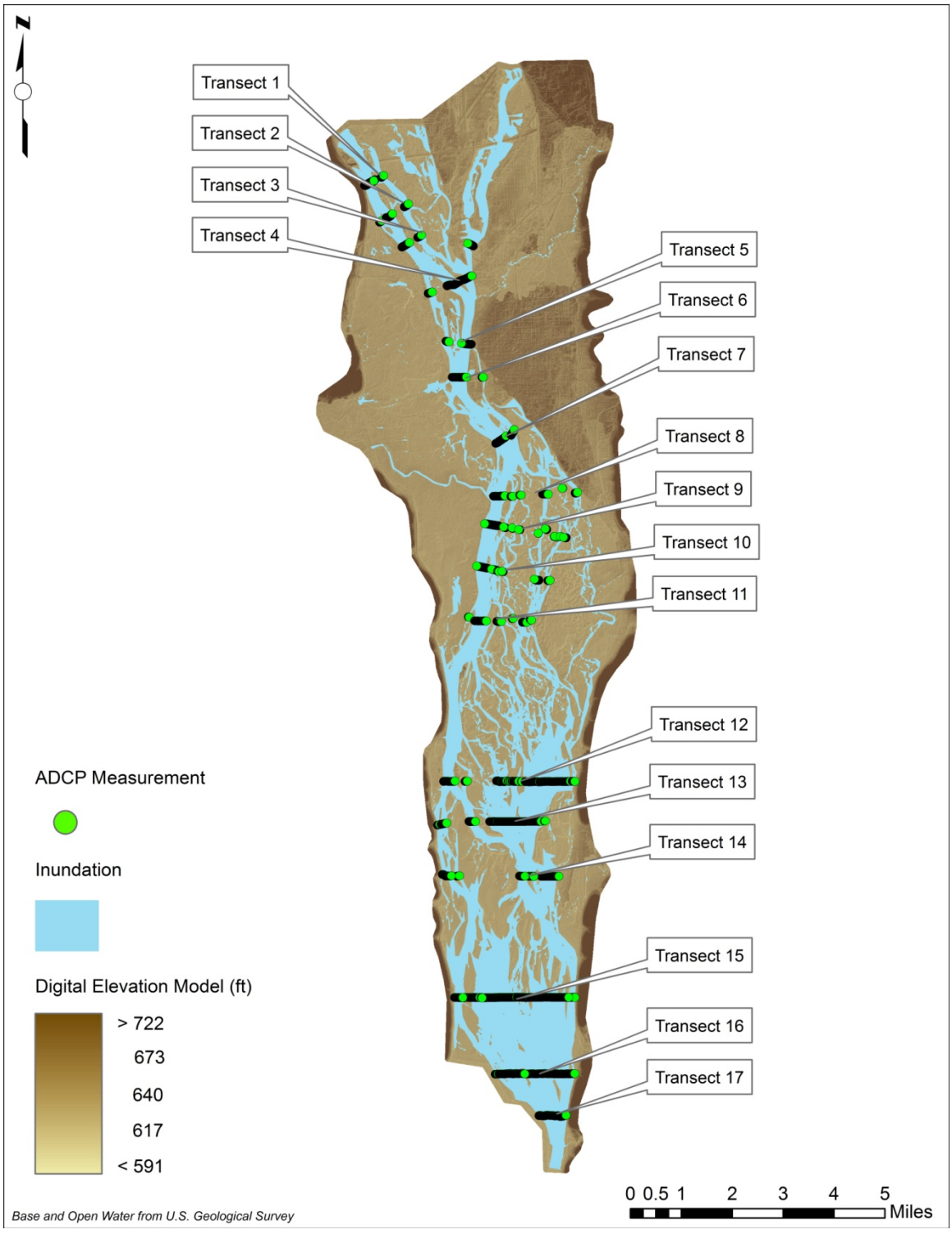

Figure 3.11. 17 ADCP transects collected by the USGS in June of 2010 in pool 8 (Data Source: USGS, 2010b). Data flooded by dark brown extends to elevation 1,178 feet and data flooded by light brown extends to elevation 561 feet.

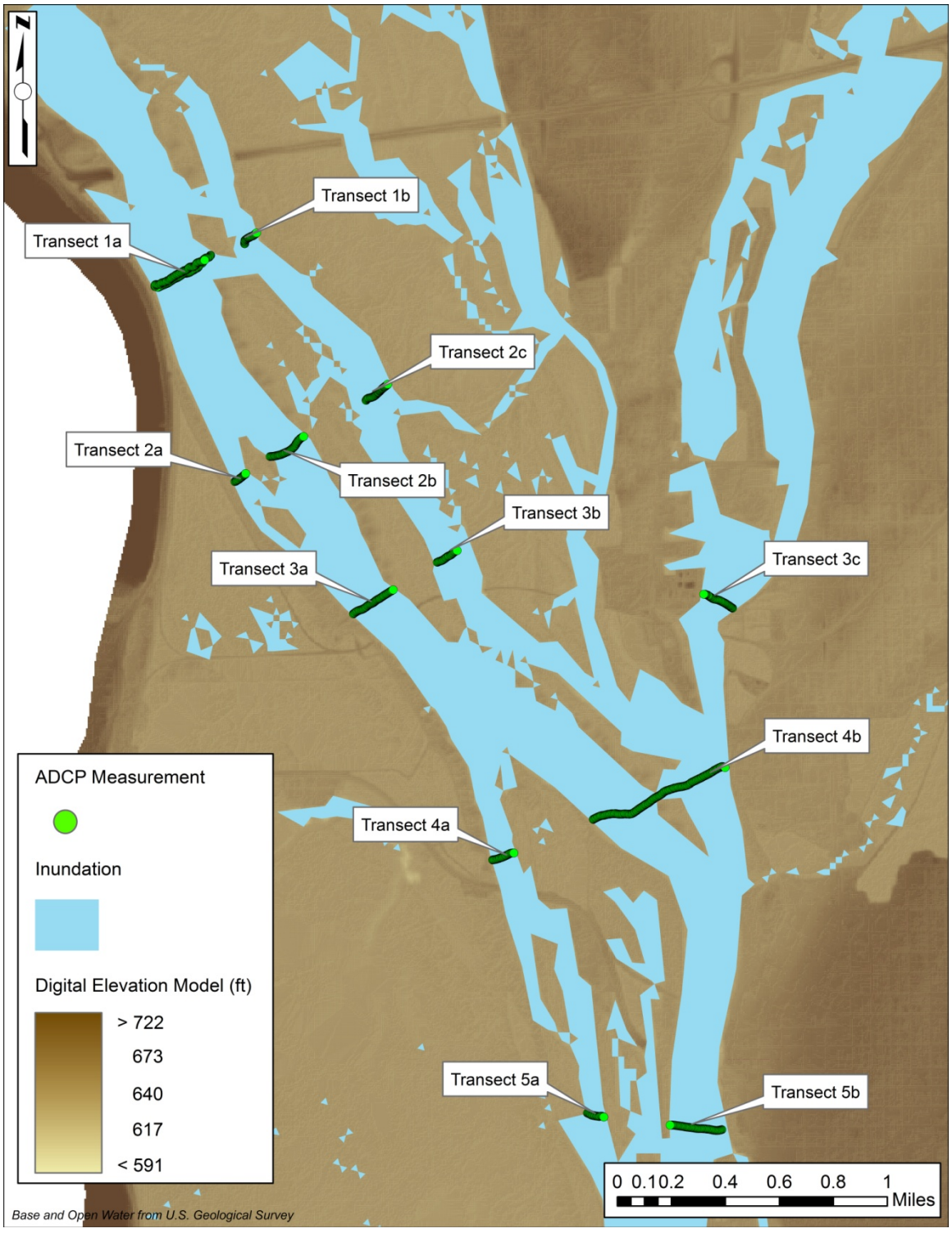

Figure 3.12. ADCP transects 1 through 5 showing location of sub transects (Data Source: USGS, 2010b). Data flooded by dark brown extends to elevation 1,178 feet and data flooded by light brown extends to elevation 561 feet.

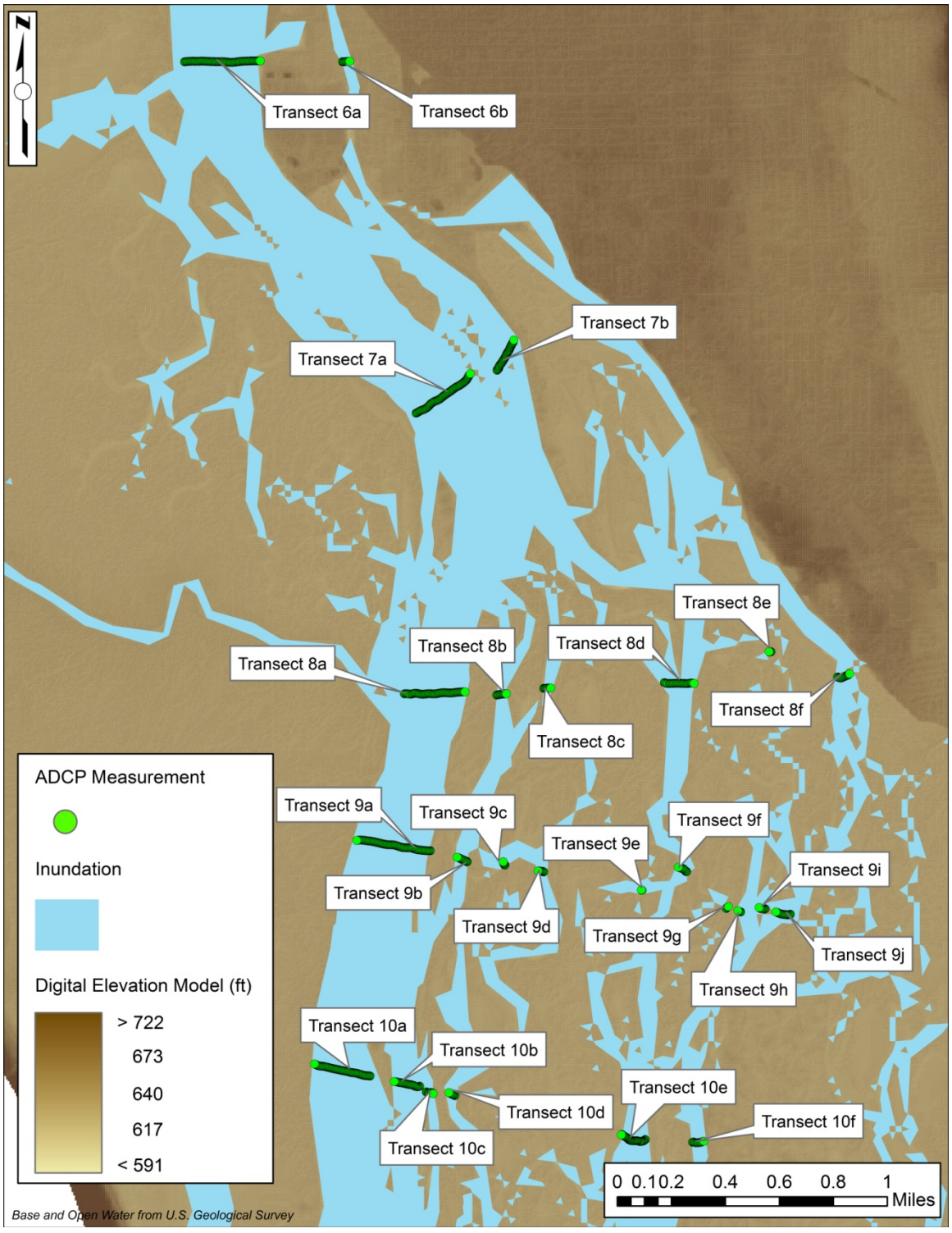

Figure 3.13. ADCP transects 6 through 10 showing location of sub transects (Data Source: USGS, 2010b). Data flooded by dark brown extends to elevation 1,178 feet and data flooded by light brown extends to elevation 561 feet.

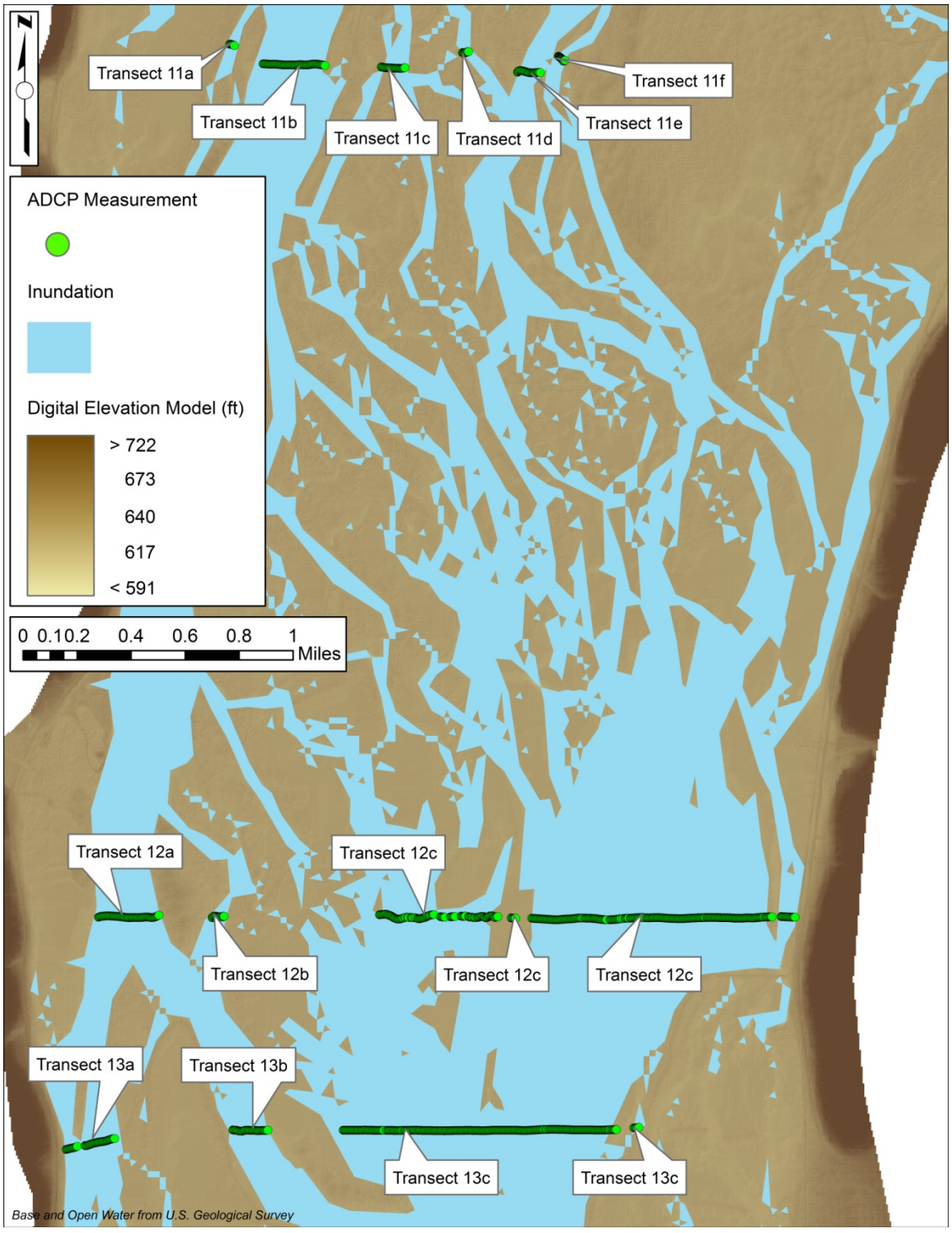

Figure 3.14. ADCP transects 11 through 13 showing location of sub transects (Data Source: USGS, 2010b). Data flooded by dark brown extends to elevation 1,178 feet and data flooded by light brown extends to elevation 561 feet.

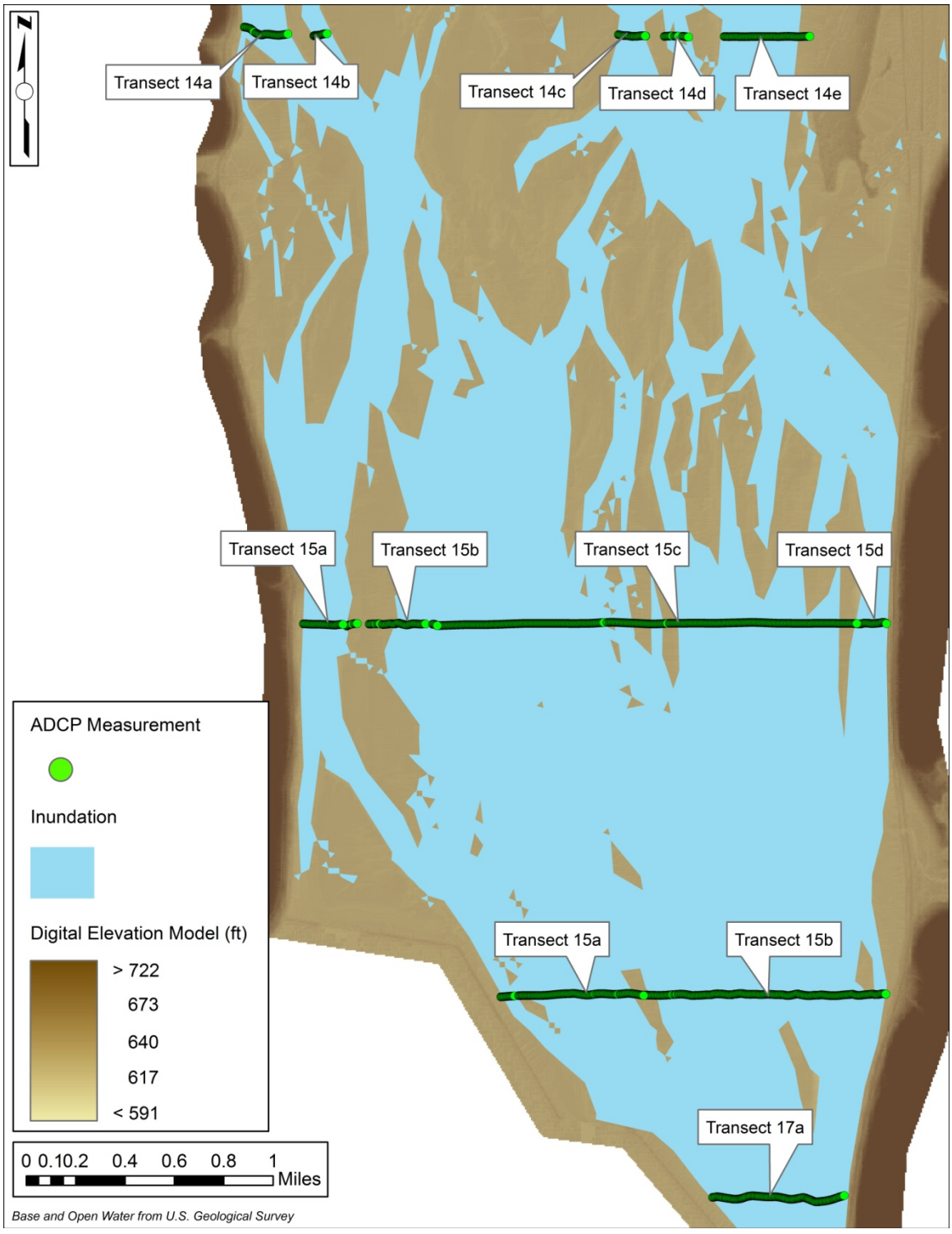

Figure 3.15. ADCP transects 14 through 17 showing location of sub transects (Data Source: USGS, 2010b). Data flooded by dark brown extends to elevation 1,178 feet and data flooded by light brown extends to elevation 561 feet.

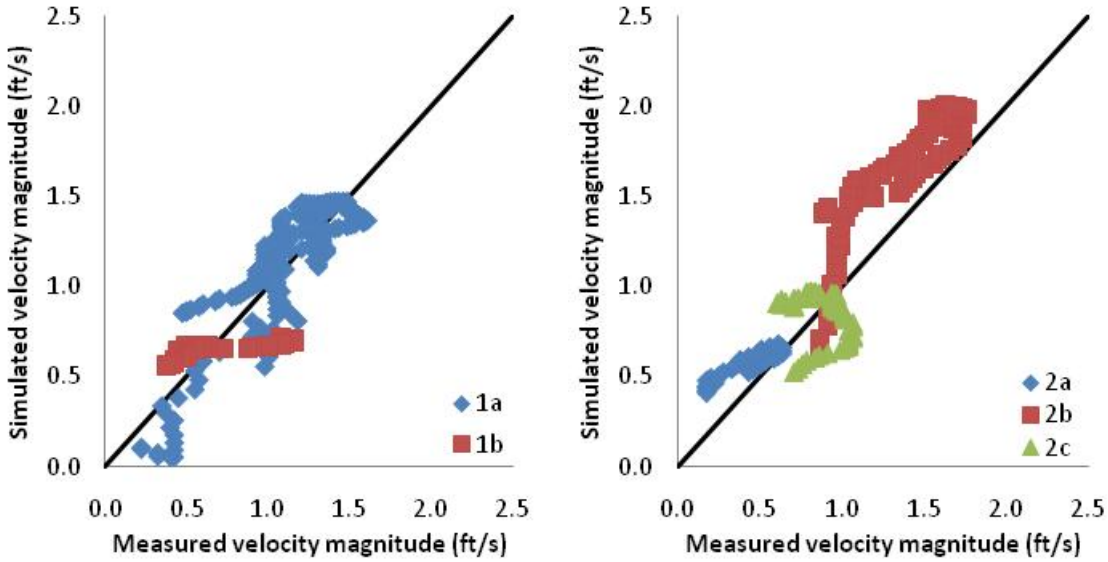

Figure 3.16. Comparison of measured and simulated velocity magnitudes at river miles 701.5 (left) and 700.6 (right).

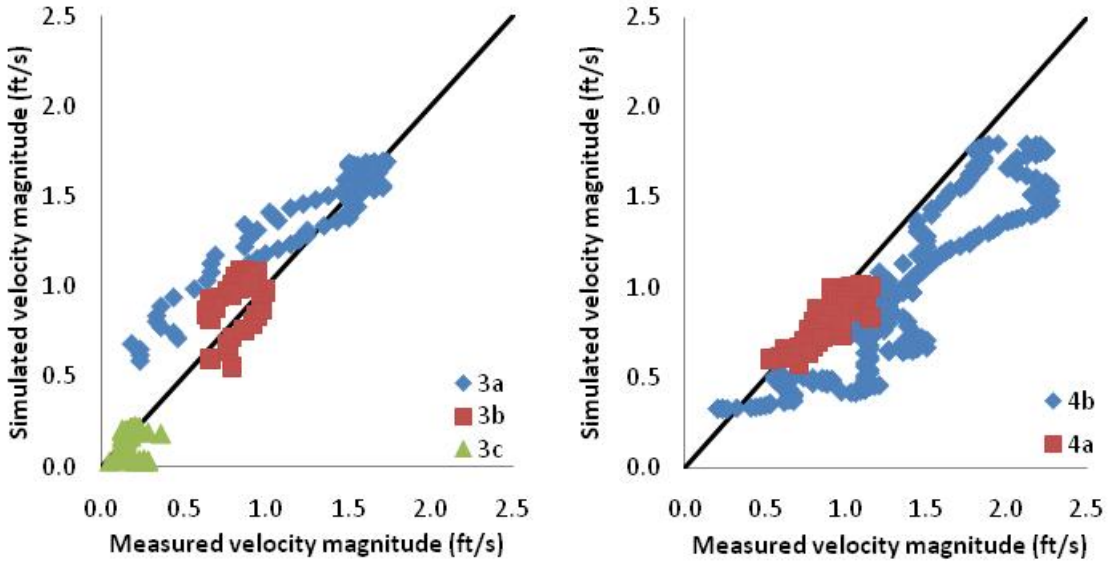

Figure 3.17. Comparison of measured and simulated velocity magnitudes at river miles 700.1 (left) and 698.7 (right).

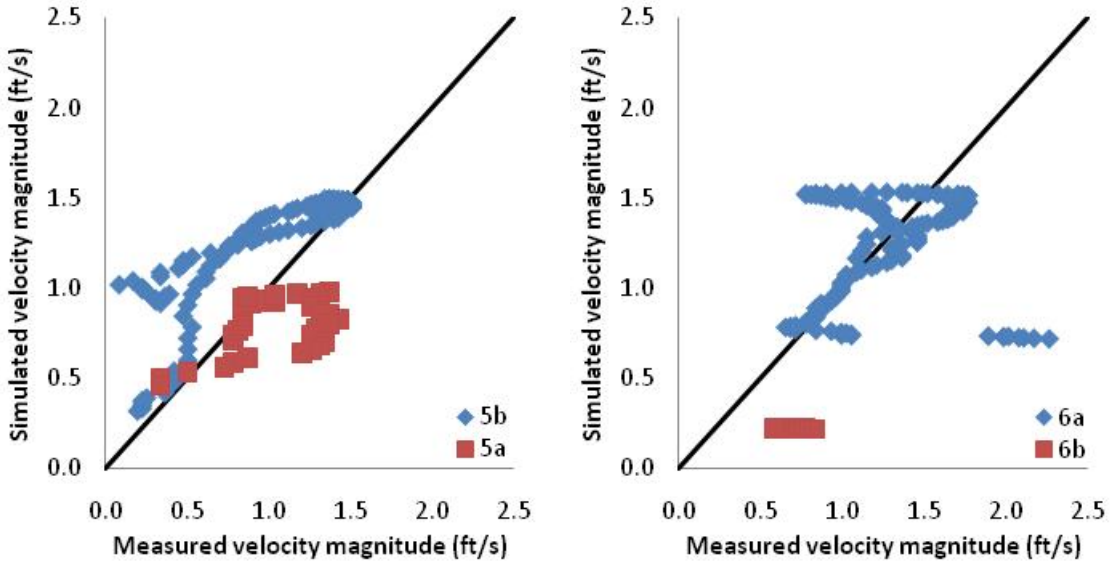

Figure 3.18. Comparison of measured and simulated velocity magnitudes at river miles 697.4 (left) and 696.8 (right).

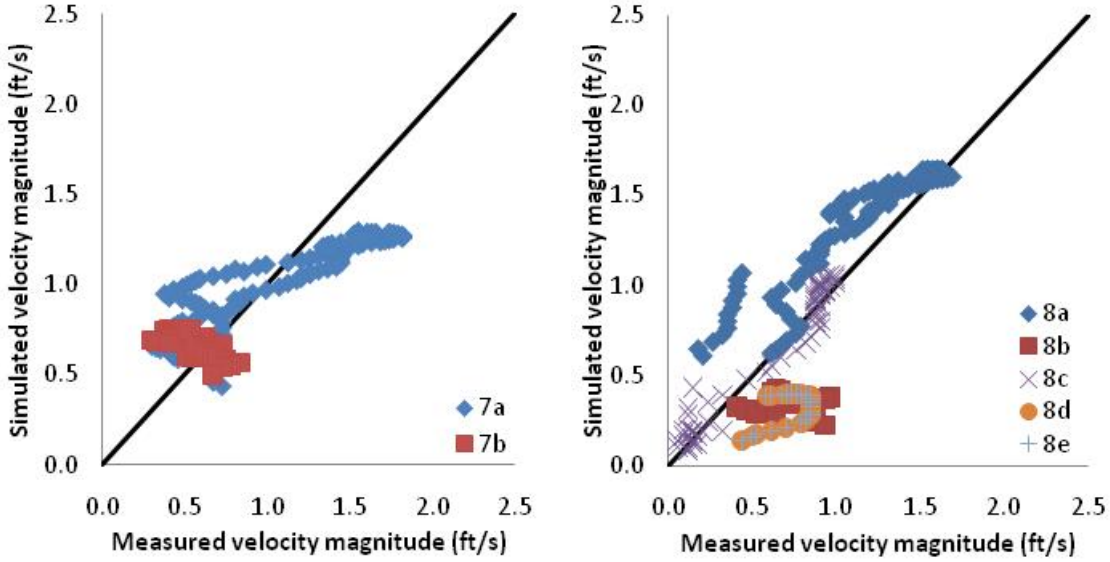

Figure 3.19. Comparison of measured and simulated velocity magnitudes at river miles 695.2 (left) and 693.9 (right).

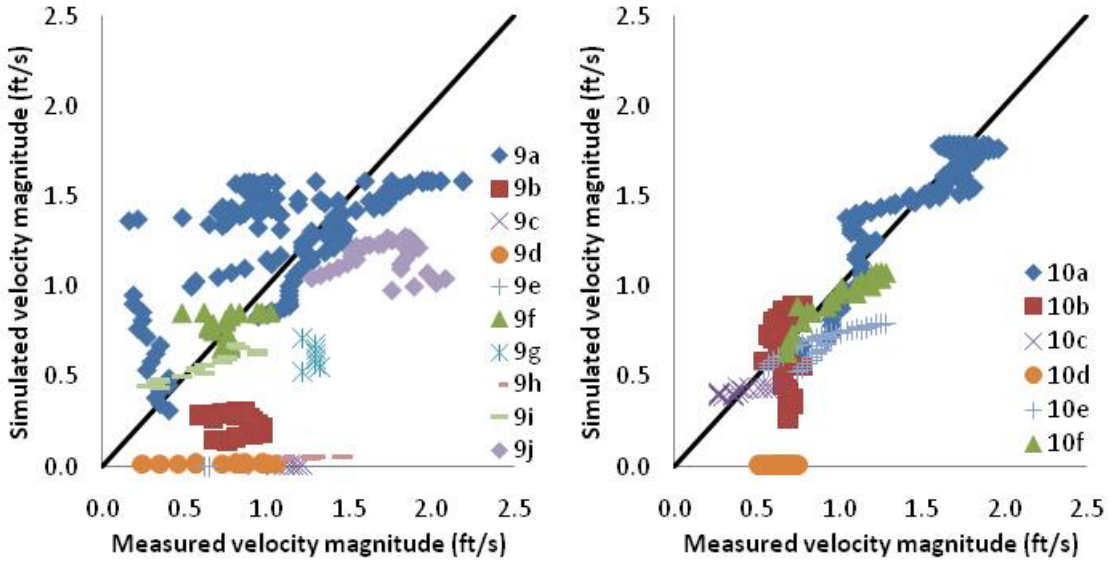

Figure 3.20. Comparison of measured and simulated velocity magnitudes at river miles 693.3 (left) and 692.5 (right).

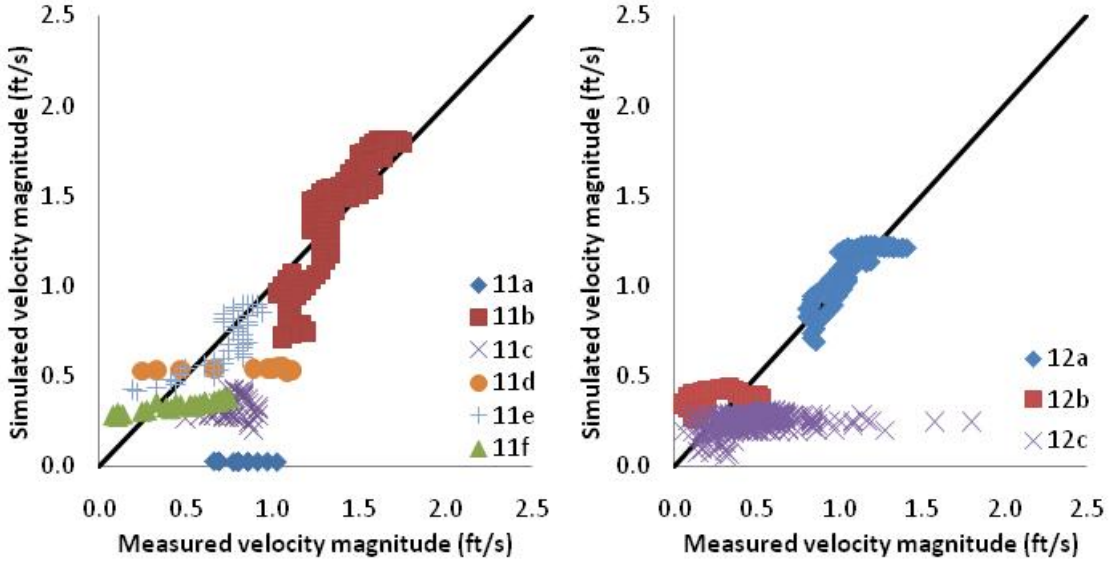

Figure 3.21. Comparison of measured and simulated velocity magnitudes at river miles 691.4 (left) and 688.7 (right).

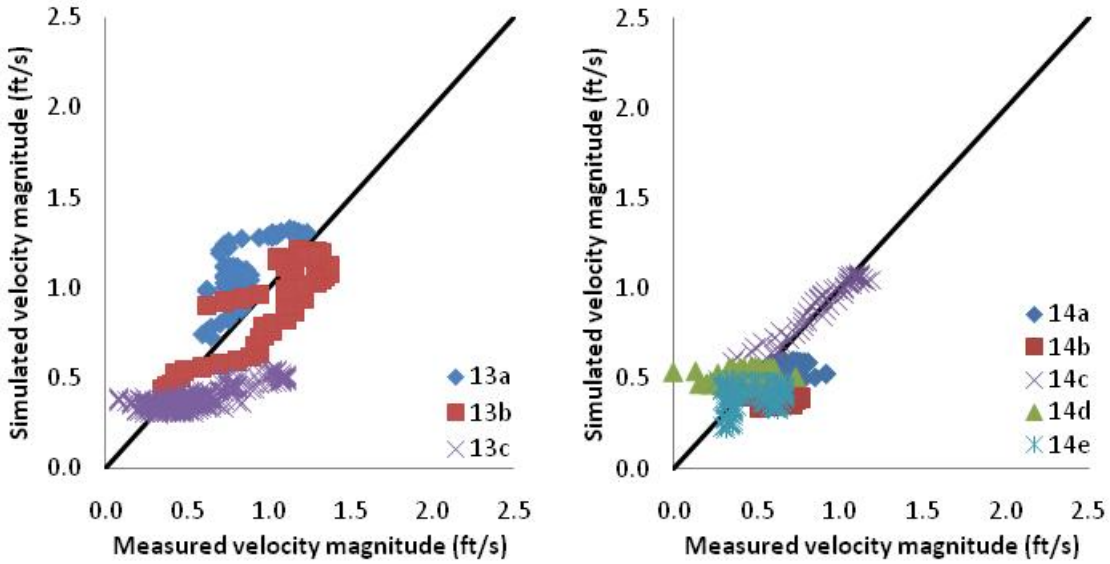

Figure 3.22. Comparison of measured and simulated velocity magnitudes at river miles 687.2 (left) and 685.6 (right).

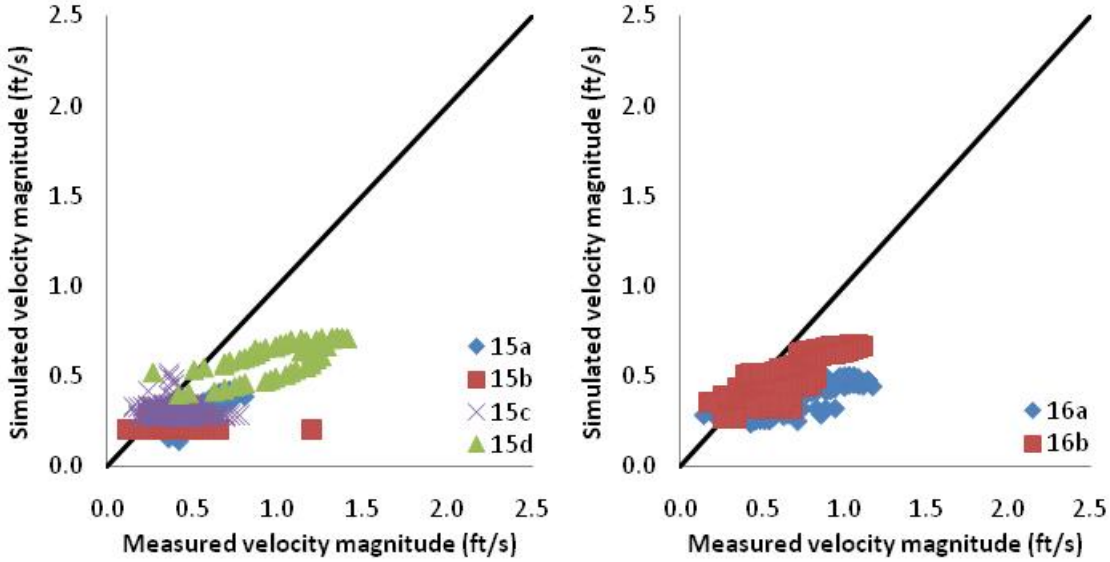

Figure 3.23. Comparison of measured and simulated velocity magnitudes at river miles 682.8 (left) and 681.3 (right).

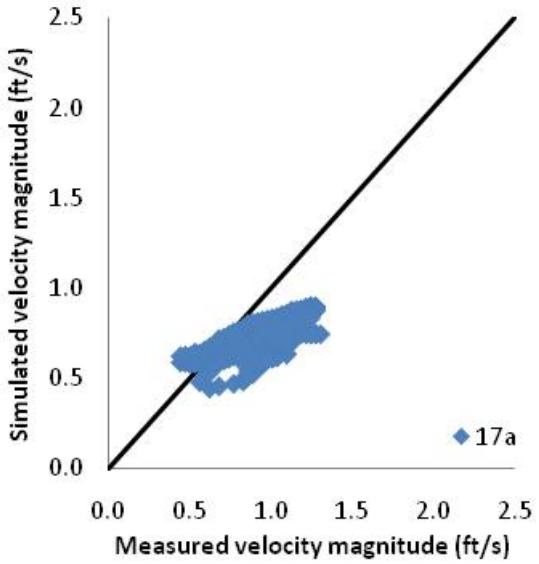

Figure 3.24. Comparison of simulated and measured velocity magnitudes at river mile 680.4.

CHAPTER 4: MODEL APPLICATION

4.1 Overview

The calibrated and validated model was utilized for a range of discharges, drawdown conditions, hypothetical island scenarios, travel time studies, and habitat suitability assessments. There were ten steady state flow scenarios simulated with the model starting at 10,000 ft^3/s (283 m^3/s) and reaching 100,000 ft^3/s (2,832 m^3/s) increasing by 10,000 ft^3/s (283 m^3/s) each time. Two steady state drawdown conditions of one and two feet (0.3 m and 0.6 m) during three flow scenarios were also modeled. A hypothetical island was placed in the lower portion of the pool in order to divert flow around the island and create an area of reduced velocities in deep water behind the island. Travel times were assessed for three flow scenarios along with a stream trace study. A habitat suitability assessment was completed for emergent vegetation within the pool using five different flow conditions.

4.2 Steady State Simulations

Numerous steady state flow scenarios were simulated with the model. Based on correspondence with USGS personnel; low, medium, and high flow rates were chosen as base flow rates. These flow rates were 10,000 ft^3/s, 33,000 ft^3/s and 90,000 ft^3/s (283 m^3/s, 934 m^3/s, and 2,549 m^3/s). Continued correspondences with USGS personnel and in collaboration with the University of Illinois, the range of flow scenarios were from 10,000 ft^3/s (283 m^3/s) to 100,000 ft^3/s (2,832 m^3/s) incrementing by 10,000 ft^3/s (283 m^3/s). The ten steady state discharges fall evenly on the flow duration curve (Figure 4.1), demonstrating the diversity of the simulated discharges. The steady state discharges were accompanied by the calibration, validation, and drawdown simulations that created the library of flow scenarios. By creating a library of flow scenarios that encompass the entire flow duration curve through Lock and Dam 8, biologists and river managers can make accurate predictions and help avoid unwanted outcomes in the river.

4.2.1 Depth and Velocity Histograms

Selecting three flow scenarios from the steady state library, velocity and depth histograms were created in order to understand their distribution around the pool. Based on correspondence with the USGS, 10,000 ft^3/s, 33,000 ft^3/s, and 100,000 ft^3/s (set A) (283 m^3/s, 934 m^3/s, and 2,832 m^3/s) flow scenarios were used to create the histograms. Code written in MATLAB took depth and velocity data from a single simulation and placed the data into a matrix. Bins were then created and utilized the matrix in order to create a plot of depth, velocity, and occurrence. Depth and velocity histograms for set A can be seen in Figure 4.2.

The figure shows how depth and velocity increase as discharge increases. At 10,000 ft^3/s (283 m^3/s) there is a high occurrence at a depth of approximately 4.0 ft (1.2 m) and at a velocity of approximately 5.5 ft/s (1.7 m/s). This dark red cluster on the 10,000 ft^3/s (283 m^3/s) plot represents occurrences in the main channel near the banks. Above the dark red cluster, there is a pyramid shape that extends to approximately 9.0 feet (2.7 m). The nine-foot mark is the navigation channel. It is apparent from the 10,000 ft^3/s (283 m^3/s) plot that a majority of the flow is in the main channel and, the rest occurs in the side channel and backwater areas. Moving to the 33,000 ft^3/s (934 m^3/s) plot, the dark red cluster starts to extend to the left side of the plot, indicating that there is an increase in side channel activity. To the left and below the dark red cluster, the occurrence becomes somewhat greater, showing an increase in velocity in the backwater and impounded areas due to the higher discharge. Focusing on the 100,000 ft^3/s (2,832 m^3/s) plot, the dark red cluster moves up and to the right on the plot. Due to the higher discharge, there is more activity in the side channel, backwater, and impounded areas which makes the red cluster decrease. From the three plots in Figure 4.2, it can be seen how a majority of the flow is in the main channel and as discharge increases, there is more activity in the secondary channels, backwater and impounded areas. The subtle changes between the flow rates that encompass the entire flow duration curve are due to

the control from the lock and dam system. The pool is controlled in order to maintain navigation conditions during all flow scenarios, which is efficiently done because there are such small changes in depth and velocity over a large range of flow scenarios.

In order to fully understand the depth and velocity histograms (Figure 4.2), velocity histograms were created (Figure 4.3 through Figure 4.5). Velocity histograms were extracted at four depths 2.6 ft, 5.2 ft, 7.8 ft, and 10.4 ft (0.8 m, 1.6 m, 2.4 m, and 3.2 m). The velocity histograms help visualize the distribution of velocity at certain depths and how the lock and dam system controls the pool. The histograms show at a depth of 7.8 ft and 10.4 ft (2.4 m and 3.2 m), the velocities are fairly consistent at 10,000 ft^3/s and 33,000 ft^3/s (283 m^3/s and 934 m^3/s). When the discharge reaches 100,000 ft^3/s (2,832 m^3/s) the velocities magnitudes slightly increase, with a greater increase in occurrence. These trends show that as discharge increases, velocity and depth will also increase. The rate at which depth and velocity increase is not dramatic due to the control the lock and dam system has over the pool.

4.3. Hypothetical Drawdowns

The Upper Mississippi River has been modified in the past years for navigation. By creating a stable, high water level within the river for navigation purposes, it has had negative ecological impacts on the river. The high water levels have resulted in nutrient and sediment becoming trapped in back water areas, erosion of islands in the lower portion of pool, and reduction in habitat diversity and quality (Water Level Management Task Force, 2007). By conducting drawdowns with Upper Mississippi pools, previously inundated areas become exposed, diversity and quality of vegetation is increased, and habitat quality is also improved.

4.3.1 Simulation Methods

Two drawdown conditions were completed for this study; one-foot and two-foot (0.3 m and 0.6 m) drawdown. Three flow scenarios were investigated during both

drawdown conditions. The three flow scenarios had to fall in the range of 20,000 ft^3/s to 100,000 ft^3/s (566 m^3/s to 2,832 m^3/s), so that normal operating levels could be maintained at Lock and Dam 8. The three flow scenarios chosen were a low, medium, and high flow; 33,000 ft^3/s, 60,000 ft^3/s and 90,000 ft^3/s (934 m^3/s, 1,699 m^3/s and 2,549 m^3/s). The flow scenarios were simulated using the one and two foot (0.3 m and 0.6 m) drawdown conditions at the exit of the model, Lock and Dam 8. Each simulation was compared using a water surface elevation profile, dewatered area, and depth and velocity histograms.

4.3.2 Results

Water surface elevation profiles along the main channel were compared for each flow condition, during normal operating conditions and the two drawdown conditions. Figure 4.6 through Figure 4.8 show the water surface elevation profiles for 33,000 ft3/s, 60,000 ft3/s, and 90,000 ft3/s (934 m3/s, 1,699 m3/s, and 2,549 m3/s). During the drawdown conditions at each flow scenario, the flat pool profile was deviated from, more during the two foot drawdown. The higher the flow rate, the closer the water surface elevation profiles are until they reach the control point within the pool. The control point is located at the La Crosse gauge, which was displayed in Chapter 3, Figure 3.7. It can be seen in Figure 4.6 that the backwater effect from the drawdown propagates throughout the entire pool up to Lock and Dam 7. Even though it is a small difference, approximately less than a half a foot, it shows how the drawdown is most effective during low flow rates.

The dewatered area comparison followed predicated trends, with area increasing between the one and two foot drawdown conditions. The low flow rate of 33,000 ft^3/s (934 m^3/s) had the largest amount of dewatered area during the two-foot drawdown and the second largest area during the one-foot drawdown. The dewatered area decreased linearly as the discharged increased. These results were recorded in Table 4.1.

Depth and velocity histograms (Figure 4.9 through Figure 4.11) were created for each of the drawdown simulations. The histograms indicated that at the low flow rate of 33,000 ft^3/s (934 m^3/s), the depth and velocity greatly decreases. The large occurrences move from the main channel and side channels to the backwater and impounded areas. This trend follows the predicted results. The drawdown decreases depths and velocities to where the higher occurrences are in the backwater and impounded areas. This trend follows suit for the 60,000 ft3/s and 90,000 ft3/s (1,699 m3/s and 2,549 m3/s) flow scenarios. Compared to the normal operating conditions, the high occurrences of depth and velocity shift from the main and side channels to the backwater and impounded areas. It can be seen through the depth and velocity histograms that the drawdown is most effective during the low flow rate of 33,000 ft3/s (934 m3/s).

4.3.3 Discussion

It can be seen from the results that drawdowns are most effective during lower flow rates. Looking at the water surface elevation profiles, the low flow rate of 33,000 ft3/s (934 m3/s) creates the greatest slope in the pool, deviating away from the flat pool profile. This slope is greatest during the two-foot drawdown, which was the case for all three flow scenarios. The dewatered area decreases as the flow rates increase. The purpose of the drawdowns is to expose previously inundated areas in order to promote vegetation growth and habitat diversity. In order to obtain the goals during a drawdown, low flows are most desirable, which means that drawdowns should occur during the low points in the annual hydrographs. One limitation to steady state drawdowns is assessing the exchange of water between backwater and main channel areas. Since the drawdowns were conducted during steady state discharges, backwater areas loose water steadily in relationship to the level of drawdown and vicinity to the exit of the model. A way to improve the drawdown results would be to simulate unsteady state discharges through the

model during the two drawdown conditions. This would make calculating exchange between backwater and main channel areas much more useful.

The depth and velocity histograms are most useful to biologists for the drawdown simulations. Habitat suitability incorporates many aspects, such as depth, velocity, substrate, turbidity, light exposure, and nutrients within the water column. The model gives biologists the two very basic parameters that drive other ecological parameters, and can help them understand the hydrodynamics within the pool. By simulating a range of drawdowns and assessing the outputs, biologists and river managers can have a better understanding of the pool, and can make more educated decisions on future drawdowns within the pool.

4.4 Implementation of Hypothetical Island

One current goal of river managers and biologists working in the UMR is to revert the river to a more natural state, increased habitat and ecological diversity. The construction of islands within impounded areas helps this goal. The main goals of the islands are to divert flow away from impounded areas and create and areas of reduced velocity in deep water behind the island (Rogala, 2009-2011). Island also protect existing habitats and create new habitat conditions so aquatic vegetation and deep water habitats can be reestablished in Pool 8 (United States Army Corps of Engineers, 2011b). The areas of reduced velocity behind the island creates new habitat for river ecology while also reducing wind fetch in shallow areas in the upper portion of the pool. From 2006 to present, the U.S. Army Corps of Engineers have been working on a three phase island rebuilding project in Pool 8. Phase one and two were completed between the years of 2006 and 2008, and phase three is currently under construction. There will be a total of 24 islands constructed in the lower portion of Pool 8 designed to aid habitat. The islands are constructed from dredged material that is protected by rock structures and vegetation.

4.4.1 Simulation Methods

Several island location options were debated based on creating an area of reduced velocity in deep water and ease of implementation of the island into the mesh. The location of the island was based on preliminary concept drawings by USGS personnel and corresponding mesh resolution. The island was created in the mesh by removing mesh cells, which meant that the island would always be dry during any flow conditions and would be considered as a wall within the model. Once the cells were removed, the original mesh was modified and used in the new simulations. The island had a high resolution of cells around it ensuring that flow structures passing the island would be captured. The island was created by removing mesh elements because of time constraints and this is the first step in a proof of concept island. The next steps in future work would be the creation of the island in the DEM with geometry and side slopes.

Three flow scenarios were simulated with the new mesh that included the island. Low, medium, and high scenarios were chosen from the library of steady state simulations so that the results from the mesh including and excluding the island could be directly compared. The three flow scenarios chosen were 10,000 ft^3/s , 33,000 ft^3/s and 100,000 ft^3/s (283 m^3/s, 924 m^3/s, and 2,832 m^3/s). Once the three simulations were complete, two analyses were done to compare the effects from the island. Results from each flow scenario including and excluding the island were used to create stream traces and visualize the flow paths in the lower portion of the pool. The results for three flow scenarios including and excluding the island were also manipulated using GIS software. Figures were constructed showing the differential velocities between the simulations with and without the island. The figures were able to accurately convey the creation of the area of reduced velocity behind the island. Tables that quantified the results accompanied these figures.

4.4.2 Results

The flow paths created in Tecplot show that a majority of the flow, for all three flow scenarios, tends to flow around the sides of the island. Since the island is treated as a wall within the model, this creates a small area of low velocities in front of the island and large area of low velocities behind the island. The low flow zone behind the island grows with the increase in discharge; and these patterns can be seen in Figure 4.12 through Figure 4.14. As the flow finds its way around the island, velocities accelerate around the island and flow is channeled into the main navigation channel and other secondary side channels. The distribution of velocity differences can be seen in Figure 4.15 through Figure 4.17. The differences are strongest on the east and west side of the sides and propagate outward. The differences also increase as discharge increases.

4.4.3 Discussion

The goals of inserting the island in the lower portion of the pool were to divert flow around the island and create an area of reduced velocities in deep water. These two goals were accomplished with the construction of the island by pushing flow into the main channel, and the creation of an area of reduced velocities behind the island. Since this was a proof of concept, some physical characteristics were not modeled properly. The first steps in the actual construction of an island would be proof of concept, showing that the island would create the desired flow regime, then the island would be given elevations and side slopes for more simulations and testing. Since the island is represented as a wall within the model, a stagnation point is created on the front of the island. In the field or with island geometry, flow would react to the slopes of the island instead of a wall.

Future work could include the construction of an island with elevations and side slopes so that hydrodynamics could be more accurately modeled. Similar tests could be performed on the island to assess the flow regime created by the islands elevations and

side slopes. Habitat suitability assessments, using the hydrodynamic model, could also be completed in order to understand if the flow regime around and behind the island is conducive for desired habitats. The island could also be simulated using the two-equation k-ε turbulence model. The k-ε model is recommended for flow separation. Future simulations could be completed with both turbulence models in SRH-2D and results compared. The proof of concept island was successfully simulated using the hydrodynamic model and it proved that it is a useful tool for such concepts.

4.5 Travel Time and Stream Trace Study

Tecplot 360 can create stream traces through the pool which are calculated by two-step second-order Runge-Kutta method. The velocity vector direction is calculated at a specific initial location set by the user. A step is made and the velocity vector direction is calculated at the new spatial location. The two vectors in the previous steps are then averaged, and the averaged vector is re-applied to the initial location (Tecplot, 2010). Once a stream trace is created, the user can then send a particle through the model domain along the stream trace. The user sets the time step and number of iterations as the particle travels along the stream trace. A large number of iterations were used in order for all particles to have a chance to exit the model domain. As the particle moves along the stream trace, position, bed elevation, water elevation, water depth, velocity components, velocity magnitude, Froude number, and bed stress are all recorded in the output file. The output file is then used to calculate the travel time based on time step size and number of iterations.

4.5.1 Simulation Methods

500 stream traces were created at the five inlets within the model and particles were released down the stream traces. The solutions from the steady state 10,000 ft^3/s, 33,000 ft^3/s and 100,000 ft^3/s (283 m^3/s, 934 m^3/s and 2,832 m^3/s) simulations were used as the data sources for the travel time study. The time step was set to 72 seconds and the

number of steps was set to 8500 iterations. The time step was calculated using the length of a cell and average velocity in the pool. The number of iterations was determined by trial and error methods tracking a particle along the stream trace within the model domain. The results from the creation of stream traces and particle calculations within Tecplot were taken into MATLAB where a script was able to calculate the travel time for each particle that exited the model domain.

4.5.2 Results

Travel time results were calculated for each inlet for three flow cases. Table 4.2 through Table 4.6 display the travel times along with amount of particles exiting the model domain from each inlet. The tables also show the travel time statistics for every inlet. Lock and Dam 7 and Onalaska Spillway had 100 percent of the particles exiting the model for all three flow cases. The French Island Spillway had zero particles exiting the model for the 10,000 ft^3/s and 33,000 ft^3/s (283 m^3/s and 934 m^3/s) cases, and only 6.8 percent of the particles exiting the model for the 100,000 ft^3/s (2,832 m^3/s) case. The La Crosse River had 100 percent of the particles exiting the model for the 10,000 ft^3/s and 100,000 ft^3/s (283 m^3/s and 2,832 m^3/s) cases, and only 78 percent of the particles exiting the model for the 33,000 ft^3/s (934 m^3/s) case. The Root River had 80, 91, and 82 percent exiting the model for the 10,000 ft^3/s, 33,000 ft^3/s and 100,000 ft^3/s (283 m^3/s, 934 m^3/s and 2,832 m^3/s) cases, respectively. The stream traces that were used to calculate the travel times can be seen in Figure 4.18 through Figure 4.22.

4.5.3 Discussion

Figure 4.18 through Figure 4.22 show the stream traces from all five inlets, which include all 500 stream traces at each inlet. Displaying all stream traces was done to capture all activity in the side channel, backwater and impounded areas. Since the stream traces were created close together at each inlet, the pool scale view showing the 500 traces at each inlet seems almost as one large stream trace. It can be seen for the flow

through Lock and Dam 7 that a majority of it is conveyed through the main channel during all flow cases. There was some divergence in the lower pool during the 100,000 ft^3/s (2,832 m^3/s) case due to the high velocities. French Island Spillway is the unique inlet among the five inlets. The flow cases of 10,000 ft^3/s and 33,000 ft^3/s (283 m^3/s and 934 m^3/s), none of the particles injected along the stream traces reached the exit of the model. The particles do not exit the model until the 100,000 ft^3/s (2,832 m^3/s) flow case is simulated. Zero particles exiting the model for the low and medium flow cases is due to extremely small flow rates over French Island Spillway and coarse discretization in that area of the model. In the 10,000 ft^3/s (283 m^3/s) case, the flow is so small that it tends to re-circulate within Round Lake, while during the 33,000 ft^3/s (934 m^3/s) case, even though discharge is increased, large amounts of re-circulation occur due to the small flow rate and coarse discretization in Round Lake. Both of these scenarios can be seen in the enlarged portion of Figure 4.19. Particles injected along stream traces near Onalaska Spillway find their way through the model by means of the main channel, except for the 100,000 ft^3/s (2,832 m^3/s) case, where the velocities are strong enough to pull them into secondary channels, which is also the case with particles injected by the La Crosse River. Particles injected by the Root River also follow the main channel as a means of reaching the exit, again, except for during the 100,000 ft^3/s (2,832 m^3/s) case where they follow secondary channels. This concludes that flow in the main channel is strong enough to attract particles from all five inlets and pull them through the main channel, except when the flow through Lock and Dam 8 is or exceeds 100,000 ft^3/s (2,832 m^3/s), in which case the velocities within the pool are strong enough to pull flow into all the secondary channels and still be able to exit the model. This also shows the limitations of the steady state stream traces developed in Tecplot, where in reality, flow will reach the secondary channels during all discharges, and it will just take longer or follow other paths to the exit. Another limitation to the steady state stream trace calculations within Tecplot is the method used to create the stream traces. Since the method uses averages during every

step, the path is somewhat skewed. A particle injected mid pool will not have the same path as a particle injected at an inlet, even if they are both injected in the main channel. The particle with the further path to travel has more velocities averaged, and will take a more generalized path through the pool.

4.6. Habitat Suitability Assessment

Construction of navigation dams and river training structures which alter the local flow in the Mississippi River (Young, 2006) have increased interest in the hydrodynamic effects on aquatic habitat. Habitat suitability indices characterizing physical habitat features are critical to ecosystem management in the heavily altered UMR. While a broad range of dynamic environmental conditions contribute to species occurrence and density within the river, habitat suitability assessments are conducted using a singular flow condition. The model was used to compare habitat suitability indices created from field and model data of emergent vegetation during multiple flow conditions in Pool 8.

4.6.1 Habitat Suitability Methods

Emergent vegetation data along with hydrodynamic data was sampled and collected by the Wisconsin Department of Natural Resources and Minnesota Department of Natural Resources. Following a method published by (Young et al., 2008), a modified version published by (Hastie et al., 2000), habitat suitability indices (HSI) of depth and velocity magnitude were created for the measured field data. Equations 4.1 and 4.2 shown below describe how proportionality is used to classify habitat suitability.

$$Pi = (Ni/N) / (Vi/V) \tag{4.1}$$

$$SI = Pi / Max\ Pi \tag{4.2}$$

In the above equations, Ni is the sampling point frequency, N is the total number of overall points, Vi is the frequency, V is the total number of sampling points, Pi is the proportional use, and SI is the suitability index value (Young et al., 2008).

Observations of emergent vegetation presence and absence were also compared with model data. Habitat suitability curves of depth and velocity magnitude were created for field results and five flow scenarios, 10,000 ft^3/s , 21,000 ft^3/s, 35,000 ft^3/s, 63,000 ft^3/s, and 90,000 ft^3/s (283 m^3/s, 595 m^3/s, 992 m^3/s, 1,784 m^3/s, and 2,549 m^3/s), which are displayed in Figure 4.23 through Figure 4.28. For each flow condition, HSI based on water depth and velocity are mapped and a minimum HSI at each computational element was calculated, using a minimum compound formula. The minimum compound formula can be seen in Equation 4.3 below which was developed in mussel study done by (Morales, 2004).

$$compound_{HSI} = minimum\ (HSI_H, HSI_V) \quad (4.3)$$

In the above equation, HSI_H is the habitat suitability index for depth and HSI_V is the habitat suitability index for velocity. The minimum of the two values at a spatial location is taken and reported as the $compound_{HSI}$.

Only perennially wet areas (defined by a discharge of 10,000 ft^3/s (283 m3/s)) were mapped because emergent vegetation can only survive in areas that are consistently inundated throughout the year. This was also done so that when comparing habitat suitability between flow rates, areas of interest were always inundated. This prevented comparing habitat areas in the floodplain during the higher discharges. Figure 4.29 through Figure 4.33 display the minimum HSI maps.

4.6.2. Results and Discussion

Results indicate that habitat suitability is independent of discharge. The habitat suitability maps, Figure 4.29 through Figure 4.33, show that there are very small areas of exceptional habitat, some small areas of adequate habitat, and a majority of the pool being poor habitat. This trend is shown in Table 4.7 and Figure 4.34. The general trend that was displayed for all five discharges was that high habitat suitability values correlated to small spatial areas and as the habitat suitability value decreases, areas of

poor habitat increase. Comparing habitat suitability index ranges and the area of suitable habitat, the area of suitable habitat was very similar for each discharge, which can be seen in Figure 4.34. All habitat suitability ranges displayed similar spatial areas of suitable habitat for each of the five flow rates confirming that habitat suitability is independent of discharge.

This conclusion could be due to the fact that the emergent vegetation samples were bias throughout the pool. Emergent vegetation samples were collected along the banks of the main channel and a few within backwater areas of the pool. It was believed that if more random samples were taken throughout the pool, the results would have concluded that discharge correlated to habitat suitability. Along with bias field data used for the habitat suitability application, steady state results could have had an effect on the results. Unsteady flow rates could possibly have resulted in a stronger correlation between discharge and habitat suitability.

4.6.3 Comparison of Habitat Suitability Outputs at Low Discharge

In section 4.6.1, habitat suitability maps were created using only perennially wet areas defined by the inundation extent of 10,000 ft^3/s (283 m^3/s). After correspondence with UMESC personnel (Rogala, 2009-2011), it was determined that in order to more accurately create the inundation extent at 10,000 ft^3/s (283 m^3/s), the output from 33,000 ft^3/s (934 m^3/s) would be used as a initial condition for the 10,000 ft^3/s (283 m^3/s) case. SRH-2D gives the option of starting a hydrodynamic model at a dry state or using a previous file as a starting point (RST file). The inundation extent from the 10,000 ft^3/s (283 m^3/s) case was not accurate to current field conditions. It was more accurately represented when the 33,000 ft^3/s (934 m^3/s) flow case was used as a starting point for the 10,000 ft^3/s (283 m^3/s) flow case. Expanding on this principle, it was determined that all flow rates under 33,000 ft^3/s did not show accurate inundation when compared to field

observations (Rogala, 2009-2011). Habitat suitability maps were created for 10,000 ft^3/s and 21,000 ft^3/s (283 m^3/s and 595 m^3/s) using both methods for inundation and compared in Figure 4.35and Figure 4.36.

It can be seen when comparing the habitat suitability maps at the different inundation extents that habitat suitability increases in the secondary channels and backwater areas. For the case of 10,000 ft^3/s (283 m^3/s), a habitat suitability index of one increases in the main channel for the larger inundation extent. A habitat suitability index of approximately 0.8 to 0.9 is largely clustered in the lower pool. This is due to the extremely low velocities and depths during this case. At 21,000 ft^3/s (595 m^3/s) a habitat suitability index of one increases in secondary channels and backwater areas. The lower pool tends to have no suitable areas due to the higher water depths at this flow rate. These results are expected because an increase in discharge will result in an increase in depth and velocity magnitude in certain locations of the pool. These maps show how during small discharges, habitat suitability tends to stay near the side banks of the main channel. When the discharge is slightly increased, enough to increase depths in backwater and impounded areas, habitat suitability moves to secondary channels, backwater and impounded areas.

Table 4.8, Figure 4.37, and Figure 4.38 show similar trends found in Section 4.6.2 for the comparison of habitat suitability during flow rates of different inundation extents. Table 4.8 and Figure 4.37 demonstrate how the areas of suitable habitat are similar for 10,000 ft^3/s (283 m^3/s) and 10,000 ft3/s (283 m^3/s) with initial conditions of 33,000 ft^3/s (934 m^3/s) except for the habitat suitability range of 0.50 to 0.75. This range is dramatically increased during the simulation with the larger inundation extent. With the larger inundation extent, more areas with adequate depths and velocities are taken into account increasing the area for the habitat suitability index range of 0.50 to 0.75. Table 4.8 and Figure 4.38 show how at 21,000 ft^3/s (595 m^3/s), areas of suitable habitat follow the same trends as in Section 4.6.2. Although area increases for all ranges, as in the

10,000 ft^3/s (283 m^3/s) case, the general trend of a large area of poor habitat suitability and a very small area of excellent habitat suitability is maintained, again showing how habitat suitability is independent of discharge. A more complete data collection process for the emergent vegetation would greatly improve the habitat suitability application use of the hydrodynamic model.

4.6.4 Habitat Suitability Map Comparison

The emergent vegetation data used in the previous sections was from the USGS Environmental Monitoring and Assessment Program (EMAP). The USGS publishes habitat suitability maps using another set of data from their Long Term Resource Monitoring Program (LTRMP). The habitat suitability maps for emergent vegetation in Pool 8 constructed by the USGS are described as being predictions and are created with the LTRMP data (United States Geological Survey, 2011a). The LTRMP data is much denser and less bias than the EMAP data, but the LTRMP data lacks corresponding spatial hydrodynamic field data. The most ideal set of data used to create the habitat suitability maps would be a combination of the two USGS data sets. The biological data would be vast and random, while having the corresponding spatial hydrodynamic field data along with the biological samples. The LTRMP emergent vegetation data in Pool 8 was spatial joined with one set of results from the hydrodynamic model. A flow rate of 35,000 ft3/s (992 m3/s) was used to create a habitat suitability map, following the same procedure as described in the above section, along with the LTRMP emergent vegetation data. The simulated map was then compared to the map that is produced by the USGS.

Figure 4.39 shows the two habitat suitability maps being compared. The green flooded areas represent areas of high suitability and the areas flooded in red represent areas of low to zero habitat suitability. This was study done not to compare the two habitat suitability methods or test the validity of the habitat suitability method developed for this model, but to show the difference between the two biological data sets used for

the emergent habitat suitability assessment. The comparison also shows that simulated habitat suitability map with the LTRMP data set, compared to the USGS habitat suitability map, shows agreement in areas of high habitat suitability.

This comparison demonstrates that data sets with copious amounts of random sampling (e.g. LTRMP data) the habitat suitability method for creating indices and maps for the current study is much improved. If the LTRMP data had corresponding spatial hydrodynamic data as well, then the habitat suitability maps could be validated. With a validated habitat suitability method, it would improve the knowledge of emergent vegetation within Pool 8 and reduce the need for more field data to be collected over time.

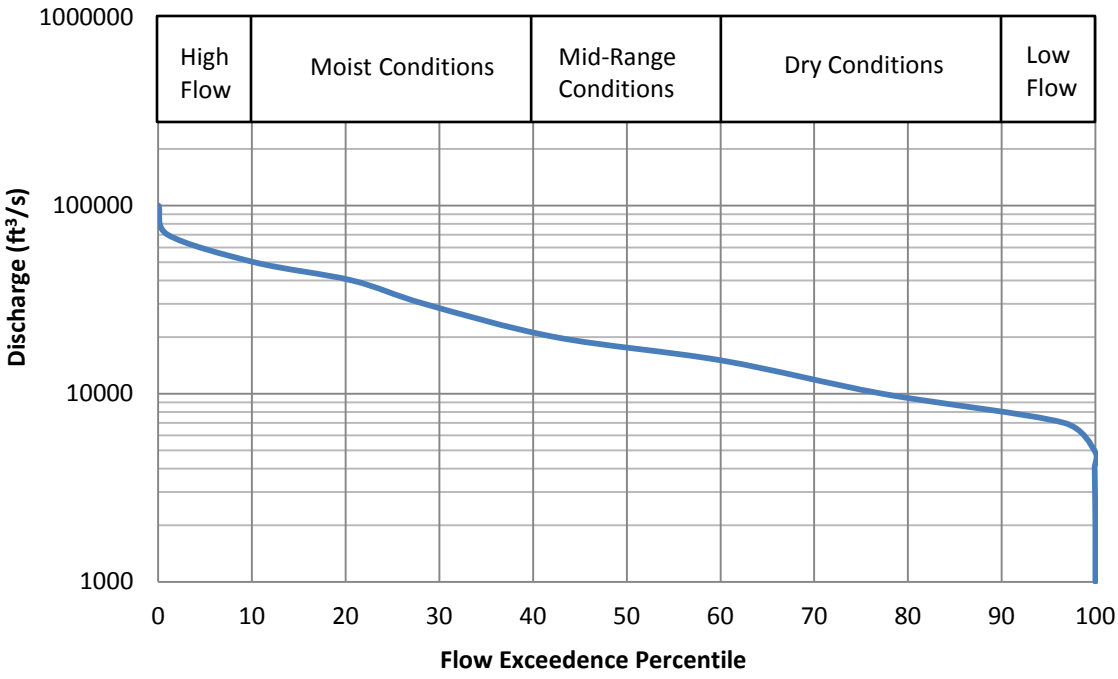

Figure 4.1. Flow duration curve from historic data recorded through Lock and Dam 8 (Data Source: USACE, 2011a).

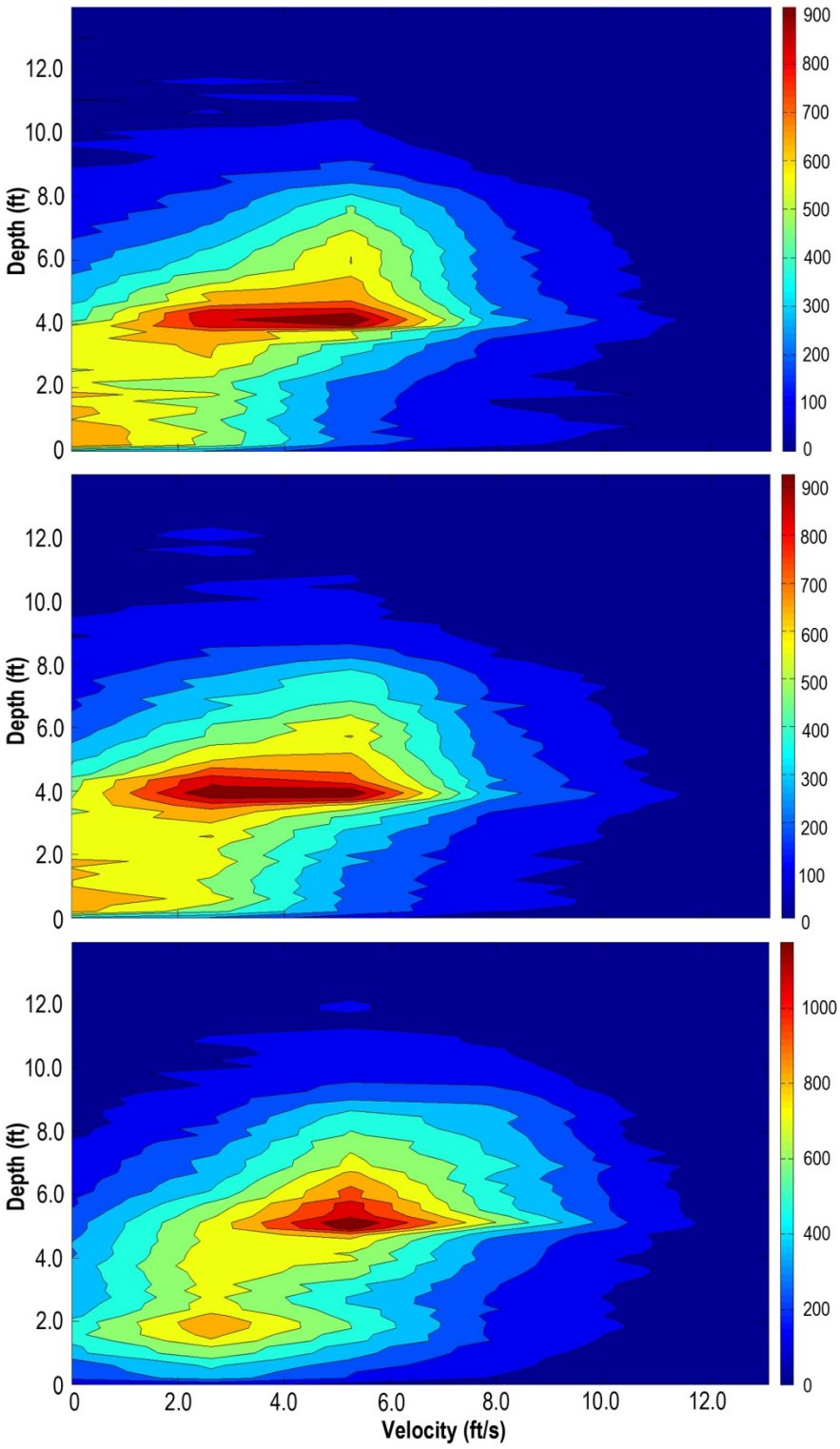

Figure 4.2. Depth and velocity histograms for 10,000 ft^3/s (top), 33, 000 ft3/s (middle), and 100,000 ft3/s (bottom) discharge through Lock and Dam 8.

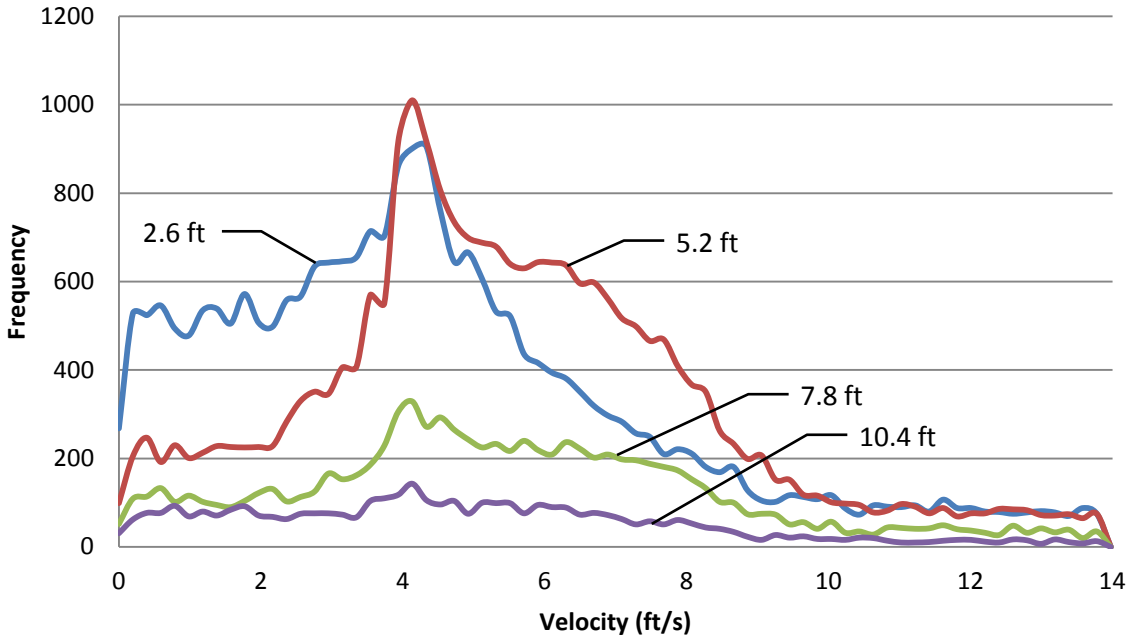

Figure 4.3. Velocity histograms at depths of 2.6 ft, 5.2 ft, 7.8 ft, and 10.4 ft for 10,000 ft^3/s discharge through Lock and Dam 8.

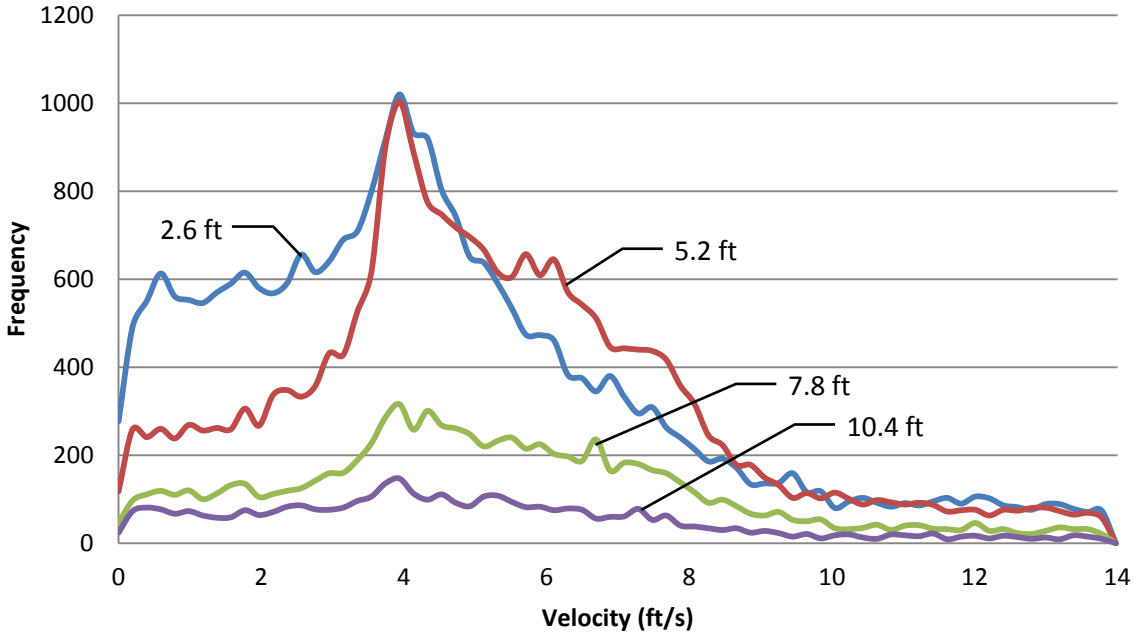

Figure 4.4. Velocity histograms at depths of 2.6 ft, 5.2 ft, 7.8 ft, and 10.4 ft for 33,000 ft^3/s discharge through Lock and Dam 8.

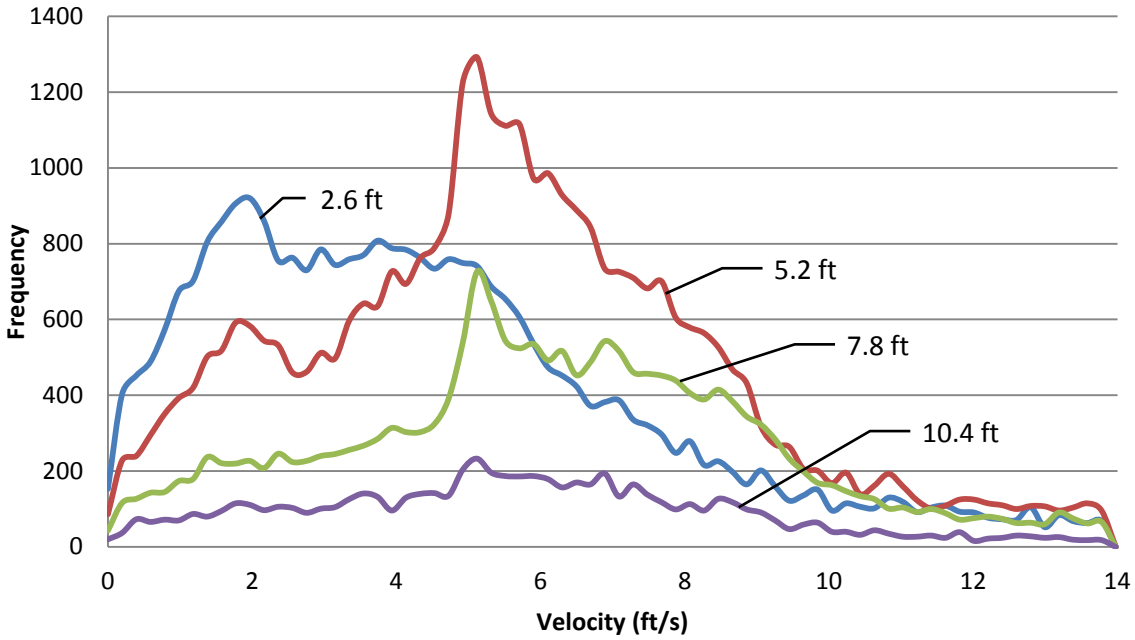

Figure 4.5. Velocity histograms at depths of 2.6 ft, 5.2 ft, 7.8 ft, and 10.4 ft for 100,000 ft^3/s discharge through Lock and Dam 8.

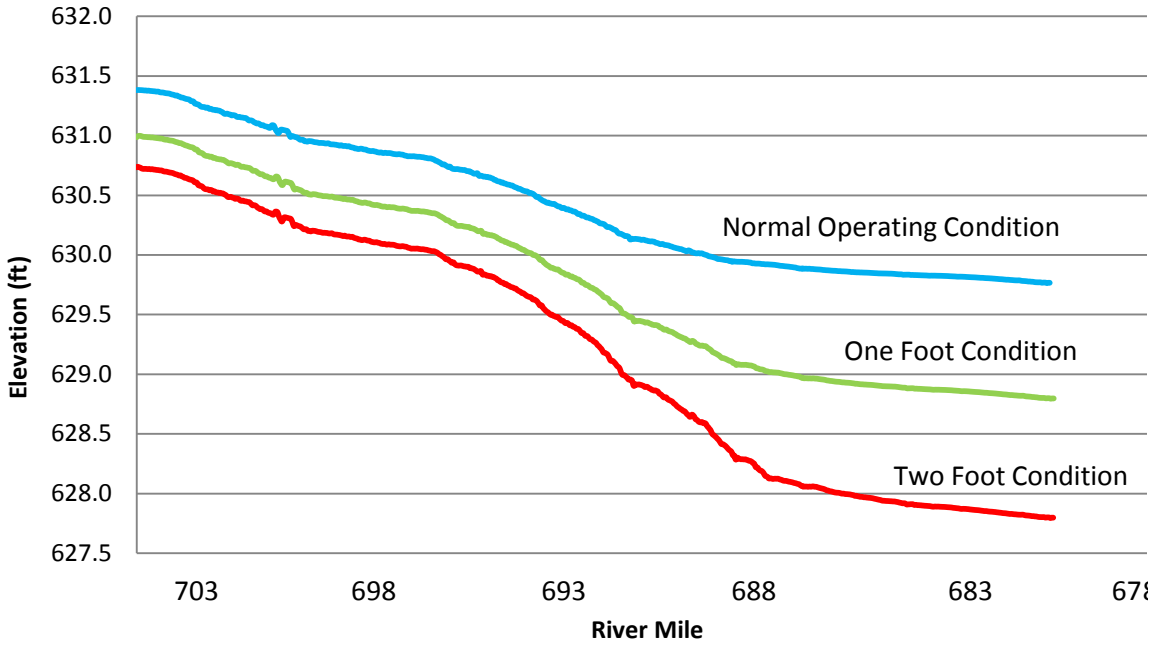

Figure 4.6. Water surface elevation profiles during normal operation, one foot drawdown and two foot drawdown for 33,000 ft^3/s discharge through Lock and Dam 8.

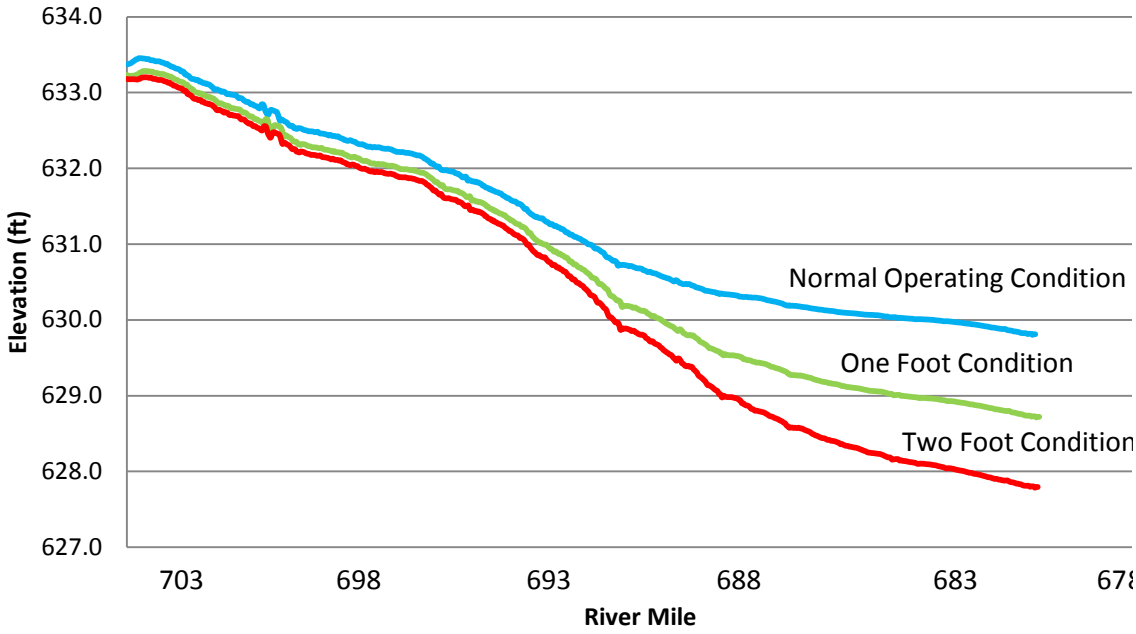

Figure 4.7. Water surface elevation profiles during normal operation, one foot drawdown and two foot drawdown for 60,000 ft^3/s discharge through Lock and Dam 8.

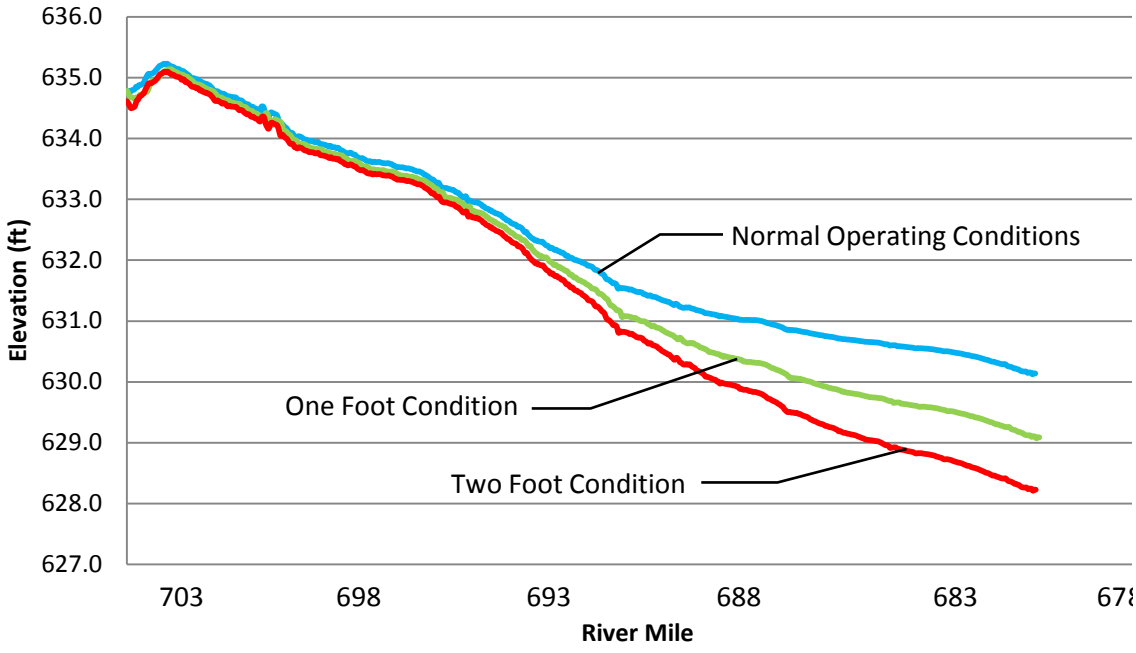

Figure 4.8. Water surface elevation profiles during normal operation, one foot drawdown and two foot drawdown for 90,000 ft^3/s discharge through Lock and Dam 8.

Table 4.1. Dewatered area for all drawdown simulations.

Drawdown Dewatered Area Results (mi^2)			
Flow Condition	33,000 ft^3/s	60,000 ft^3/s	90,000 ft^3/s
Normal Conditions	41.52	47.35	51.90
One Foot Drawdown	37.85	45.83	51.39
One Foot Dewatered Area	3.68	1.52	0.51
Two Foot Drawdown	35.98	44.80	51.02
Two Foot Dewatered Area	5.55	2.54	0.88

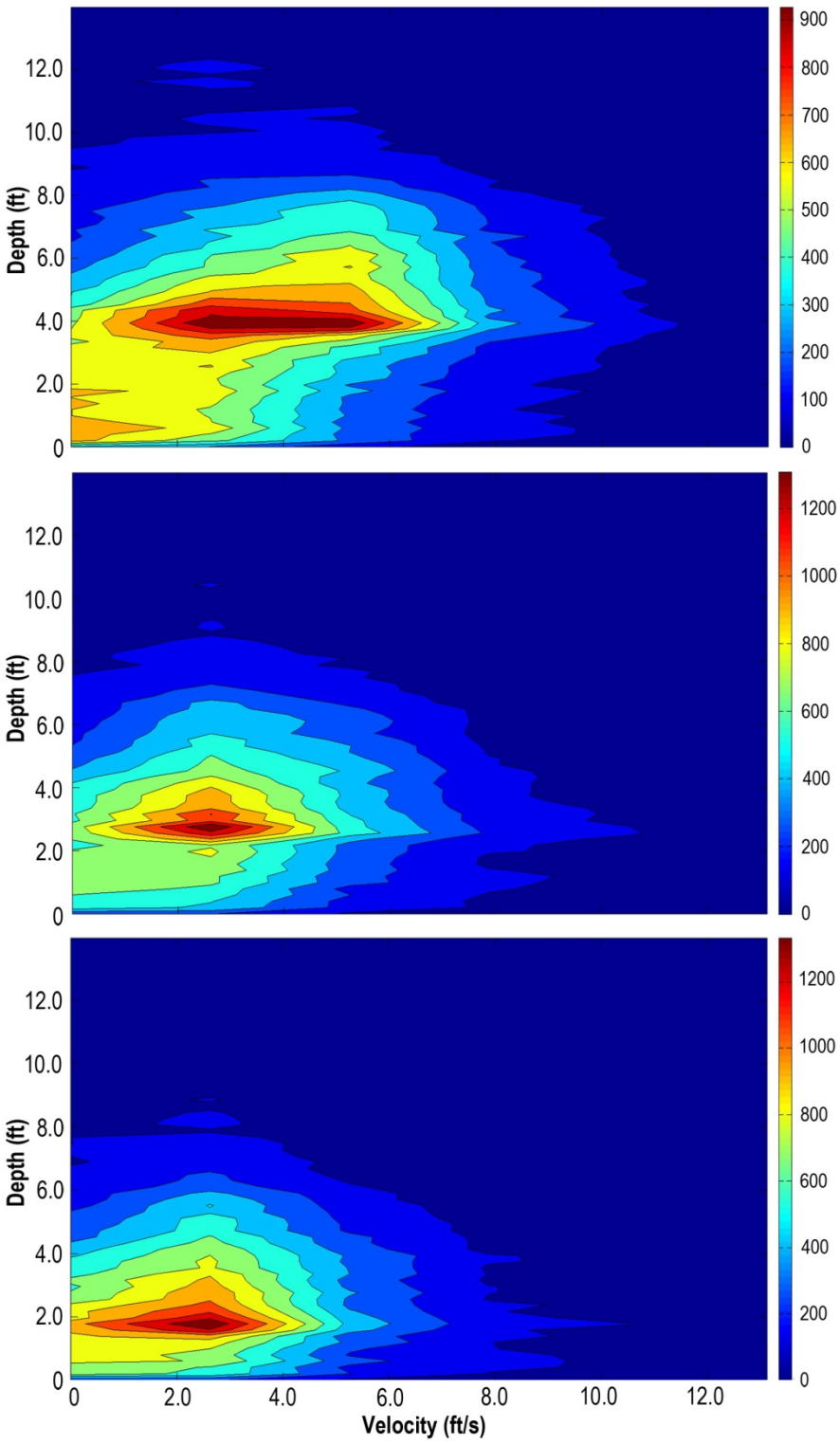

Figure 4.9. Depth and velocity histograms for 33,000 ft^3/s discharge through Lock and Dam 8 normal conditions (top), one foot drawdown (middle), and two foot drawdown (bottom).

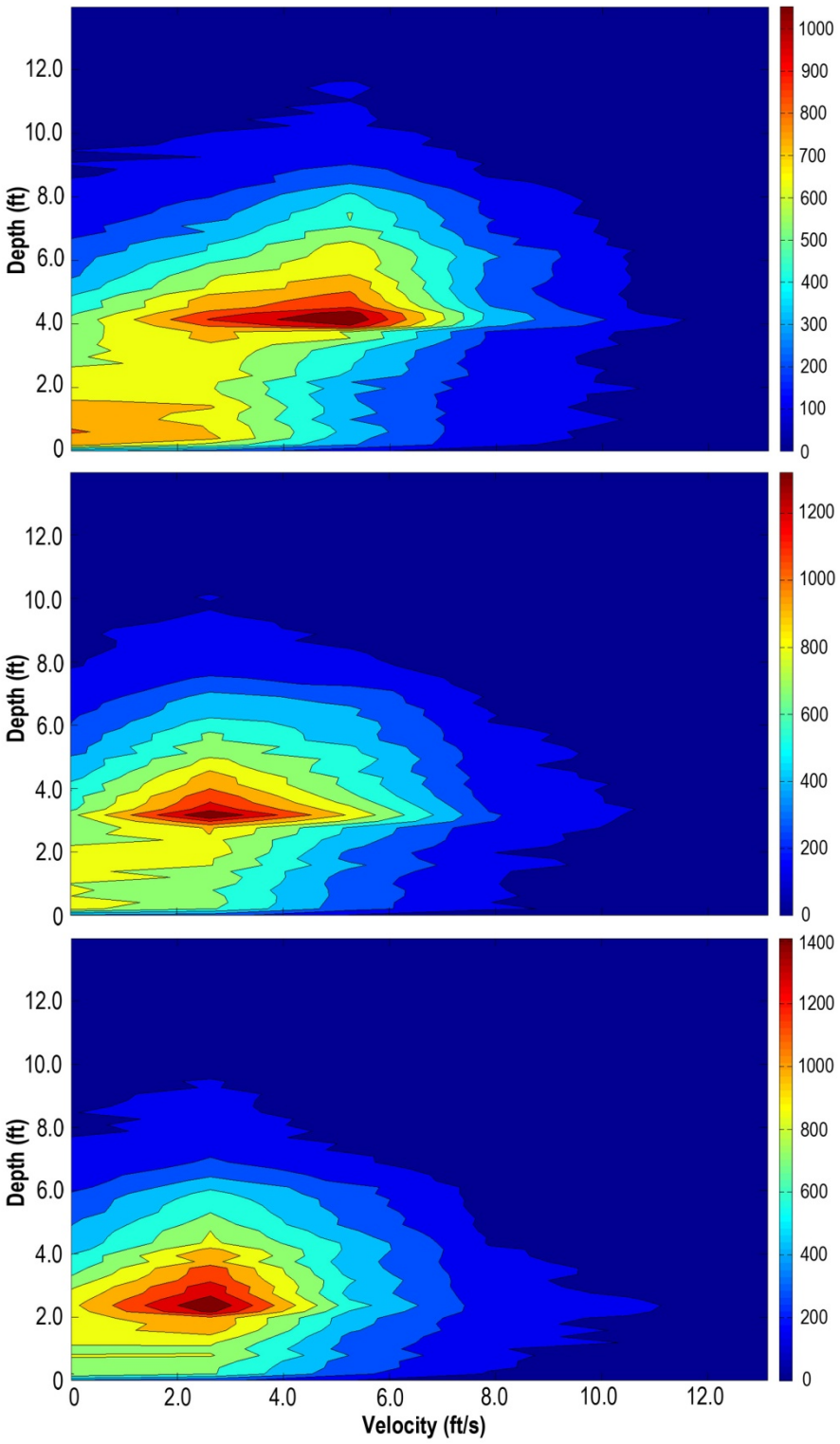

Figure 4.10. Depth and velocity histogram for 60,000 ft^3/s discharge through Lock and Dam 8 normal conditions (top), one foot drawdown (middle), and two foot drawdown (bottom).

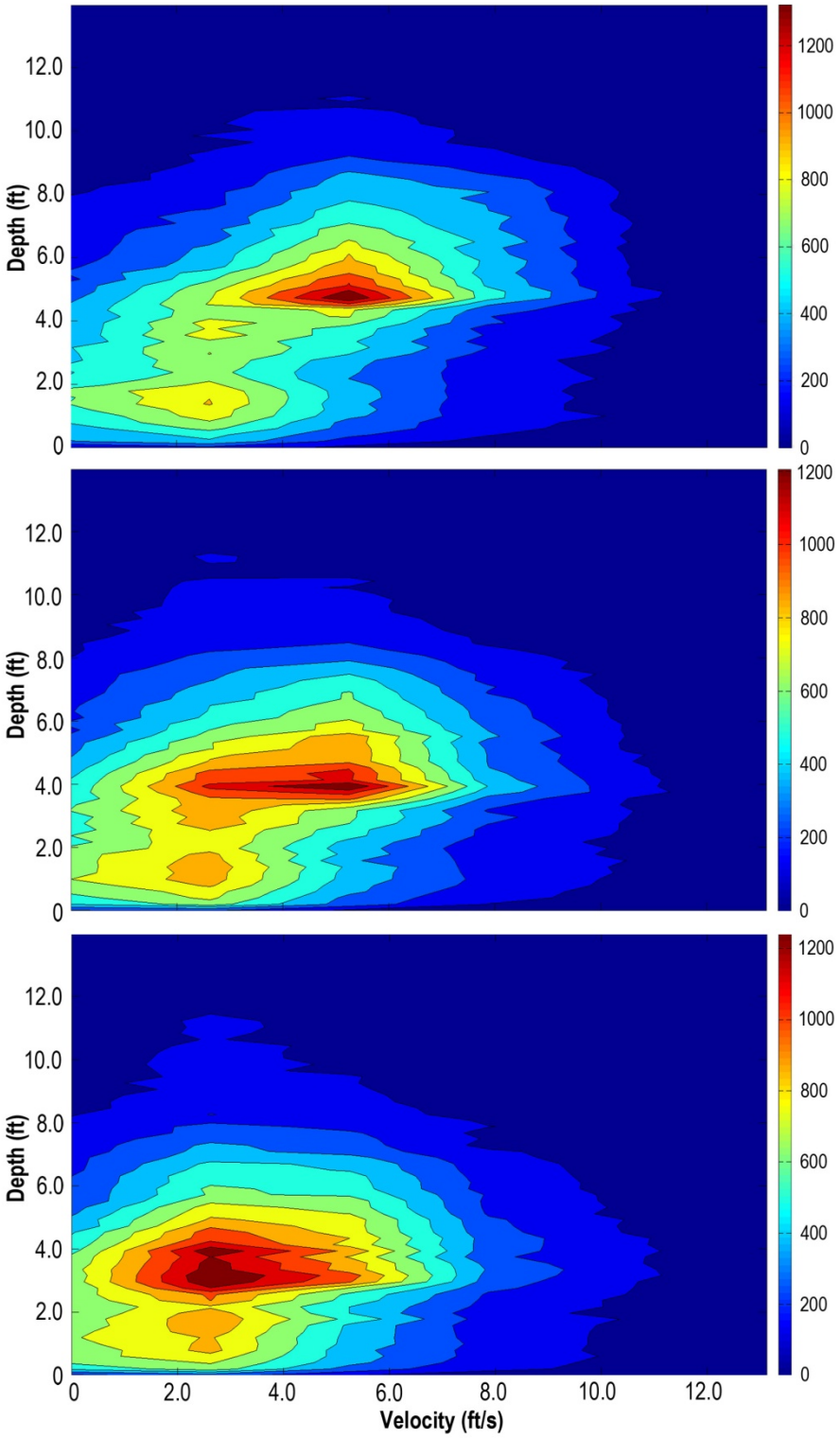

Figure 4.11. Depth and velocity histogram for 90,000 ft^3/s discharge through Lock and Dam 8 normal conditions (top), one foot drawdown (middle), and two foot drawdown (bottom).

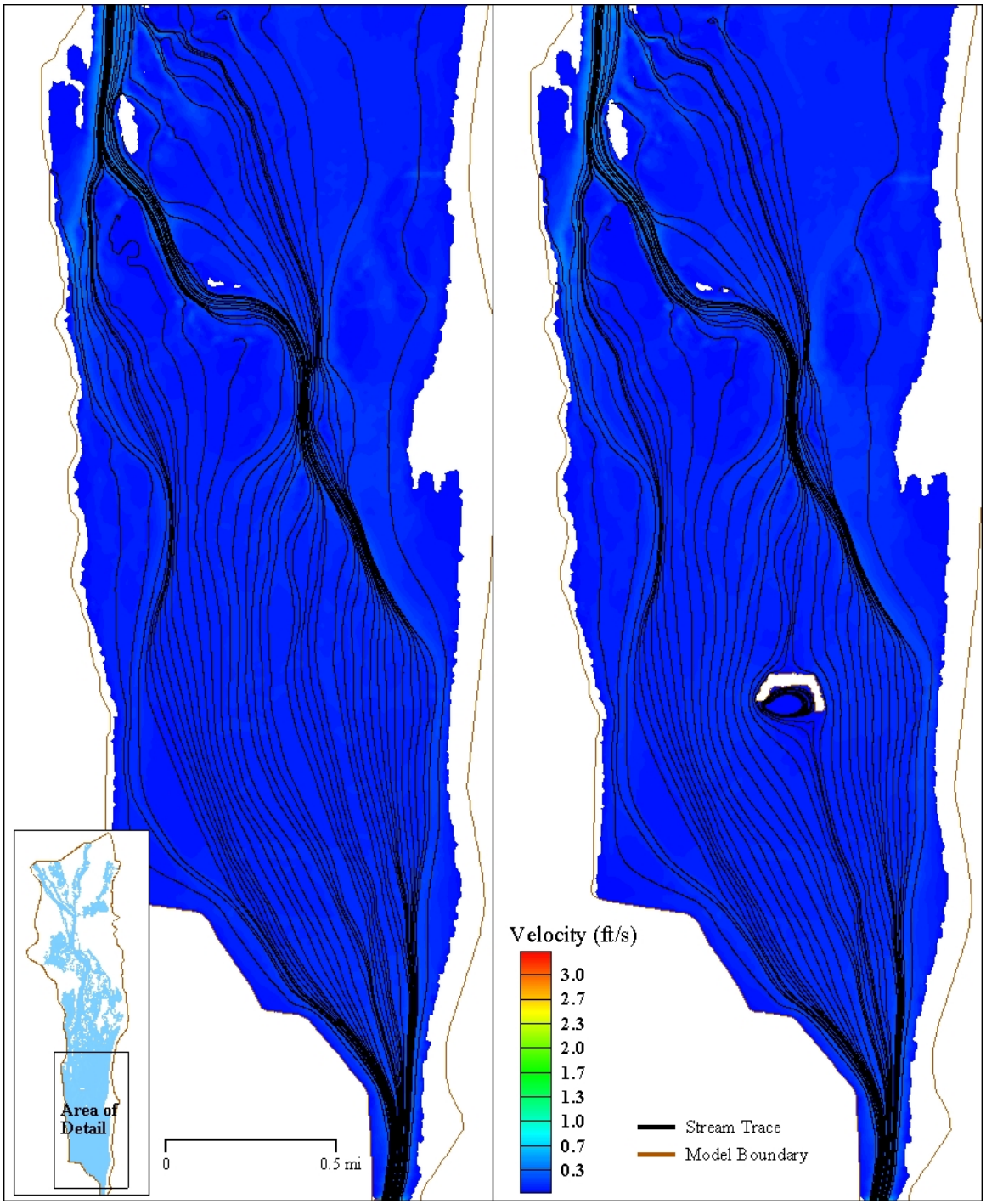

Figure 4.12. Stream trace paths and velocity distribution without island (left) and around hypothetical island (right) implemented in lower pool at 10,000 ft^3/s discharge through Lock and Dam 8.

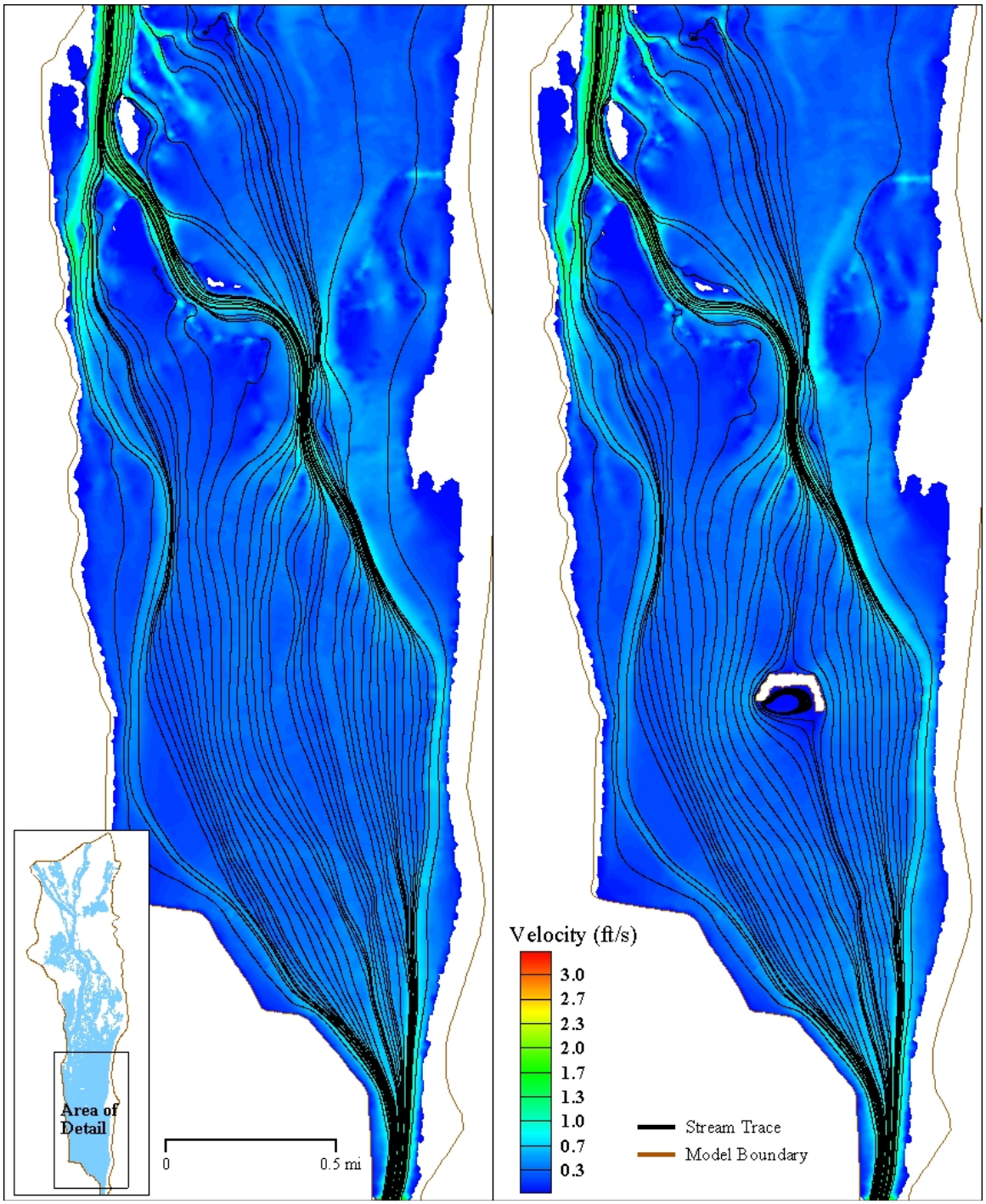

Figure 4.13. Stream trace paths and velocity distribution without island (left) and around hypothetical island (right) implemented in lower pool at 33,000 ft^3/s discharge through Lock and Dam 8

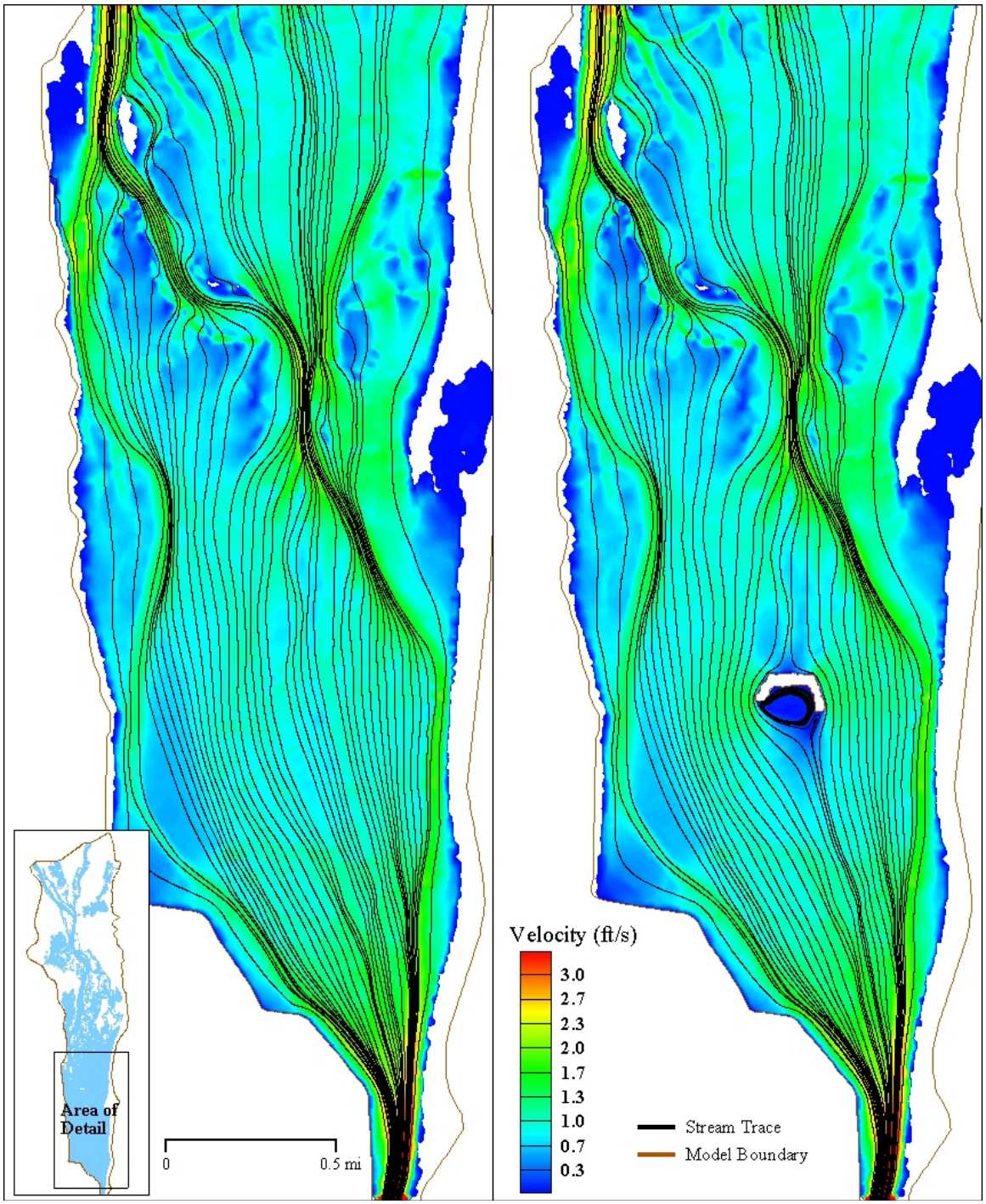

Figure 4.14. Stream trace paths and velocity distribution without island (left) and around hypothetical island (right) implemented in lower pool at 100,000 ft^3/s discharge through Lock and Dam 8.

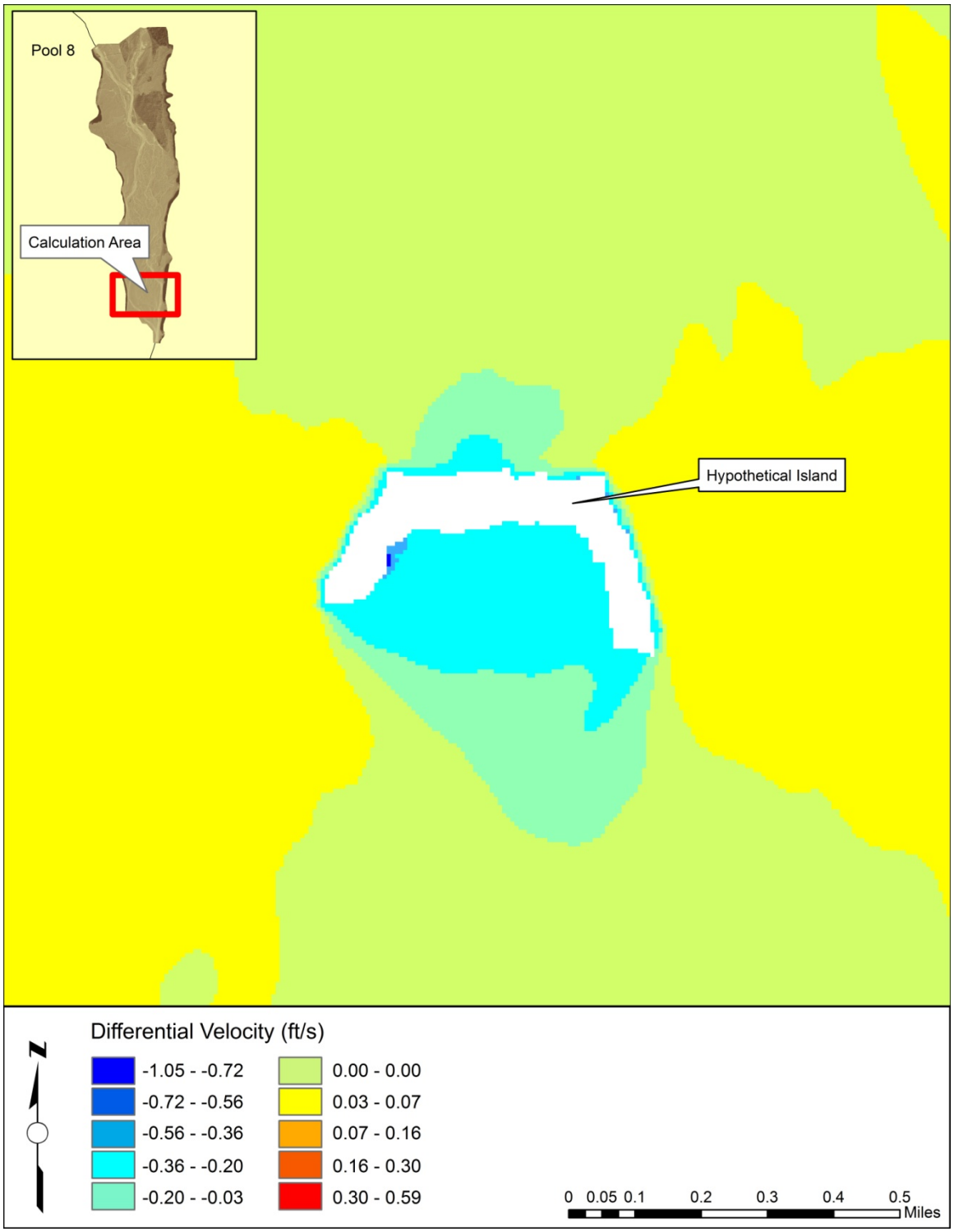

Figure 4.15. Velocity differential around hypothetical island at 10,000 ft^3/s discharge through Lock and Dam 8.

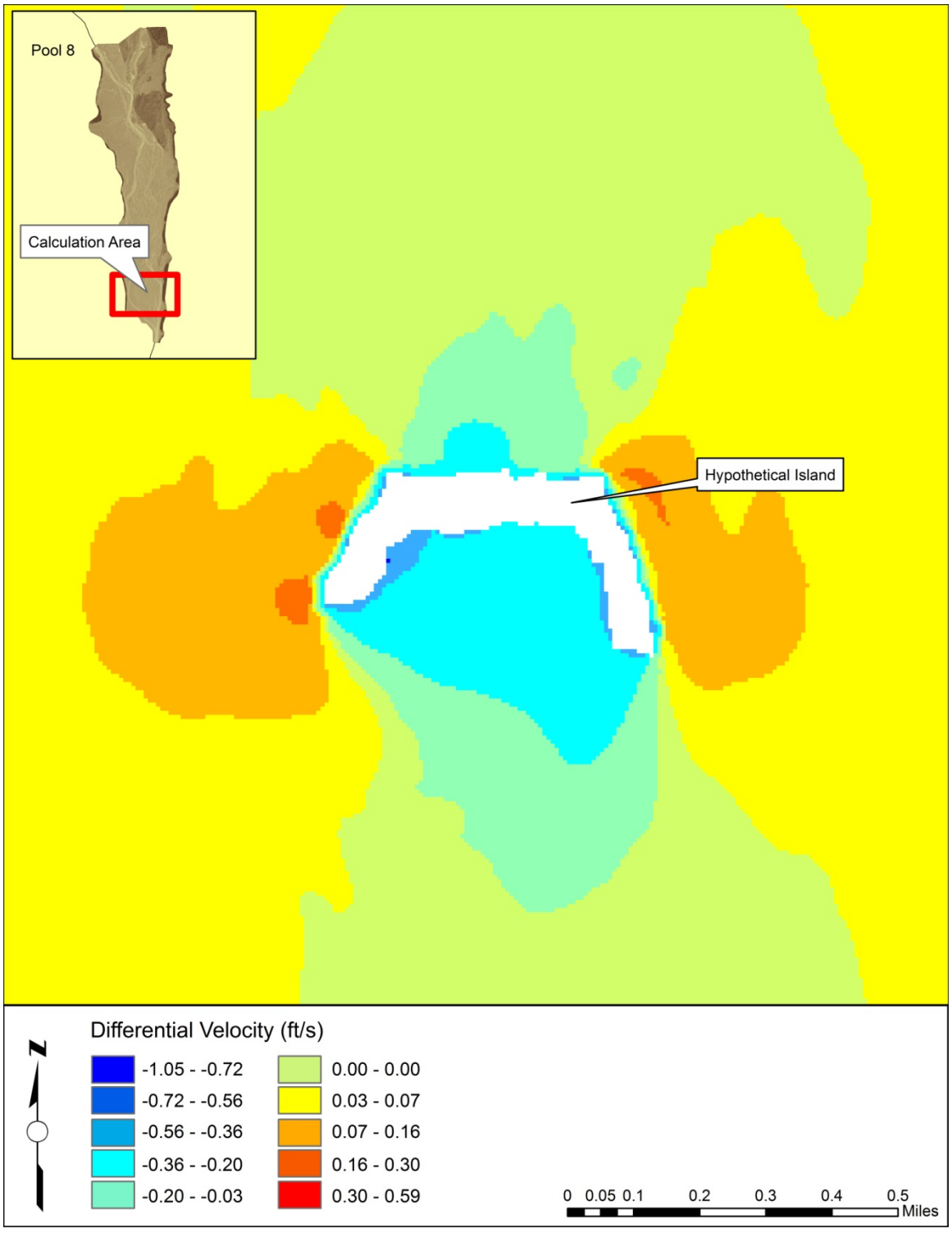

Figure 4.16. Velocity differential around hypothetical island at 33,000 ft^3/s discharge through Lock and Dam 8.

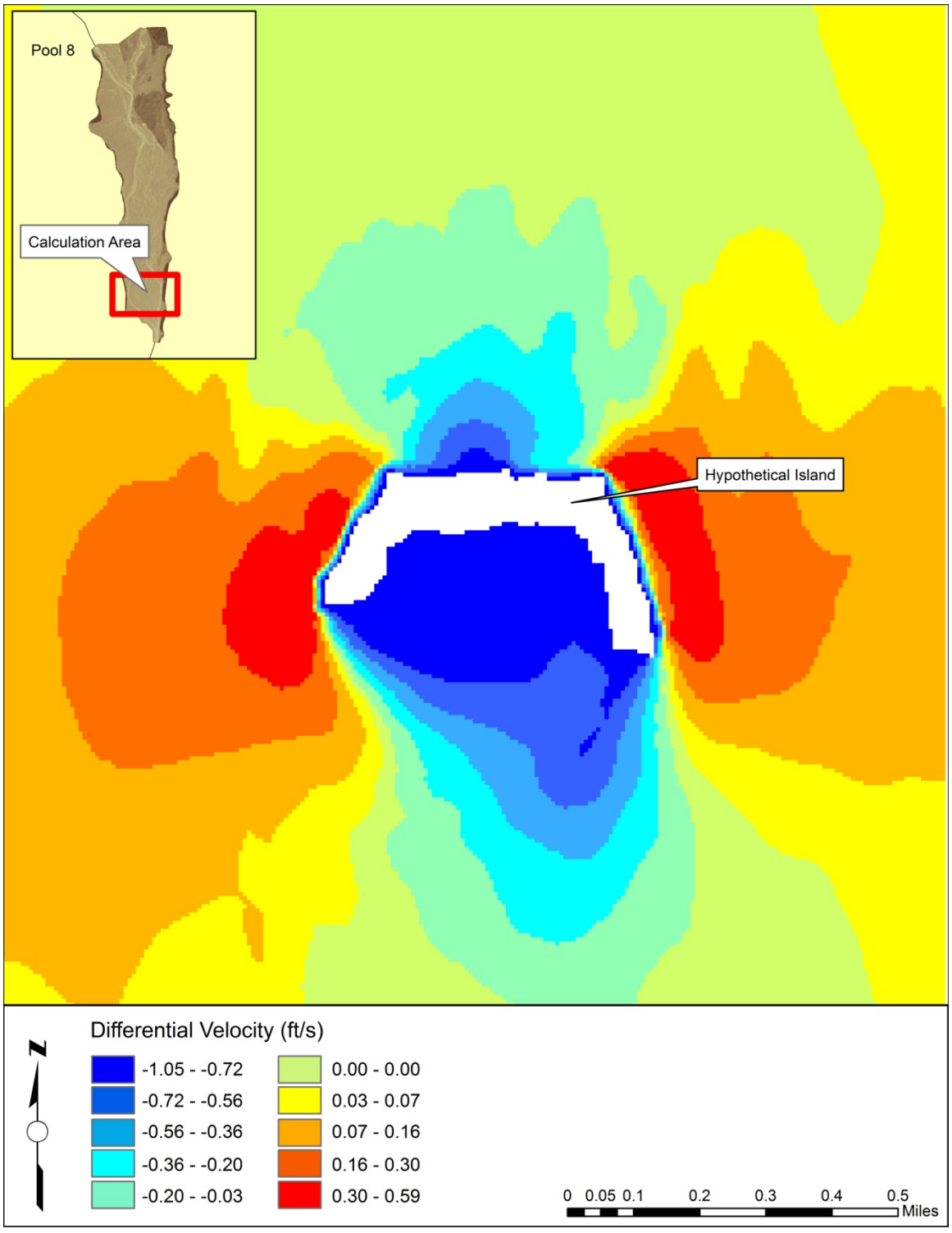

Figure 4.17. Velocity differential around hypothetical island at 100,000 ft^3/s discharge through Lock and Dam 8.

Table 4.2. Travel time results and amount of particles exiting model for Lock and Dam 7.

Residence Time for Lock and Dam 7 (days)					
Flow Case (ft^3/s)	Average	Maximum	Minimum	Standard Deviation	% of Particles Exiting
10,000	4.99	5.14	4.91	0.06	100.00
33,000	1.47	1.52	1.44	0.02	100.00
100,000	0.73	0.80	0.69	0.03	100.00

Table 4.3. Travel time results and amount of particles exiting model for French Island Spillway.

Residence Time for French Island Spillway (days)					
Flow Case (ft^3/s)	Average	Maximum	Minimum	Standard Deviation	% of Particles Exiting
10,000	0.00	0.00	0.00	0.00	0.00
33,000	0.00	0.00	0.00	0.00	0.00
100,000	1.07	1.12	1.06	0.01	7.00

Table 4.4. Travel time results and amount of particles exiting mode for Onalaska Dam.

Residence Time for Onalaska Spillway (days)					
Flow Case (ft^3/s)	Average	Maximum	Minimum	Standard Deviation	% of Particles Exiting
10,000	10.40	11.07	10.21	0.22	100.00
33,000	3.99	4.33	3.92	0.10	100.00
100,000	3.41	3.66	3.31	0.10	100.00

Table 4.5. Travel time results and amount of particles exiting the model for Root River.

Residence Time for Root River (days)					
Flow Case (ft^3/s)	Average	Maximum	Minimum	Standard Deviation	% of Particles Exiting
10,000	5.55	5.57	5.53	0.01	80.00
33,000	1.83	2.71	1.78	0.15	91.00
100,000	0.80	3.66	0.78	0.16	82.00

Table 4.6. Travel time results and amount of particles exiting the mode for La Crosse River.

Residence Time for Lacrosse River (days)					
Flow Case (ft^3/s)	Average	Maximum	Minimum	Standard Deviation	% of Particles Exiting
10,000	7.51	7.75	7.39	0.09	100.00
33,000	2.92	2.98	2.88	0.03	78.00
100,000	1.85	1.92	1.80	0.03	100.00

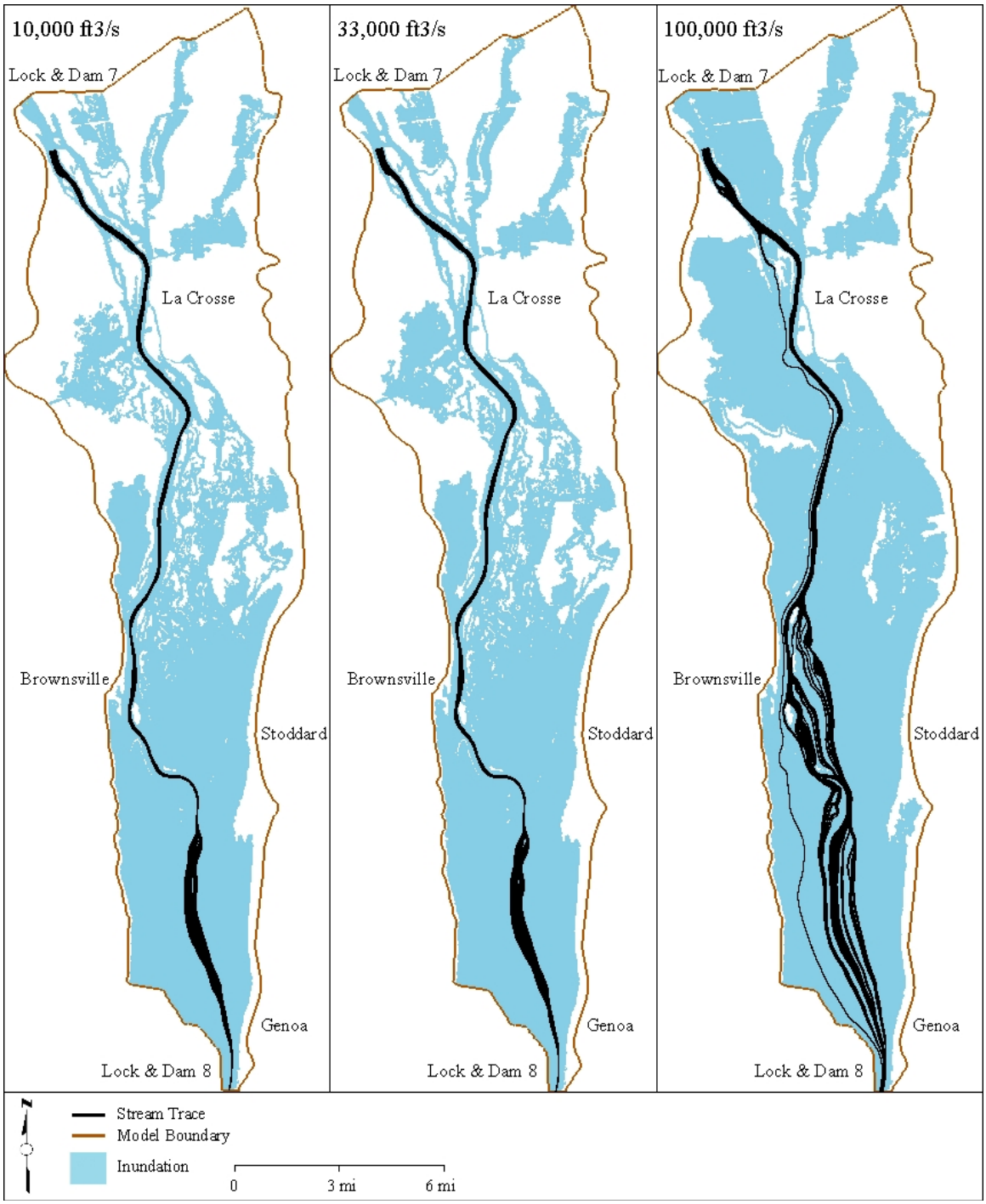

Figure 4.18. Stream trace paths for 500 particles injected at Lock and Dam 7 inlet.

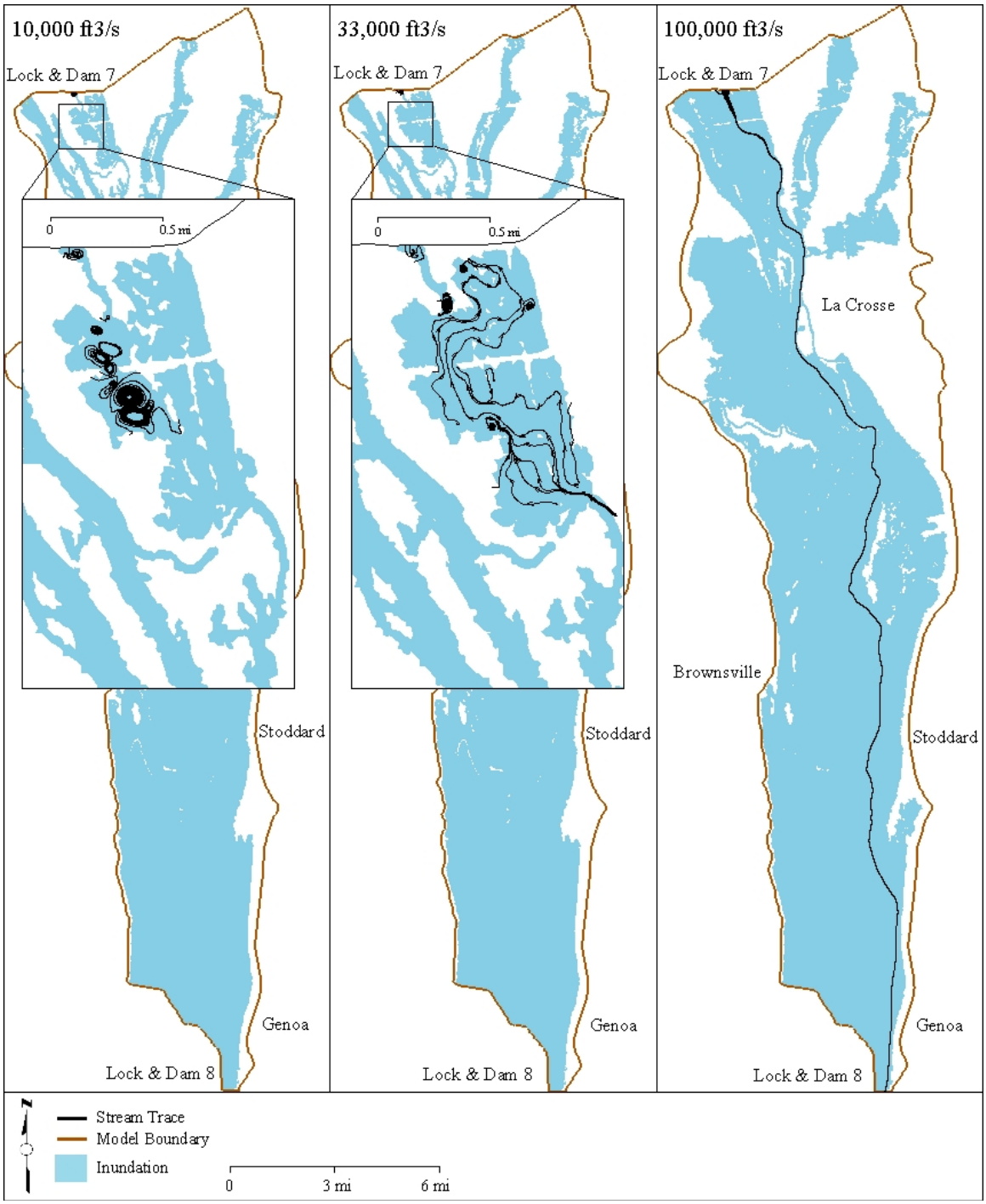

Figure 4.19. Stream trace paths for 500 particles injected at French Island Spillway inlet.

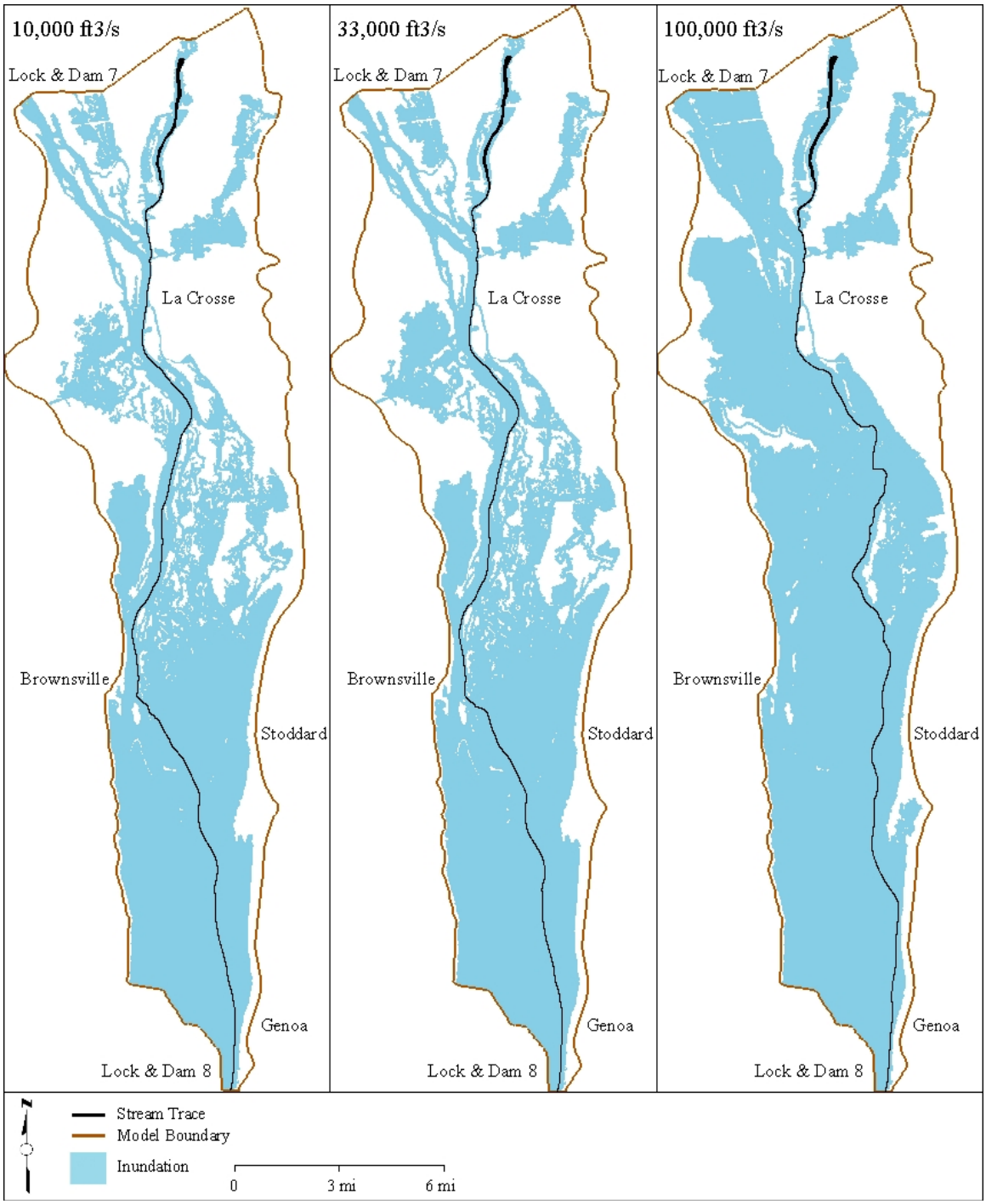

Figure 4.20. Stream trace paths for 500 particles injected at Onalaska Dam inlet.

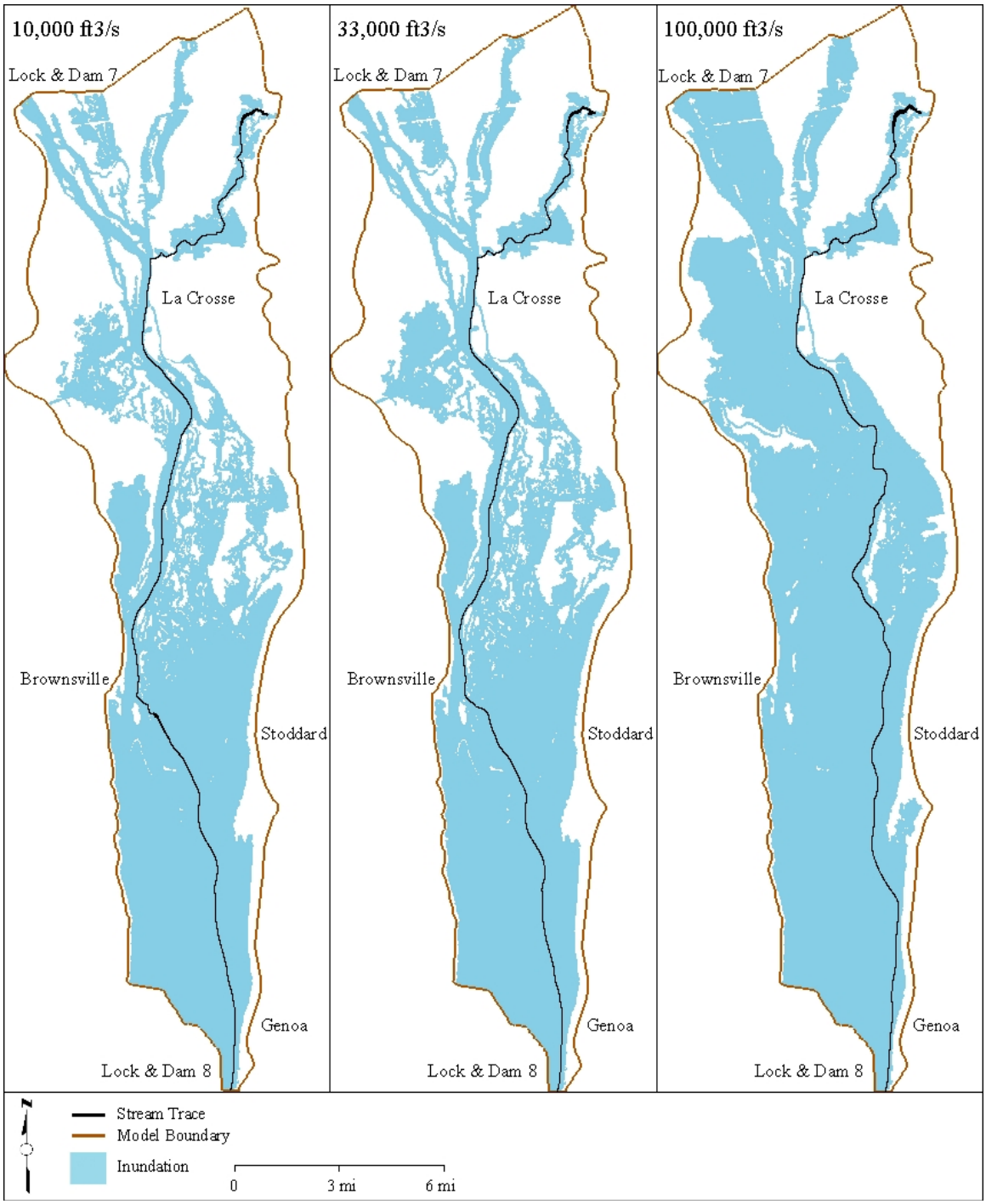

Figure 4.21. Stream trace paths for 500 particles injected at the La Crosse River inlet.

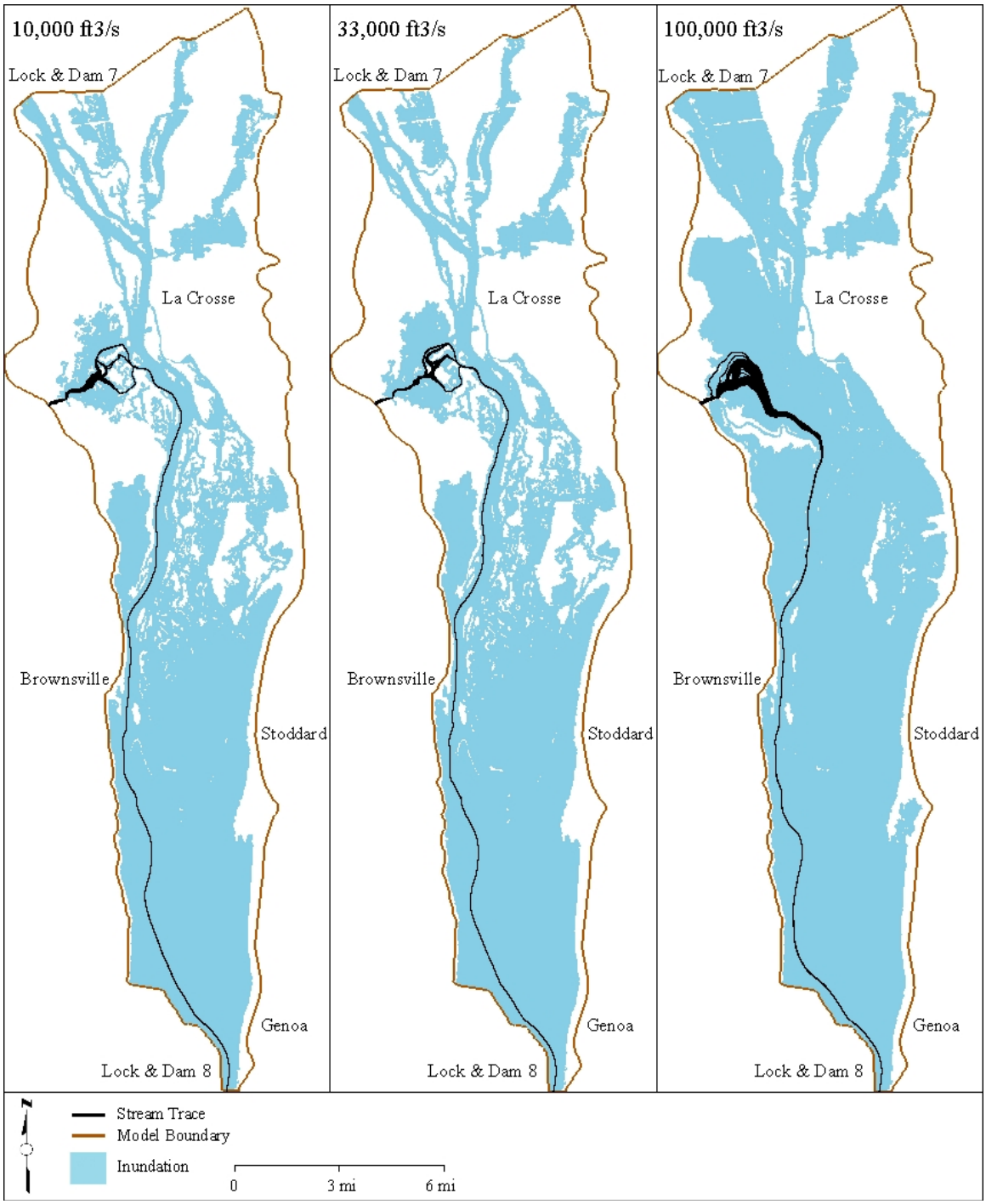

Figure 4.22. Stream trace paths for 500 particles injected at the Root River inlet.

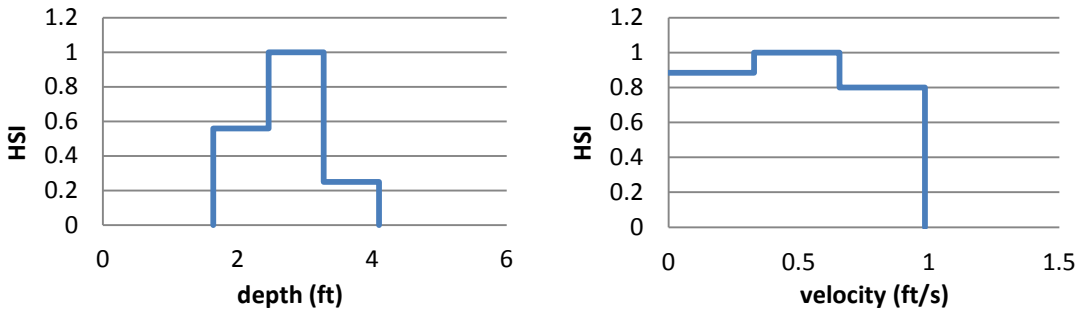

Figure 4.23. Potential habitat suitability curves for emergent vegetation of depth (left) and velocity (right) for field data.

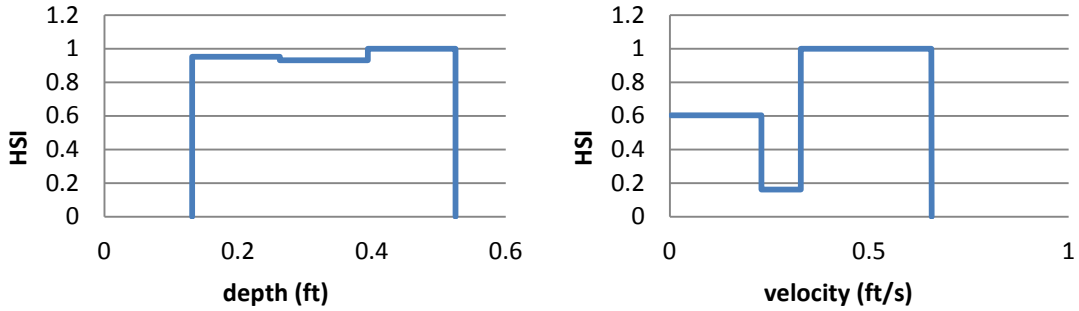

Figure 4.24. Potential habitat suitability curves for emergent vegetation of depth (left) and velocity (right) for 10,000 ft^3/s discharge through Lock and Dam 8.

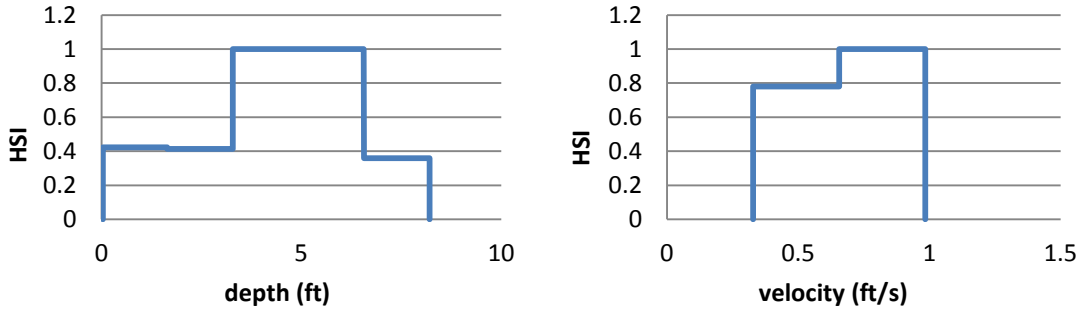

Figure 4.25. Potential habitat suitability curves for emergent vegetation of depth (left) and velocity (right) for 21,000 ft^3/s discharge through Lock and Dam 8.

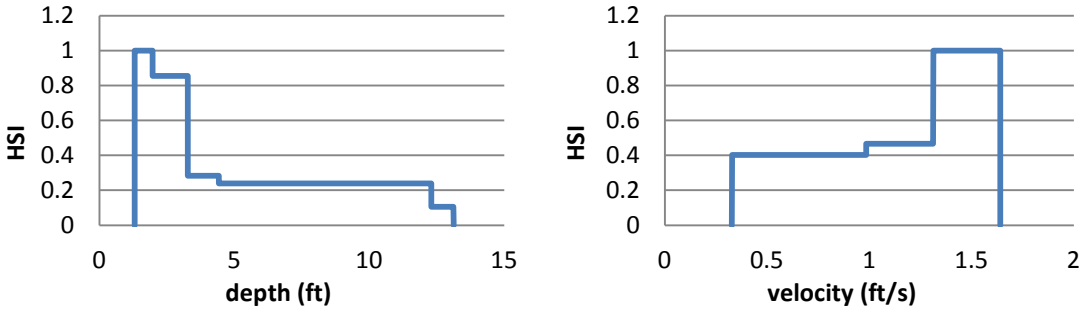

Figure 4.26. Potential habitat suitability curves for emergent vegetation of depth (left) and velocity (right) for 35,000 ft^3/s discharge through Lock and Dam 8.

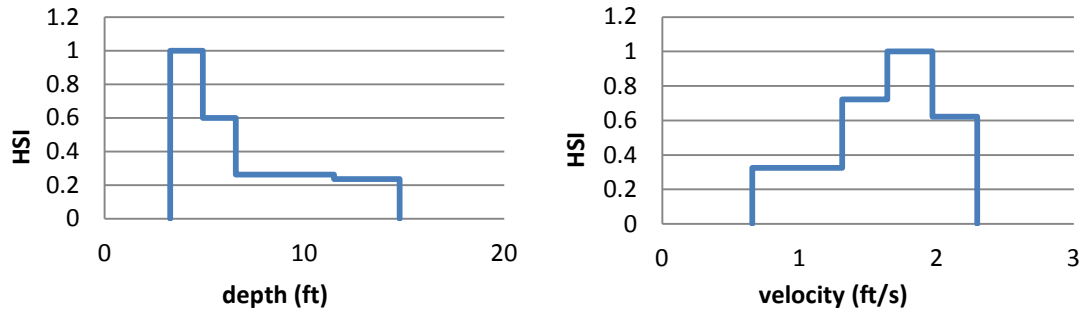

Figure 4.27. Potential habitat suitability curves for emergent vegetation of depth (left) and velocity (right) for 63,000 ft^3/s discharge through Lock and Dam 8.

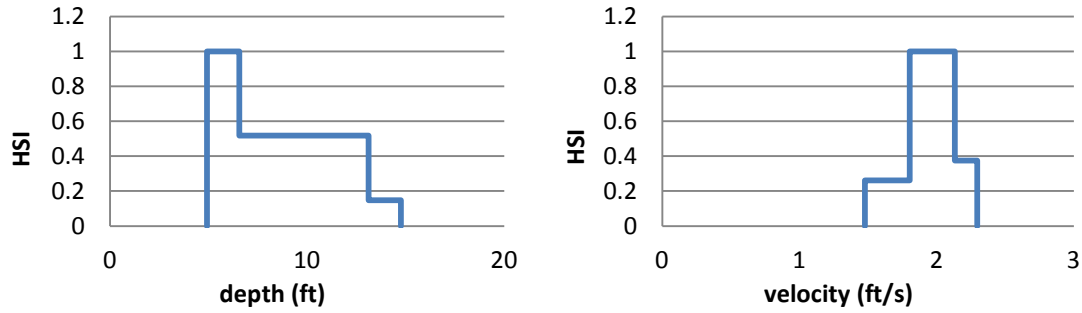

Figure 4.28. Potential habitat suitability curves for emergent vegetation of depth (left) and velocity (right) for 90,000 ft^3/s discharge through Lock & Dam 8.

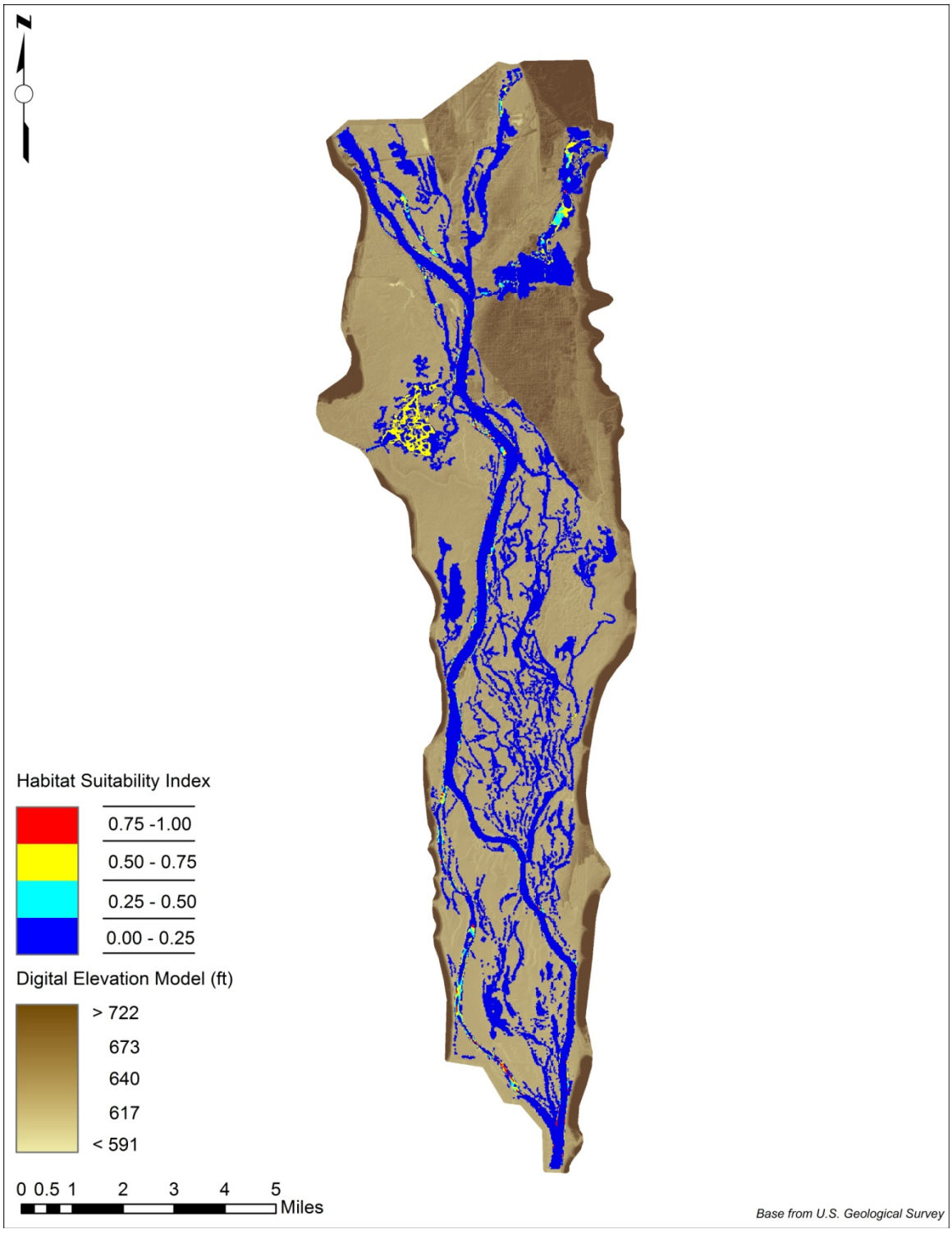

Figure 4.29. Potential habitat suitability map of emergent vegetation for 10,000 ft^3/s discharge through Lock and Dam 8 (Base Data Source: USGS, 2010b). Data flooded by dark brown extends to elevation 1,178 feet and data flooded by light brown extends to elevation 561 feet.

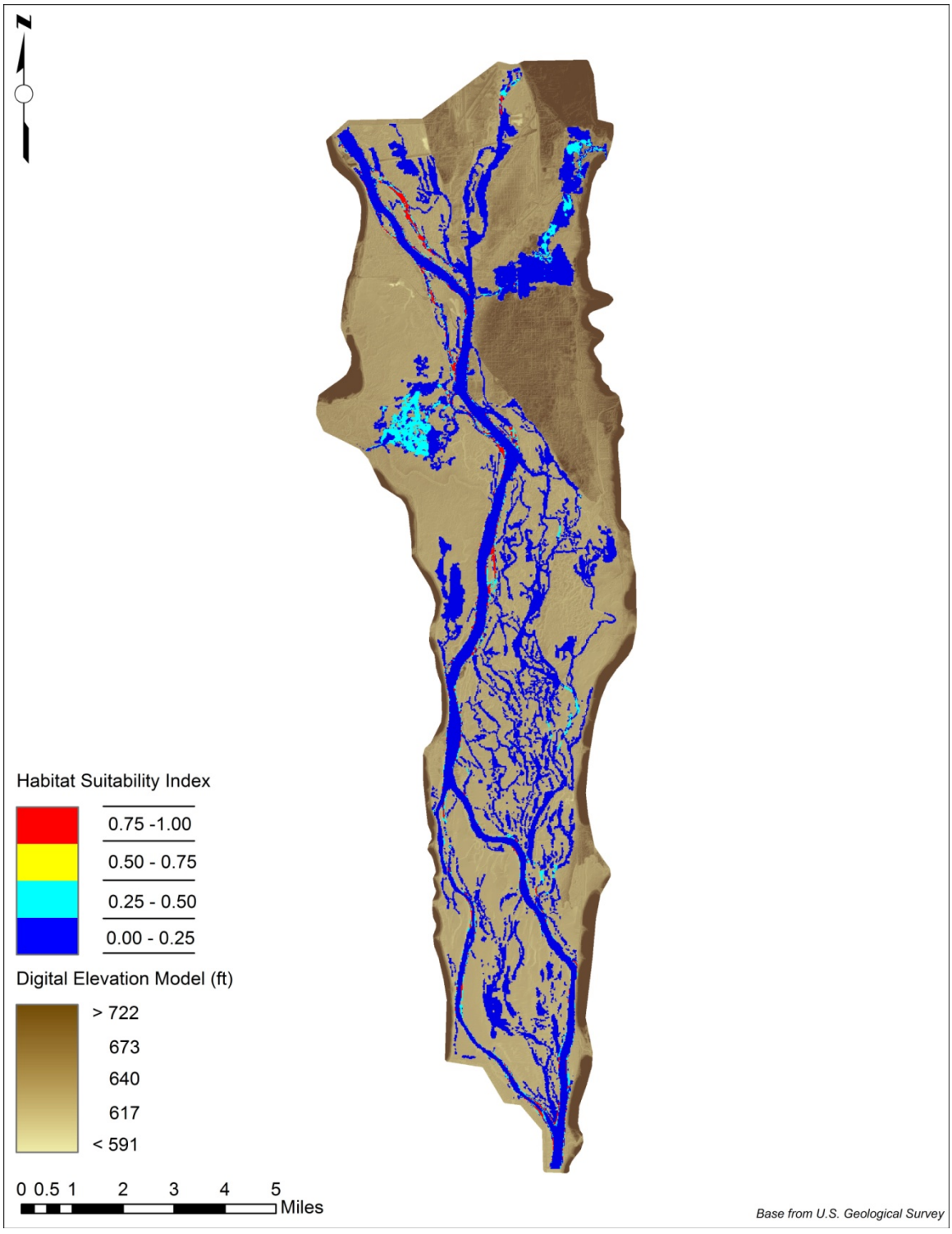

Figure 4.30. Potential habitat suitability map of emergent vegetation for 21,000 ft^3/s discharge through Lock and Dam 8 (Base Data Source: USGS, 2010b). Data flooded by dark brown extends to elevation 1,178 feet and data flooded by light brown extends to elevation 561 feet.

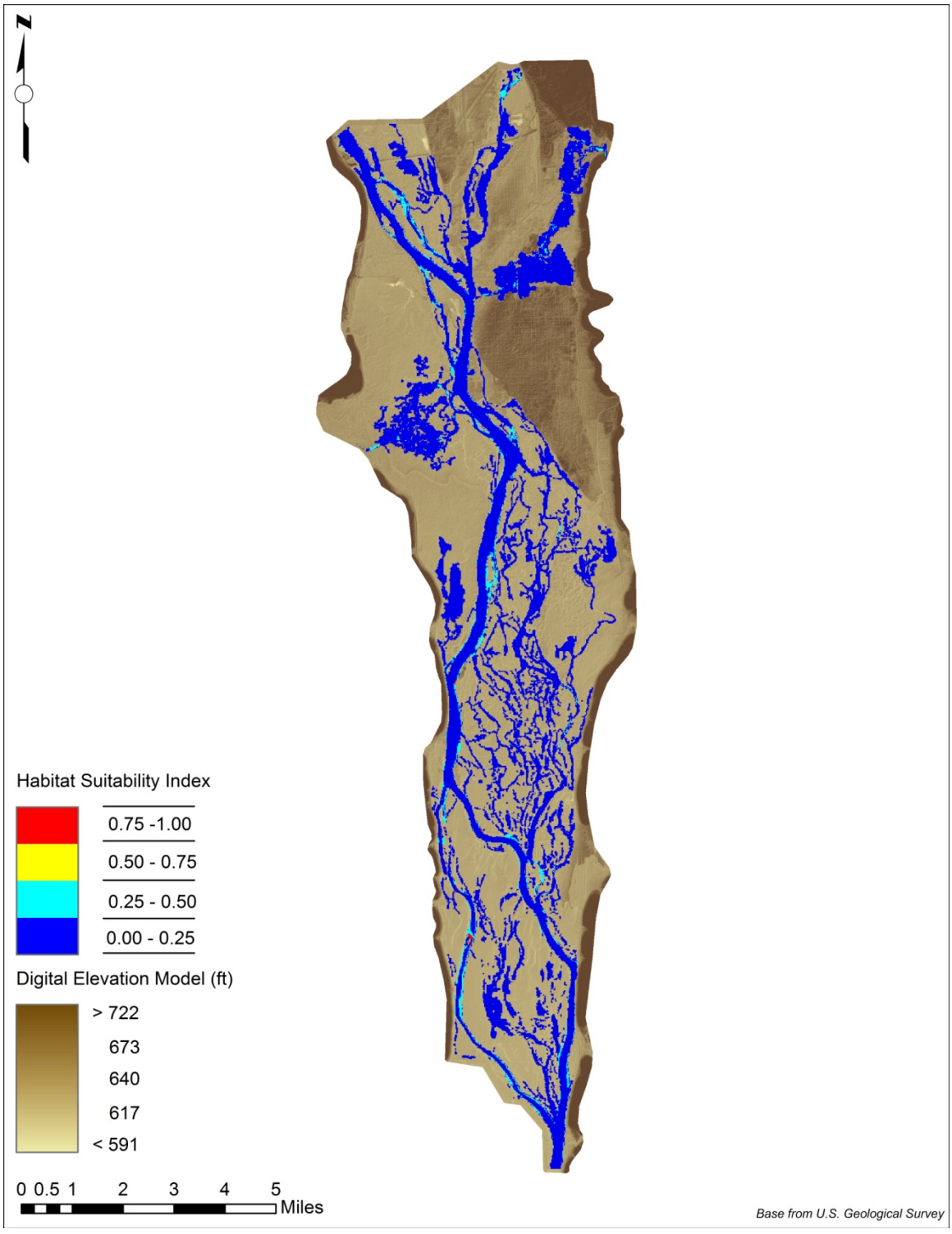

Figure 4.31. Potential habitat suitability map of emergent vegetation for 35,000 ft^3/s discharge through Lock and Dam 8 (Base Data Source: USGS, 2010b). Data flooded by dark brown extends to elevation 1,178 feet and data flooded by light brown extends to elevation 561 feet.

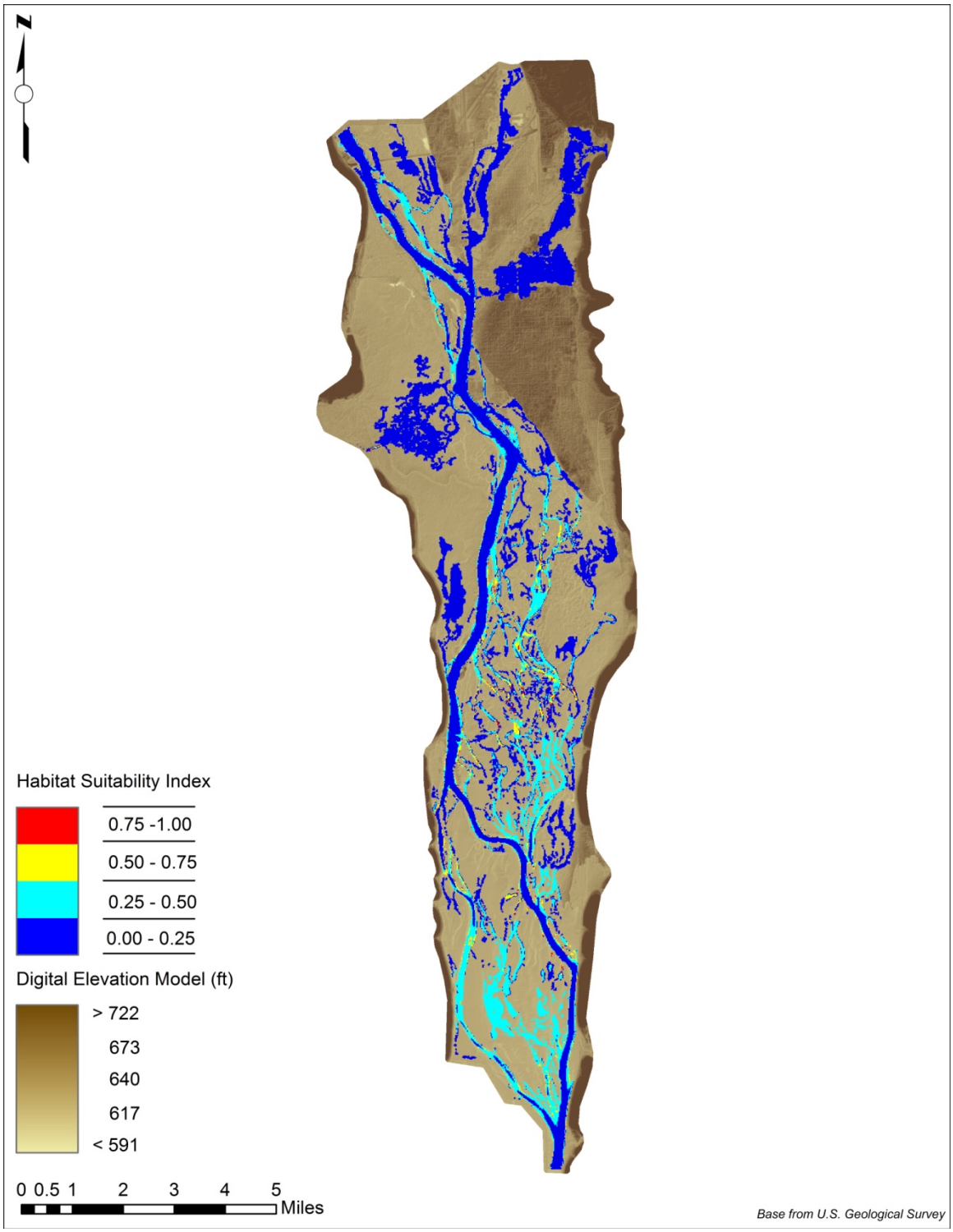

Figure 4.32. Potential habitat suitability map of emergent vegetation for 63,000 ft^3/s discharge through Lock and Dam 8 (Base Data Source: USGS, 2010b). Data flooded by dark brown extends to elevation 1,178 feet and data flooded by light brown extends to elevation 561 feet.

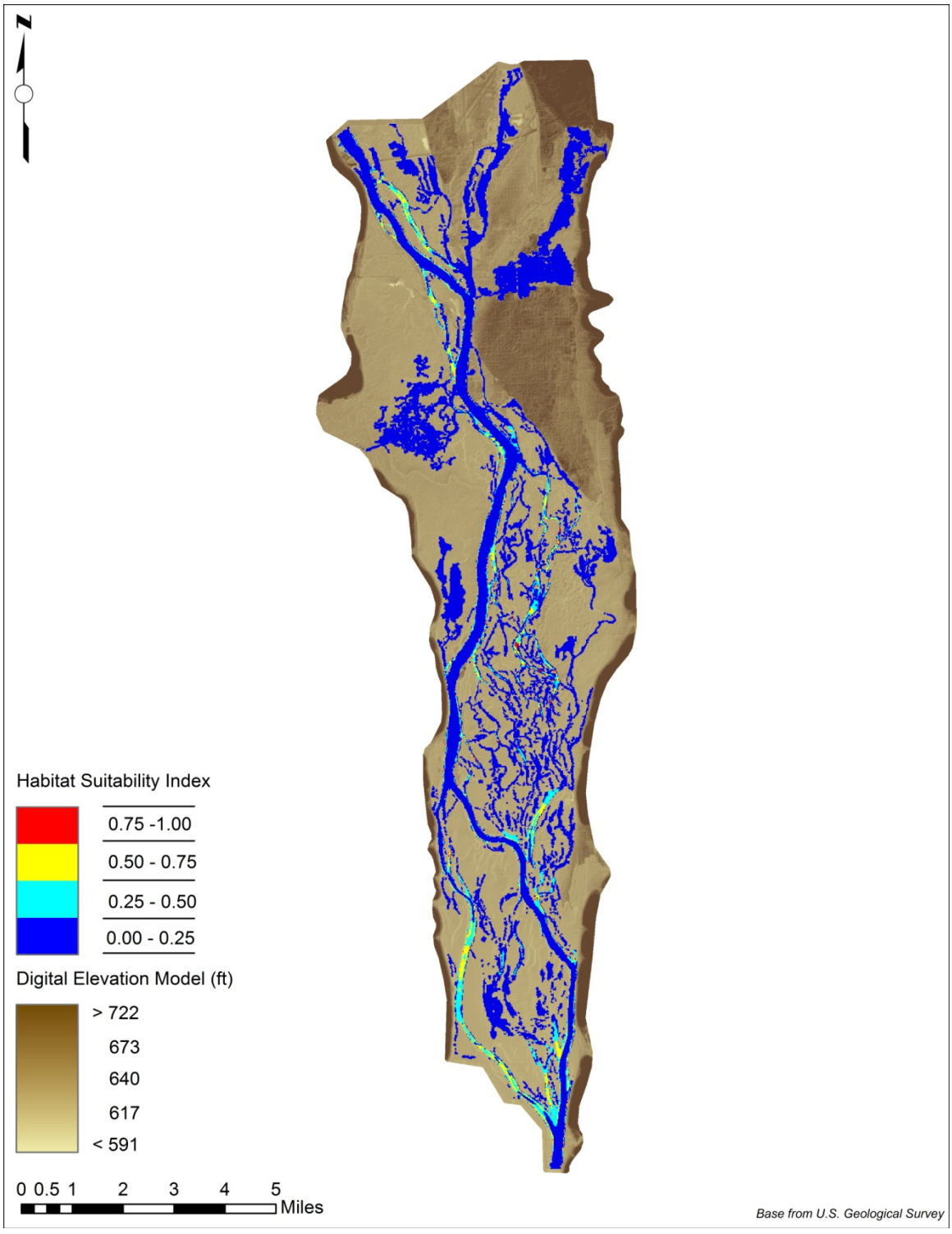

Figure 4.33. Potential habitat suitability map of emergent vegetation for 90,000 ft^3/s discharge through Lock and Dam 8 (Base Data Source: USGS, 2010b). Data flooded by dark brown extends to elevation 1,178 feet and data flooded by light brown extends to elevation 561 feet.

Table 4.7. Comparison of habitat suitability area for emergent vegetation during 10,000 ft^3/s, 21,000 ft^3/s, 35,000 ft^3/s, 60,000 ft^3/s and 90,000 ft^3/s.

Area of Suitable Habitat for Emergent Vegetation (mi^2)					
Suitability Index	10,000 ft^3/s	21,000 ft^3/s	35,000 ft^3/s	63,000 ft^3/s	90,000 ft^3/s
0.75 - 1.00	0.16	0.63	0.06	0.08	0.15
0.50 - 0.75	1.04	0.00	0.00	0.66	0.74
0.25 -0.50	0.33	1.51	0.95	4.58	1.58
0.00 - 0.25	17.86	16.41	17.53	13.81	16.68

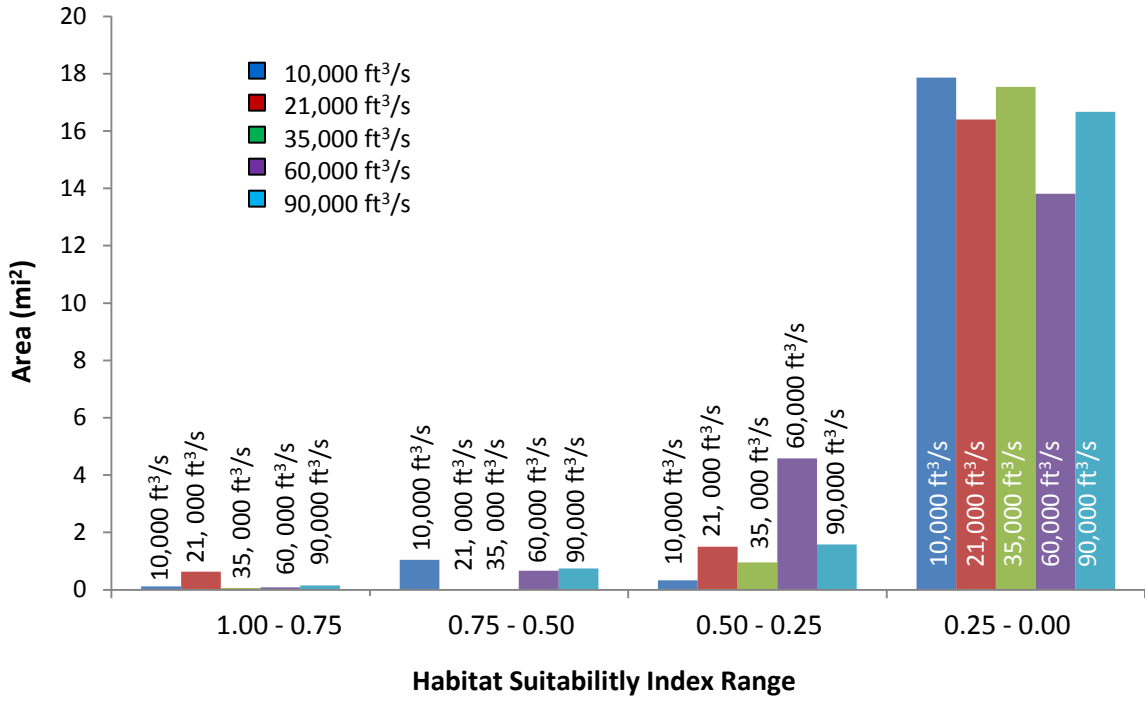

Figure 4.34. Comparison of habitat suitability area for emergent vegetation during 10,000 ft^3/s, 21,000 ft^3/s, 35,000 ft^3/s, 60,000 ft^3/s and 90,000 ft^3/s.

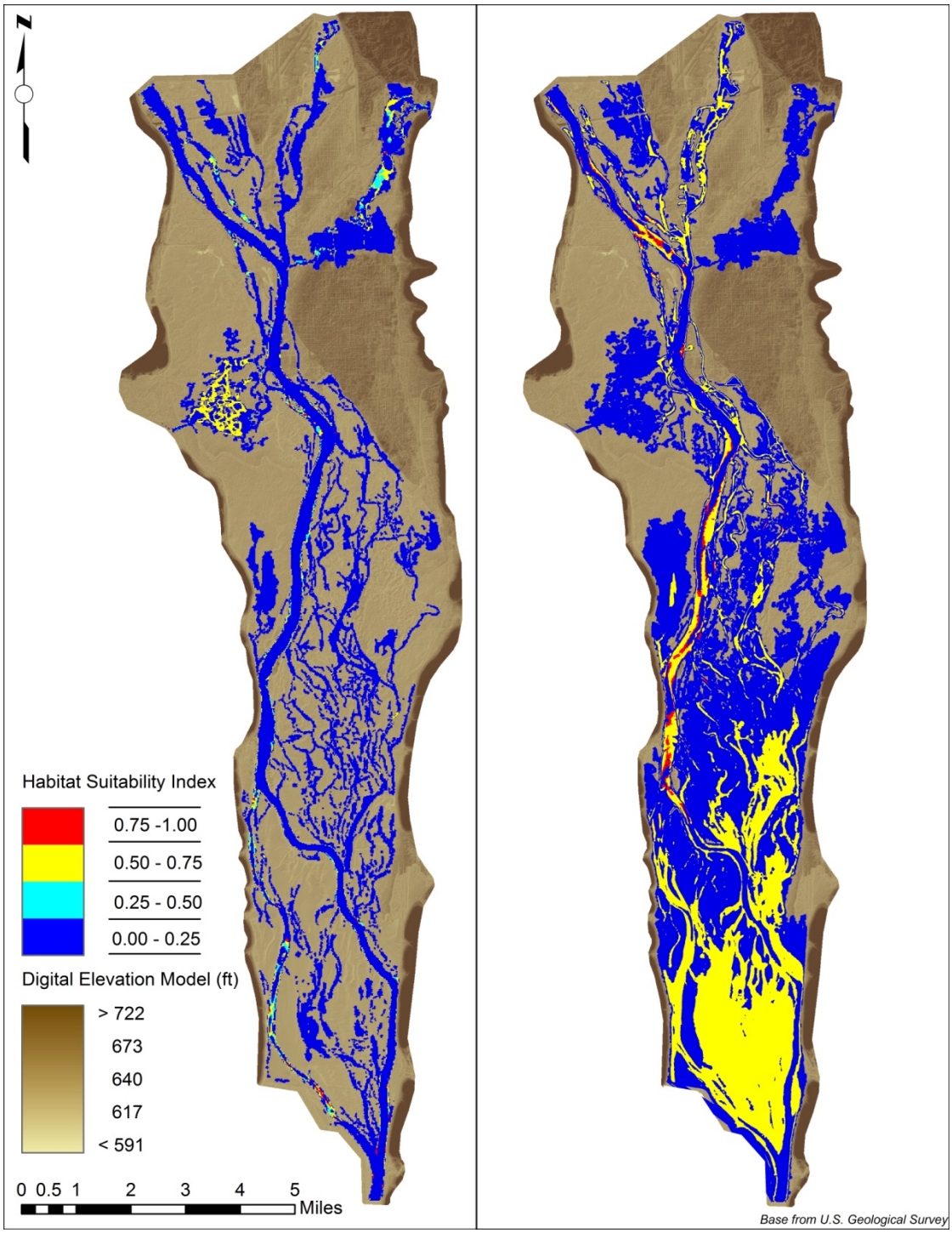

Figure 4.35. Comparison of emergent vegetation habitat suitability maps at 10,000 ft^3/s (left) and 10,000 ft^3/s with initial conditions of 33,000 ft^3/s simulations (right) (Base Data Source: USGS, 2010b). Data flooded by dark brown extends to elevation 1,178 feet and data flooded by light brown extends to elevation 561 feet.

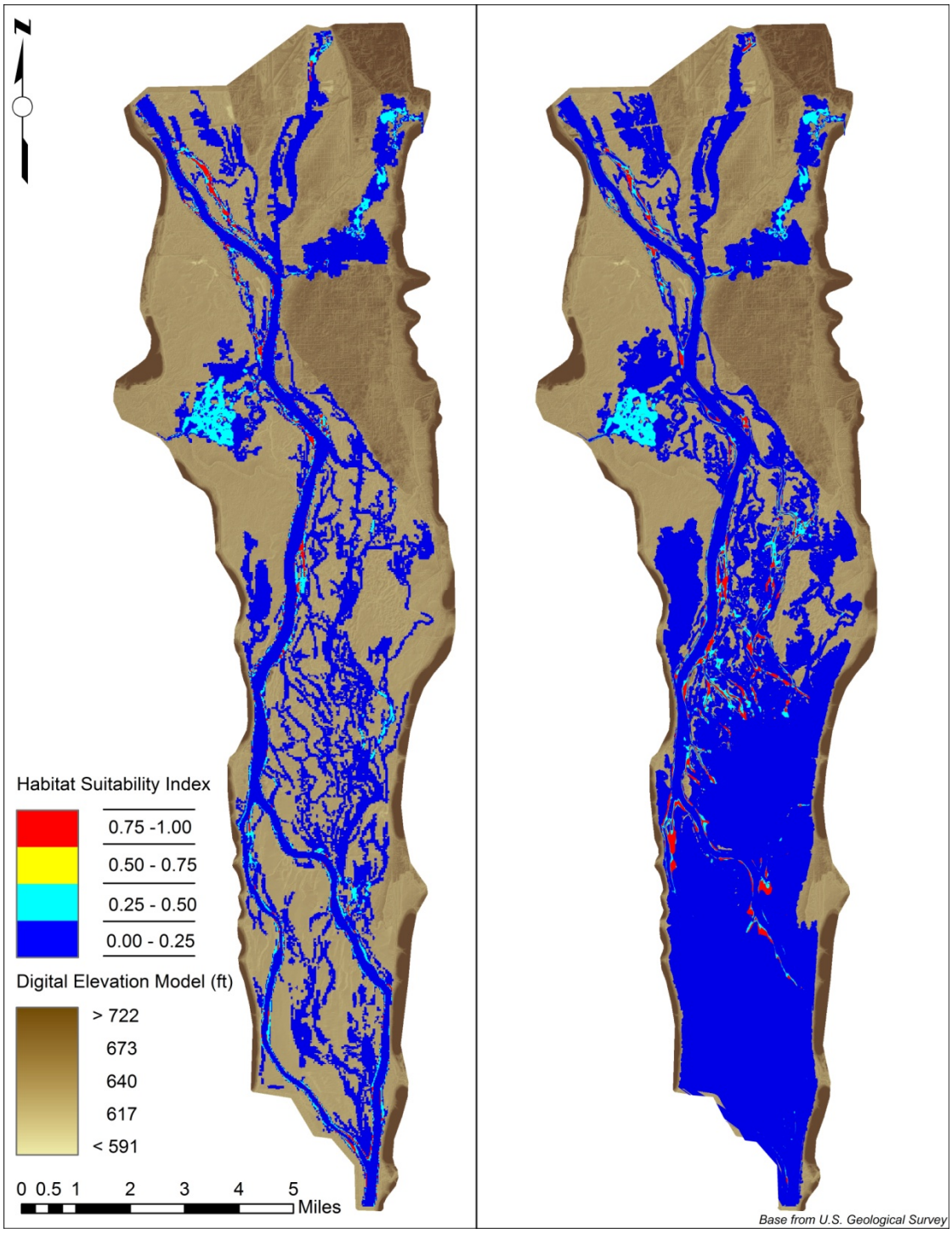

Figure 4.36. Comparison of emergent vegetation habitat suitability maps at 21,000 ft^3/s (left) and 21,000 ft^3/s with initial conditions of 33,000 ft^3/s simulations (right) (Base Data Source: USGS, 2010b). Data flooded by dark brown extends to elevation 1,178 feet and data flooded by light brown extends to elevation 561 feet.

Table 4.8. Comparison of 10,000 ft3/s and 21,000 ft3/s for emergent vegetation habitat suitability area.

Area of Suitable Habitat for Emergent Vegetation (mi2)				
Suitability Index	10,000 ft3/s	10,000 ft3/s with 33,000 ft3/s initial condition	21,000 ft3/s	21,000 ft3/s with 33,000 ft3/s initial condition
0.75 - 1.00	0.12	0.44	0.63	1.31
0.50 - 0.75	1.04	11.61	0.00	0.00
0.25 -0.50	0.33	0.00	1.51	2.08
0.00 - 0.25	17.86	28.93	16.41	37.78

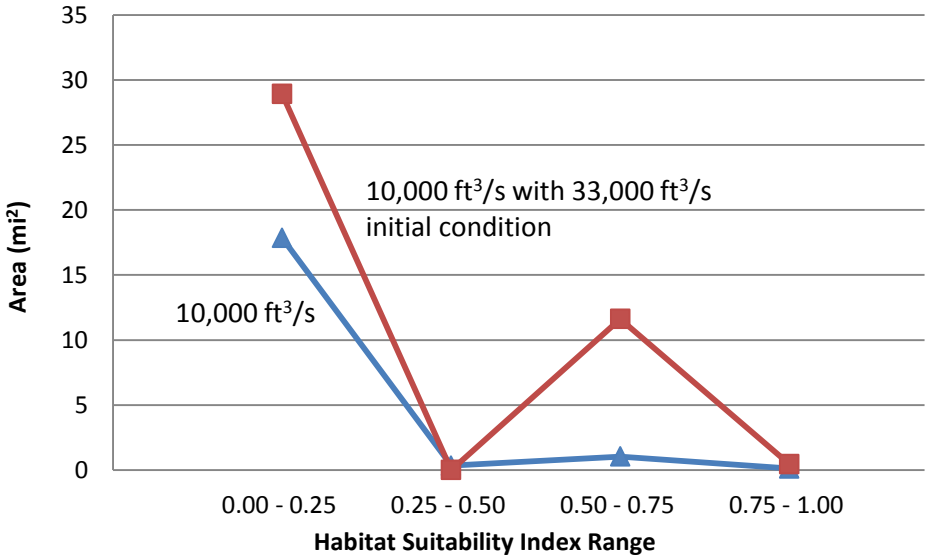

Figure 4.37. Comparison of habitat suitability area for emergent vegetation during 10,000 ft^3/s and 10,000 ft3/s with 33,000 ft^3/s initial condition.

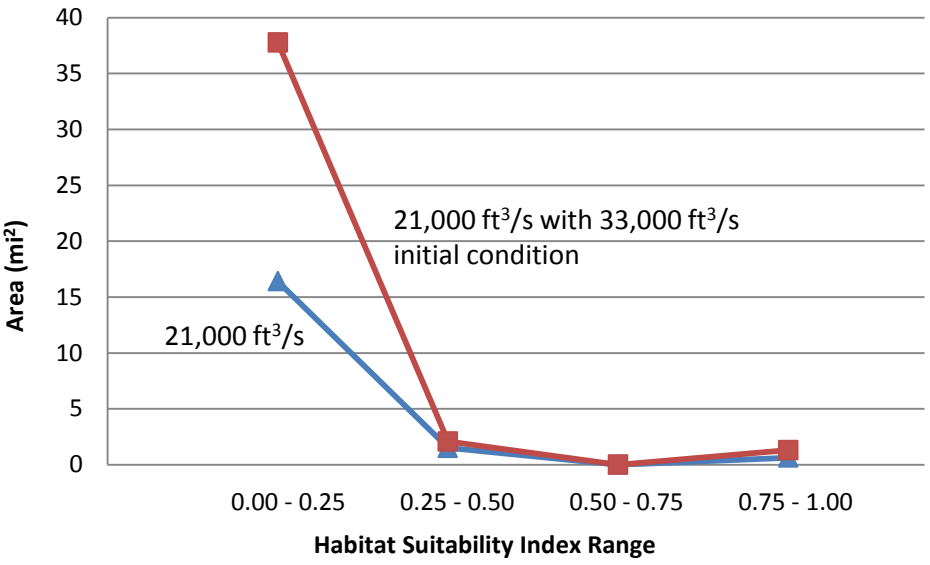

Figure 4.38. Comparison of habitat suitability area for emergent vegetation during 21,000 ft3/s and 21,000 ft3/s with 33,000 ft3/s initial condition.

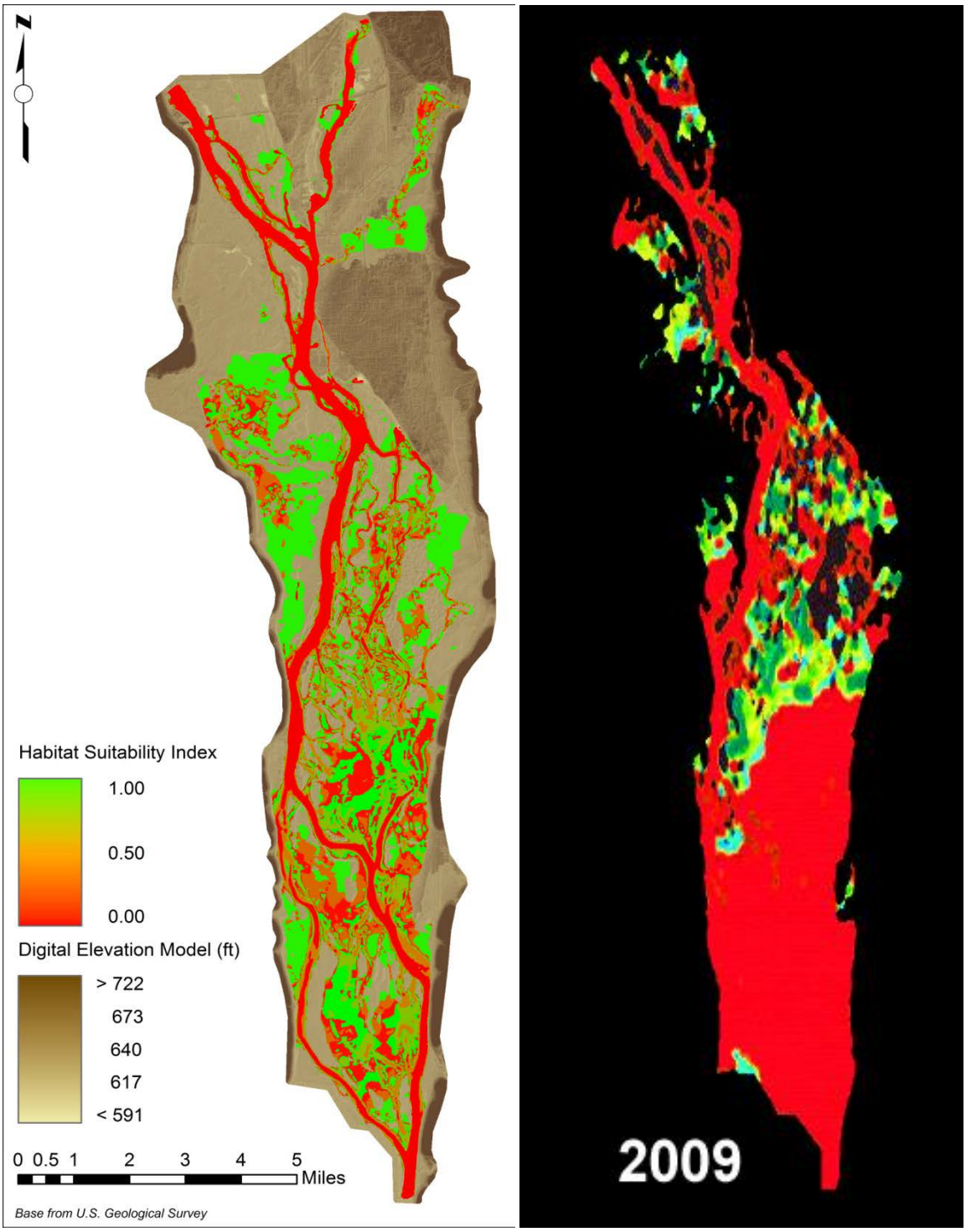

Figure 4.39. Comparison of habitat suitability area for emergent vegetation simulated map (left) and USGS map (right). (Base Data Source: USGS, 2010b). Data flooded by red represents habitat suitability index of zero and data flooded by green represents a habitat suitability index of one for both maps.

CHAPTER: 5 JOINING HYDRODYNAMIC AND ECOLOGICAL MODELS

5.1 Overview

Understanding the hydrodynamics of large river systems is crucial for ecological and river management assessments. Not only are the hydrodynamic parameters important, but understanding the ecological phenomena within large rivers can aid in restoration, management, and future data collection. In order to recognize ecological processes in aquatic environments, the source of productivity must be discovered. There are three methods in which organic material can be supplied to river systems, by the river continuum concept, the river productivity model, and the flood-pulse-concept (Dettmers et al., 2001). The river continuum concept conveys that organic material is due to terrestrial inputs at headwaters and then travels downstream due to flow patterns. The river productivity model states that productivity comes from organic producers from within the river system. The flood pulse concept states that production originates from when rivers flow out of bank into the floodplain and when the river recedes, it brings the organic material from the floodplain into the river (Amato et al., 2010).

5.2 Ecological Model

Amato et al., (2010) have been developing an ecological model that simulates the carbon cycle within a reach of the UMR. The model joins ecological and hydrodynamic properties in order to assess the carbon cycle and determine what the primary sources of productivity are within the system. The models goals are to simulate productivity, in which the model will support the river productivity model theory. If the model dose not accurately simulate productivity, the two other river productivity theories will have to be incorporated into future work.

The model simulates basic carbon cycles using simple food webs that are interwoven into the hydrodynamic parameters (Amato et al., 2010). The model was first

implemented in Pool 5 of the UMR. The general concept behind the model is a system of grid cells that are pushed along by the hydrodynamic properties, while at each time step within a grid cell, carbon is consumed or released (Amato et al., 2010). Early results prove that the model could successfully simulate the transfers of carbon through the river reach, which was a difficult task due to spatial, temporal, and anthropogenic variability within the pool. The model supported the river productivity model by proving the productivity within the river is greatly influenced by the hydrodynamics parameters. Many ecological phenomena in the river system depend on depth and velocity in order to successfully occur, and this model proved that those phenomena depend on the hydrodynamics of the river (Amato et al., 2010).

5.3 IIHR – Hydroscience and Engineering Contribution

The ecological models next steps were to be implemented in Pool 8 of the UMR along with some improvements made by the University of Illinois and UMSEC. IIHR – Hydroscience and Engineering was tasked with compiling a library of flow data for Pool 8 in which the model would use as the hydrodynamic input. The completed library of flow scenarios cover an annual hydrograph ranging from 10,000 ft^3/s to 100,000 ft^3/s (283 m^3/s to 2831 m^3/s) incrementing by 10,000 ft3/s (283 m^3/s). Along with the ten average flow scenarios, a drawdown flow condition was modeled. The drawdown conditions were taken from a historic drawdown performed in Pool 8 in 2001. There were six steady state flows simulated, which corresponded to six days along the drawdown process. The days that were simulated during the drawdown period can be seen in Figure 5.1.

5.4 Future Work

The next step in the process is to take the results from the ecological model and incorporate them into the hydrodynamic model. This would require manipulation of the SRH-2D source code from the United State Bureau of Reclamation (USBR). The code

would be manipulated so that the equations used in the ecological model would be set in the hydrodynamic code and the two models could run simultaneously. This would require a great deal of coding and effort from both parties. An increase in funding from government sources and corporation from the USBR would be needed so that the future work could be completed.

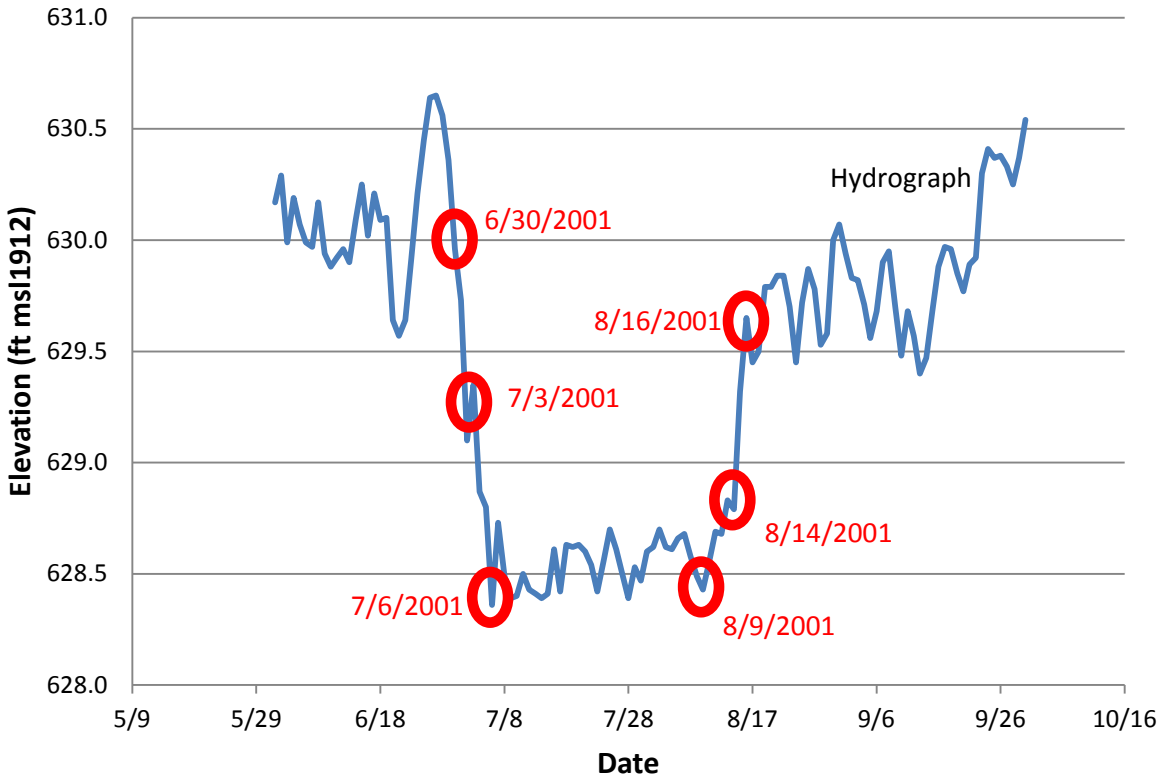

Figure 5.1. 2001 Pool 8 drawdown hydrograph showing dates for University of Illinois steady state drawdown simulations (Data Source: USGS, 2010b).

CHAPTER: 6 SUMMARY AND CONCLUSIONS

Hydrodynamic models are efficient and powerful tools for resource planning and management in river systems. These models can simulate future scenarios and predict field events on the river improving the knowledge of biologists and river managers, for informed decision making, cost savings, and intended project outcomes. Hydrodynamic models provide field biologists with new information on flow, velocity, depth, roughness, and travel times (to name a few parameters) to build a framework for habitat restoration and adaptive management.

Hydrodynamic model can be one-, two-, or three-dimensional depending on the specific objectives and goals of the project. A two-dimensional model in large river systems often provides a good balance between accuracy, detail, and time. The current study's goal, conducted in Pool 8 of the UMR near La Crosse, Wisconsin, was to create a two-dimensional hydrodynamic model that resolved flow in the main channel and backwater areas. The model was constructed using 18 unique roughness coefficients based on primary literature and land cover values provided by U.S. Geological Survey, Upper Mississippi River Environmental Science Center. The model was calibrated to an extracted water surface elevation profile from LiDAR data provided by the U.S. Geological Survey and validated using water surface elevation profile measurements along with a discharge comparison at 17 transects within Pool 8. Applications for the model included a hypothetical island, travel time study, drawdown scenarios, habitat suitability assessment, and collaboration with the University of Illinois in joining the model results with an ecological model that they are developing.

The Pool 8 model was able to accurately simulate a range of steady state flow scenarios in 10,000 ft^3/s (283 m^3/s) increments from 10,000 ft^3/s to 100,000 ft^3/s (283 m^3/s to 2,832 m^3/s) which provided the results for a "flow library" used in all the model applications. Products included depth and velocity histograms for three steady state flow

scenarios low, 10,000 ft^3/s (283 m^3/s); medium, 33,000 ft^3/s (943 m^3/s); and high, 100,000 ft^3/s (2,832 m^3/s) which showed how depth and velocity increased in the pool as discharge increased. The drawdown results demonstrated that conducting a drawdown is more successful during lower flows, and provided depth and velocity histograms that can be very useful to biologists in improving their knowledge about the hydrodynamics in the pool during a drawdown. Implementation of the hypothetical island demonstrated the creation of an area of reduced velocities in deeper water behind the island along with increased flow rates in the main and secondary channels. Travel time studies completed from every inlet into Pool 8 illustrated the effect that as discharge increased the travel time for the five inlets increased as well with increased recirculation at the higher discharges The habitat suitability assessment demonstrated that emergent vegetation habitat is independent of discharge and the area of suitable habitat stays constant during all simulated flow rates. Lastly, the results from the steady state simulations provided the driving parameters for an ecological model developed at the University of Illinois and UMSEC, which can educate biologists and river managers on how nutrients move and interact within the pool.

Future work for the Pool 8 model might include several new scenarios and techniques as data becomes more readily available. For example, constructing the same model with improved bathymetry would allow the model to be more accurate and capture local flow patterns, which biologists need to understand habitat suitability. A new habitat suitability assessment in the pool could be conducted that included more field data other than presence and absence of a species. Including more habitat parameters, e.g. substrate, turbidity, light, and nutrients would allow for a more comprehensive habitat suitability assessment. New data on substrate and sediment type in the pool would also improve roughness coefficients and now the model reacts to flow conditions.

A pool wide scale unsteady state model that incorporated a large portion of the annual hydrograph would provide biologists with often needed unsteady data in order to

understand species fate transport. Biologists are also interested in smaller scale areas within the pool involving nutrient removal, which would require more detailed three-dimensional models that include the vertical aspects, similar to an earlier research study by The University of Iowa, IIHR conducted in Round Lake of Pool 8. A few locations of specific interest in Pool 8 would be selected for small nested three-dimensional models using the results from the two-dimensional model as boundary conditions.

Lastly, incorporation of the ecological data, from the University of Illinois carbon model, into the hydrodynamic model has the potential to more fully couple these two models. However, incorporating the ecological equations would require manipulation of the source code in SRH-2D. Implementing ecological processes within the hydrodynamic model may result in a very comprehensive model that would be invaluable to all biologists and river managers in the UMR.

BIBLIOGRAPHY

Amato, K. R., et al. "A Spatially - Explicit Carbon Cycle Model in Pool 5 of the Mississippi River." *INDO-US Bilateral Workshop of Sedimentation, Erosion, and Ecological Health of Rivers.* Kolkata, India, 2010. 57-74.

Anderson, J.D. *Computational Fluid Dynamics.* New York, NY: McGraw-Hill, Inc., 1995.

AQUAEVO. *SMS 10.0 Overview.* 2011. http://www.ems-i.com/SMS/SMS_Overview/sms_overview.html (accessed 2010-2011).

Bates, P. D., and A.P.J. De Roo. "A Simple Raster-Based Model for Flood Inundation Simulation." *Journal of Hydrology*, 2000: 54-77.

Chow, V. T. *Open-Channel Hydraulics.* New York: McGraw-Hill, 1959.

Crowder, D. W. "Reporducing and Quantifying Spatial Flow Patterns of Ecological Imporatnace with Two-Dimensional Hydraulic Models." *Ph.D. Diss.* Blacksburg, VA: Virginia Polytechnic Institute and State University, 2002.

Crowder, D. W., and P. Diplas. "Applying Spatial Hydraulic Principles to Quantify Stream Habitat." *River Research and Applications*, 2006: 79-89.

Crowder, D. W., and P. Diplas. "Using Two-Dimensional Hydrodynamic Models at Scales of Ecological Importance." *Journal of Hydrology*, 2000: 172-191.

Cunge, J. A., F. M. Holly, and A. Verwey. *Practical Aspects of Computational River Hydraulics.* London: Pitman Publishing Limited, 1980.

Delaney, Robert L. *Ecological Status and Trends of the Upper Mississippi River System.* Long Term Resource Monitoring Program, La Crosse, Wisconsin: USGS Upper Midwest Environmental Science Center, 1998.

Dettmers, J. M., D. H. Wahl, D. A. Soluk, and S. Gutreuter. "Life in the Fast Lane: Fish and Foodweb Structure in the Main Channel of Large Rivers." *Journal of the North American Benthological Society*, 2001: 255-265.

ESRI. *ArcGIS.* 2011. http://www.esri.com/software/arcgis/arceditor/index.html (accessed 2009-2011).

Ghanem, A., P. Steffler, and F. Hicks. "Two-Dimensional Hydraulic Simulation of Physical Habitat Conditions in Flowing Streams." *Regulated Rivers: Research & Management*, 1996: vol. 12 185-200.

Hastie, L.C., Boon, P.J., Young, M.R. “Physical Microhabitat Requirements of Freshwater Pearl Mussels, Margaritifera margaritifera (L.).” *Hydrobiologia*, 2000: vol. 492 59-71

He, Z., W. Wu, and S. S.Y. Wang. "A Depth-averaged 2-D Analysis of Fish Habitat Suitability Impacted by Vegetation and Sediment." *World Environmental and Water Resources Congress.* Omaha, NE: American Society of Civil Engineers, 2006.

Hendrickson, J. S. "Island Construction - Rebuilding Natural Levess to Restore Connectivity in the Northern Reaches of the Upper Mississippi River." *Federal Interagency Sedimentation* . Las Vegas, 2010.

Hendrickson, J. S., and A. W. Buesing. "Floodplain Restoration for Fish and Wildlife Habitat on the Upper Mississippi River." *American Society of Civil Engineers* . Minneapolis, 2000.

Hendrickson, J.S. "Personal Correspondence." United States Army Corps of Engineers, 2010-2011.

Ickes, B. "Personal Correspondence." LaCrosse, Wisconsin: United States Geological Survey, 2010-2011.

Jirka, G.H. "Large Scale Structures and Mixing Processes in Shallow Flows." *Journal of Hydraulic Research*, 2001: 567-573.

Johnson, B. "Personal Correspondence." LaCrosse, Wisconsin: United States Geological Survey, 2010-2011.

Knox, J. C. "The Mississippi River System." In *Large Rivers Geomorphology and Management*, by Avijit Gupta, 145-177. Jon Wiley & Sons, Ltd, 2007.

Lai, Y. G. *Two-Dimensional Depth-Averaged Flow Modeling with an Unstructured Hybrid Mesh.* Denver: Bureau of Reclamation Sedimentation and River Hydraulics, 2009.

Mays, L. W. *Water Resource Engineering.* New Jersey: Wiley & Sons, Inc., 2005.

Microsoft. *Excel 2010.* 2011. http://office.microsoft.com/en-us/excel/.

Morales, Y. “Analysis of Mussel Popultaion Dynamics in the Mississippi River.” *Ph.D.* Diss. Iowa City. University of Iowa, 2004.

Natinal Oceanic and Atmospheirc Administration. *National Geodetic Survey.* March 21, 2011. http://www.ngs.noaa.gov/ (accessed 2011).

Papanicolaou, A. N., Ad. Elhakeem, D. Dermisis, and N. Young. "Evaluation of the Missouri River Shallow Water Habitat Using a 2D-Hydrodynamic Model." *River Research and Applications.* Wiley InterScience, 2010.

Piotrowski, J. A. "Development of a High-Resolution Two-Dimensional Urban/Rural Flood Simulation." *Masters Thesis.* Iowa City: University of Iowa, 2010.

Piotrowski, J. "Personal Correspondence." Iowa City, Iowa: University of Iowa, 2011.

Rogala, J. "Personal Correspondence." LaCrosse, Wisconsin: United States Geological Survery, 2009-2011.

Rueda, F., E. Monreno-Ostos, and J. Armengol. "Calibration and Verification of a 2D-Hydrodynamic Model for Simulating Flow Around Emergent Bendway Weir Structures." *Journal of Hydraulic Engineering*, 2011: 75-89.

Schnoebelen, D.J. "Written Communication." Iowa City, Iowa: The University of Iowa, 2009-2011.

Schubert, M. A. "Computational Fluid Dynamics Applications for Nitrate Removal in an Upper Mississippi River Backwater." *Masters Thesis.* Iowa City: University of Iowa, 2009.

Schwarz, C.R. *The North American Datum of 1983.* NOAA Professional Paper NOS 2, Rockville, MD: National Geodetic Survey , 1989.

Silberstein, R. P. "Hydrological models are so good, do we still need data?" *Environmental Modeling and Software*, 2006: 1340-1352.

Tecplot, Inc. *Tecplot 360 User's Manual.* Bellevue, WA, 2010.

The University of Iowa. *Lucille A. Carver Mississippi Riverside Environmental Research Station.* October 4, 2010. http://www.iihr.uiowa.edu/projects/mrers/ (accessed 2011).

United State Army Corps of Engineers. *River Gauges.* 2011a. http://www2.mvr.usace.army.mil/WaterControl/new/layout.cfm (accessed 2009-2011).

United State Department of Agriculture Natural Conservation Service. *Geospatial Data Gateway.* March 9, 2011. http://datagateway.nrcs.usda.gov.GDGOrder.aspx (accessed 2011).

United States Army Corps of Engineers. *US Army Corps of Engineers St. Paul District.* March 2, 2011b. http://www.mvp.usace.army.mil/environment/default.asp?pageid=80 (accessed 2010-2011).

—. *Water Control Center, St. Paul District.* 2010. http://www.mvp-wc.usace.army.mil/ (accessed 2010-2011).

United States Bureau of Reclamation. *SRH-2D version2: Theory and User's Manual.* Software User's Manual, Denver, CO: U.S. Department of the Interior , 2008.

United States Geological Survey. *Seamless Data Warehouse.* December 28, 2010a. http://seamless.usgs.gov/ (accessed 2010).

—. *The Long Term Resource Monitoring Program.* March 11, 2011a. http://www.umesc.usgs.gov/ltrmp.html (accessed 2010-2011).

—. *Upper Midwest Environment Science Center.* December 3, 2010b. http://www.umesc.usgs.gov/ (accessed 2010-2011).

—. *Upper Mississippi River - Select a Reach.* March 7, 2011b. http:www.umesc.usgs.gov/rivers/upper_mississippi/select_a_reach.html (accessed 2009-2011).

—. *Water Watch.* March 16, 2011c. http://waterwatch.usgs.gov/new/ (accessed 2010-2011).

Water Level Management Task Force. *A Summary of the Research and Monitoring Results from the 2001 and 2002 Experimental Drawdowns of Pool 8 Upper Mississippi River Pool 8 Frawdown Results* . Reseach Monitoring, La Crosse, Wisconsin: United Geological Survery, 2007.

Young, N. C,. "Physical Characterization of Freshwater Mussel Habitats in Upper Mississippi River Pool 16." *Ph.D. Diss.* Iowa City: University of Iowa, 2006.

Young, N. C., A. J. Peck, D. Baldrige, and A. D. Christian. "Relationships Betweem Benthic Sediments, Hydrodynamics, and Animal Occurrences: Identifying Appropriate Structural Habitat for Potamilus Capax." *Fifty-Six Annual Meeting of the North American Benthological Society.* Salt Lake City, 2008.